THEORETICAL STUDIES OF THE LIGHT REACTIONS IN PHOTOSYNTHESIS

Richard A. Friesner
(Ph. D. thesis)

March 1979

Prepared for the U. S. Department of Energy
under Contract W-7405-ENG-48

DISCLAIMER

LBL-8953

THEORETICAL STUDIES OF THE LIGHT REACTIONS IN PHOTOSYNTHESIS

by

Richard A. Friesner

Lawrence Berkeley Laboratory
University of California
Berkeley, California 94720

THEORETICAL STUDIES OF THE LIGHT REACTIONS IN PHOTOSYNTHESIS

by

Richard A. Friesner

Kenneth Sauer

ABSTRACT

This thesis is concerned with the study of the light reactions of photosynthesis by electron paramagnetic resonance spectroscopy (EPR). The author's original contributions are primarily in two areas; development of magnetic resonance formalism, and utilization of theoretical formulations to interpret EPR spectra arising from photosynthetic systems. The latter analysis has provided information about the orientations, interactions, and identity of the electron transport cofactors involved in the photosynthetic light reactions in both green plants and photosynthetic bacteria.

The first two chapters present introductory material. Chapter 1 briefly outlines the magnetic resonance formalism which is used throughout; Chapter 2 is a short introduction to the light reactions of photosynthesis. These sections are intended to serve as a review for a reader familiar with these topics, or as a guide for one who is new to them; more extensive references are provided.

In Chapter 3 a general method of determining the orientational distribution function of a partially ordered ensemble of paramagnetic systems from its EPR lineshape is developed. The formalism represents a significant departure

from the usual technique, expansion of the distribution function in Wigner rotation matrix elements. Instead, a model for the ordering is constructed from the symmetry operations of the ensemble, and the EPR lineshape is simulated by varying parameters which can be assigned explicit physical interpretations. A prescription is also given for determining the relationship of the principal magnetic axis system (PMAS) of the paramagnetic species to the preferred alignment direction of the ensemble if this is not already known. The approach is currently being extended to other types of spectroscopy, *e.g.* linear dichroism.

In Chapter 4 the theory of Chapter 3 is applied to a partially ordered ensemble of triplet states localized on the primary donor in photosynthetic bacteria. Ordering is achieved by magnetic field orientation (*Rps. viridis* and *Rps. palustris*) or magnetophotoselection (*Rps. spheroides*). An analysis of the spectrum from a randomly oriented ensemble allows determination of the D and E values of the triplet and the relative intersystem crossing rates $K_x:K_y:K_z$; the parameters so obtained are then used in conjunction with a model for the distribution function to determine the orientation of either the normal to the photosynthetic membrane (magnetic field alignment) or the appropriate optical transition moment (magnetophotoselection) in the PMAS of the triplet.

Chapter 5 is an analysis of a spin polarized EPR signal arising from photosystem I (PSI) of higher plants which can be observed in chloroplast suspensions. The chloroplasts can

be oriented by means of a flow gradient; this causes an alteration in the polarized EPR lineshape.

A radical pair theory of spin polarization for systems of membrane bound radicals with anisotropic g tensors is developed, and used to explain the orientation dependence of the lineshape of the polarized signal. The quantitative features of the oriented and unoriented signals can be satisfactorily reproduced only if the sequence of electron transport cofactors in PSI is taken to be

$$P700 \rightarrow A_1 \rightarrow A_2 \rightarrow P430,$$

where A_1^- is an isotropic radical with a g value close to that of $P700^+$ (probably a chlorophyll anion) and A_2 is X, an anisotropic species which can be observed in steady state EPR experiments at low temperature when P430 is reduced.

ACKNOWLEDGEMENTS

The time I have spent at Berkeley has been a time for growing, both intellectually and emotionally. This thesis is one of the end products of that process, so it is fitting that I have an opportunity here to give thanks to some of the people who have contributed something of themselves to my life:

Harry Frank, John Bolt, Ann McGuire, Mary Mclean, and Chuck Dismukes, for their first-class experimental work and subatantive collaboration in development of theoretical models.

John Nairn, for the contribution of his considerable talents to the development of the orientation averaging theory.

All of the members of the Sauer research group, for their encouragement in both scientific and personal matters.

Marshall Tuttle, for an exemplary job of thesis typing in a very short amount of time.

The men and women who I have come to feel close to over the past six years: Donna, David, Philip, Bobby, Gary, Michael, Tim, Barbara, Hank, Lisa, Beth, Michael, Karen, Kenny, Shelley, Mary, Harry, Warren, Lew, and many others.

My parents, for their unwavering faith, love and financial support.

My adviser, Kenneth Sauer, for his patience, understanding, and insight in both science and personal relations. Without his support this thesis would never have been completed.

TABLE OF CONTENTS

INTRODUCTION

The application of physics and chemistry to biology has produced a scientific revolution of astonishing dimensions during the past twenty years. Enormous quantities of detailed structural and functional information have been obtained concerning a wide variety of biological entities: chromosomes, enzymes, membranes, etc. Our picture of the biological micro-world has undergone a gestalt-switch to a sharper focus.

In a certain sense, it is the structural information which has primacy in biological theory construction; function often can be deduced directly from structural considerations, as in the obvicus conclusions drawn immediately from the Watson-Crick double helix structure for DNA, or the elucidation of enzyme mechanisms from the geometry of the active site. Where structure does not lead directly to function, it can often suggest key experiments needed to provide mechanistic information.

X-ray diffraction has, to date, been the most important and successful method for determining the structures of components of biological systems. Macroscopic bodies like large protein molecules have been crystallized, and their three-dimensional structures refined to within a few angstroms by the use of heavy-atom derivatives. The wealth of data obtained by this technique has been of incomparable value in constructing a model of the way things are in biological systems, and the way they work.

Nevertheless, there are serious limitations of the application of x-ray diffraction techniques to biological studies. Preparation of crystalline material requires isolating and purifying the component of interest; even if this can be successfully accomplished, crystallization may prove to be impossible. Furthermore, the structural determination must be carried out in a chemical environment which is vastly different from the natural biological state. Not only is this likely to distort the structure from the *in vivo* one, but it prevents determination of the spatial relations between the molecule of interest and neighboring molecules. Such relations can be of crucial importance in discovering biological function.

The above considerations suggest that it would be valuable to perform structural determinations on biological components *in vivo*. Unfortunately, this presents a far more difficult problem than the determination of the geometrical arrangement of crystalline material. Any single crystal, even one of a complex protein, possesses a great deal of symmetry: the repeating unit cell. It is this symmetry that allows one to reconstruct the spatial arrangement of atoms within a single unit cell, because the scattered x-rays from diverse cells interfere coherently and in predictable fashion.

Biological structures are normally dispersed in aqueous or lipid phases in a more or less heterogeneous manner. An ensemble of particular entities (*e.g.* a group of cells suspended in solution, or protein molecules bound to membrane fragments)

will at best be partially ordered with respect to one another. Furthermore, the entire intact system contains many types of molecules in various environments. To sort out information obtained from such a system, and obtain quantitative conclusions, is a problem which appears on the surface to be so difficult that one is tempted to give up before starting.

The most common method of probing molecular properties in solution has been the use of appropriate frequencies of electromagnetic radiation. Microwaves will interact with paramagnetic species (either nuclear or electronic spins, depending on frequency) and provide information about the environment and identity of these species. Infrared radiation induces vibrational transitions, while optical wavelengths stimulate electronic transitions; the location, width and intensity of the absorption bands can be related to the molecular entities present in the sample. Optical rotation and circular dichroism are more subtle probes which can be utilized to study molecules which possess a fundamental asymmetry. Light scattering, particularly Raman and resonance Raman measurements, is also a useful investigative method.

Nevertheless, the detailed structural information obtained from such experiments on biological systems has been remarkably scarce and uncertain. Molecular species can, in principle, be characterized by their EPR or absorption spectrum, but these can change appreciably with environment, particularly in a protein matrix. Also, chromophores are often aggregated in

some fashion, with consequent changes in their observed properties. Finally, there is often the problem of specificity; the absorptive regions of different species may overlap, making it difficult to sort out the signal due to an individual molecule. A typical absorption profile of a biological system is a superposition of heterogeneous signals; some from identical molecules in different environments, others from different molecules.

This thesis will be concerned with a specialized problem; investigation of the light reactions of photosynthetic systems via EPR spectroscopy. All of the difficulties described above are evident in this work. Some can be alleviated by suitable experimental techniques, *e.g.* judicious sample preparation, observation methods, *etc.* However, the focus will be on the theoretical aspects of the problem - the use of quantum mechanical formalism to extract structural and interactional information from the EPR signals in photosynthetic systems. From this viewpoint there are two major hurdles to overcome:

(1) Formulation of fundamental theory.

This involves creating a correct quantum mechanical formulation which can actually be applied to the problem at hand. Sometimes such a theory already exists, but often it is necessary to modify an existing formalism or construct an entirely new approach. The theory of CIDEP of membrane-bound radicals in Chapter 5 is an example of the former sort, while the theory of partially ordered systems developed in Chapter 3 contains a new conceptual framework.

(2) Application of the theory to experiments.

The critical factors here are building a physically reasonable model and having a good intuitive feel for how to extract the maximum useful quantitative information from it. With the theory in hand it is then a matter of technique to utilize computer methods to obtain the desired results. Of course, one must also have relevant experimental results to interpret; I have been fortunate in my career at Berkeley to have been able to work with a number of careful and imaginative experimentalists who were able to provide such data.

The material in the following chapters is of importance for an understanding of photosynthesis and as an advancement of funadmental EPR theory; as such, it can be evaluated in the appropriate independent context. What I wish to suggest here is that it also represents a contribution, albeit a small one, towards structural determination in heterogeneous media. I expect that ultimate solution to this problem will involve the combined use of a number of spectroscopic techniques; unfortunately, this is beyond the scope of the present work. What is here, though, can be thought of as a paradigmatic step along the path which must be followed.

CHAPTER 1

INTRODUCTION TO EPR THEORY

The theory of electron paramagnetic resonance has been explicated by many authors. A wide range of treatments ranging from introductory textbooks to advanced treatises and specialized journal articles are available, and we shall not attempt here to replicate in detail material that has already been presented. Our approach will be to briefly outline the development of magnetic resonance formalism, with particular emphasis on topics which will be needed later. References 1-5 provide a starting point for those who wish to work through the theory more comprehensively.

1.1 Phenomenological Description of Magnetic Resonance

The process characteristic of all magnetic resonance experiments is absorption of microwave radiation by a paramagnetic species. The experimental EPR apparatus is designed to measure and quantify this absorption process, in the presence of an external magnetic field $\underset{\sim}{H}_o$ which is applied at right angles to the microwave magnetic field direction. An EPR spectrum consists of a set of measurements of microwave absorption for different magnitudes of $\underset{\sim}{H}_o$.

The microwave radiation is produced by a klystron; a set of standard frequency ranges (*e.g.* X band $\approx$ 9.0 GHz, Q band $\approx$ 35.0 GHz, K band $\approx$ 25.0 GHz) are available. All of the

experiments relevant to this thesis were done at X band. Detailed discussion of the klystron, microwave cavity, and detection system can be found in reference 5. We shall assume simply that the sample experiences a uniform oscillatory microwave field of frequency 9.0 GHz, and that net absorption of radiation is quantitatively measured.

The absorption of radiation is due to transitions among the spin sublevels of the paramagnetic system. The simplest case is that of a single, unpaired free electron ($S = 1/2$). In the absence of an applied magnetic field, the two spin sublevels are degenerate. In the presence of $\underset{\sim}{H}_o$, the system is characterized by two distinct eigenstates, α and β, corresponding to $\underset{\sim}{S}$ aligned parallel or antiparallel to $\underset{\sim}{H}_o$.

The energy splitting between these states is $g_e\beta|\underset{\sim}{H}_o|$, where $\frac{1}{2} g_e\beta$ is the intrinsic magnetic moment of the free electron. The EPR spectrum of an ensemble of non-interacting free electrons would thus consist of a delta function located at $h\nu = g_e\beta H_o$. By substituting $h\nu = 9$ GHz, we obtain the resonant magnetic field for a free electron in an X band experiment;

$$H_o = \frac{h\nu}{g_e\beta} = 3227 \text{ gauss} \qquad (1\text{-}1)$$

For more complicated systems, we need to investigate the totality of the magnetic environment of each of the unpaired electrons in the ensemble. Our program will be to formulate a magnetic, or spin Hamiltonian for each paramagnetic system

under consideration, and then diagonalize it to obtain transition energies and resonant field positions. The observed EPR spectrum will be an ensemble average over all species in the sample.

1.2 Magnetic Resonance Formalism

We shall restrict consideration to systems with at most two electrons; generalization to multi-electron systems is straightforward in principle. The spin operators for the two electrons are

$$\begin{aligned} \underset{\sim}{S}_1 &= (S_{1x} \quad S_{1y} \quad S_{1z}) \\ \underset{\sim}{S}_2 &= (S_{2x} \quad S_{2y} \quad S_{2z}) \end{aligned} \tag{1-2}$$

The total spin is

$$\underset{\sim}{S} = \underset{\sim}{S}_1 + \underset{\sim}{S}_2 \tag{1-3}$$

or, in terms of components

$$\underset{\sim}{S} = (S_x \quad S_y \quad S_z) = (S_{1x}+S_{2x} \quad S_{1y}+S_{2y} \quad S_{1z}+S_{2z})$$

The spins are coupled to the external magnetic field $\underset{\sim}{H}_o$ (Zeeman field) by the g tensors $\hat{g}_1$ and $\hat{g}_2$, and to each other by the dipole-dipole coupling tensor, $\hat{D}$, and the exchange tensor, $\hat{J}$. Interaction with paramagnetic nuclei is represented via the hyperfine tensors $\hat{A}_1$ and $\hat{A}_2$. The spin operators for the nuclei are $\underset{\sim}{I} = (I_x \quad I_y \quad I_z)$, and the z component eigenvalues are M_{iz}.

The theory of electron paramagnetic resonance consists of determining the experimental EPR signal (as defined in 1.1) from a knowledge of the elements of the vector and tensor operators defined above. The procedure we shall employ is as follows:

(1) Characterization of a spin Hamiltonian in terms of an effective spin, $\underset{\sim}{S}'$, which includes spin-orbit coupling effects.

(2) Diagonalization of the Hamiltonian matrix to obtain eigenvalues, eigenvectors, transition energies and oscillator strengths.

(3) Convolution of the "stick spectrum" obtained in (2) with a broadening function to phenomenologically take into account random dipolar interactions, lifetime broadening, *etc.*

(4) Ensemble averaging over all orientations, hyperfine states, and distinct species to obtain the desired experimental signal.

1.3 The Spin Hamiltonian

A. Effective Spin

Our first step is to incorporate the orbital and intrinsic magnetic moments of the electron i into an effective magnetic moment characterized by a new spin operator $\underset{\sim}{S}_i'$. A free electron has no orbital angular momentum (*i.e.* $\underset{\sim}{L} = 0$) so that here $\underset{\sim}{S}_i' \equiv \underset{\sim}{S}_i$. When we constrain an electron to a bound state (as in an atom or molecule), other values of $\underset{\sim}{L}$

are possible, and there will be a corresponding orbital moment associated with the circulation of charge. The interaction between the orbital and intrinsic magnetic moments gives rise to a term in the molecular Hamiltonian

$$\mathcal{H}_{soc} = \chi(r)\underset{\sim}{L}\cdot\underset{\sim}{S} \qquad (1\text{-}4)$$

where $\mathcal{H}_{soc}$ is the spin-orbit coupling operator, and χ is a parameter characterizing the magnitude of the interaction as function of electron position. This term will mix basis states with differing L_z and S_z quantum numbers.

The total interaction of a magnetic field $\underset{\sim}{H}$ with the electron can be written as

$$U = \beta\underset{\sim}{H}\cdot\underset{\sim}{L} + g_e\beta\underset{\sim}{H}\cdot\underset{\sim}{S} \qquad (1\text{-}5)$$

where β is the Bohr magneton, and $g_e\beta$ the magnetic moment of a free electron. We wish to combine the two terms on the right hand side of eq. (1-5) into a single term; *i.e.*

$$U = \beta\underset{\sim}{H}\cdot\hat{g}\cdot\underset{\sim}{S}' \qquad (1\text{-}6)$$

where $\underset{\sim}{S}'$ is the effective spin, and $\hat{g}\beta$ represents an effective magnetic interaction which may be anisotropic.

In the absence of spin-orbit coupling it can be shown that $\langle\psi_g|\beta\underset{\sim}{H}\cdot\underset{\sim}{L}|\psi_g\rangle = 0$, for the ground state ($\psi_g$) of a molecule with an unpaired electron. Therefore, spin-orbit mixing of the ground state wave function with other (L,S) states provides the only orbital contribution to the effective g value.

In the first order of perturbation theory the new ground state with $\underset{\sim}{S}$ parallel to $\underset{\sim}{H}$ is given by

$$|+\rangle = |\psi_o\ \alpha\rangle - \sum_n \frac{\langle n|\mathcal{H}_{soc}|\psi_o\ \alpha\rangle}{E_n - E_o}\ |n\rangle \qquad (1\text{-}7)$$

where ψ_o is the ground state space part of the wavefunction, and n runs over all excited states, including $|\psi_i\ \beta\rangle$ states.

Similarly, $|\psi_o\ \beta\rangle$ is altered to

$$|-\rangle = |\psi_o\ \beta\rangle - \sum_n \frac{\langle n|\mathcal{H}_{soc}|\psi_o\ \beta\rangle}{E_n - E_o}\ |n\rangle \qquad (1\text{-}8)$$

The $|+\rangle$ and $|-\rangle$ states are the new eigenstates of the molecule; the effective spin is defined to act on the $|+\rangle$ and $|-\rangle$ states in the same fashion that S acts on $|\alpha\rangle$ and $|\beta\rangle$, *i.e.*

$$\begin{aligned} S'_z\ |+\rangle &= \tfrac{1}{2}\ |+\rangle \\ S'_z\ |-\rangle &= -\tfrac{1}{2}\ |-\rangle \\ \langle +|S'^2|+\rangle &= \langle -|S'^2|-\rangle = \tfrac{1}{2} \end{aligned} \qquad (1\text{-}9)$$

The elements of the g tensor are given by

$$g_{ij} = g_e - \Sigma \frac{\langle\psi_o|L_i|\psi_n\rangle\langle\psi_n|L_j|\psi_o\rangle}{E_n - E_o} \qquad (1\text{-}10)$$

where i,j = x, y, or z.

In the sections that follow, we shall drop the prime and always understand S to be the effective spin, $|\alpha\rangle$ and $|\beta\rangle$ to be the $|+\rangle$ and $|-\rangle$ states, and $\hat{g}$ to be the g tensor as defined above.

B. Zeeman Interaction

We shall use the term "Zeeman field" to mean "static EPR field" (usually produced by an electromagnet which is part of the experimental apparatus) and shall label this field by $\underset{\sim}{H}_o$. In the laboratory axis system, $\underset{\sim}{H}_o$ is normally taken to be in the z direction.

The Zeeman interaction is the magnetic interaction of the Zeeman field with the magnetic dipoles of the paramagnetic electrons. If the two electrons have distinct g tensors (*e.g.* they are on different molecules), the Zeeman term in the Hamiltonian is

$$\mathcal{H}_{Zeeman} = [\underset{\sim}{H}_o \cdot \hat{g}_1 \cdot \underset{\sim}{S}_1 + \underset{\sim}{H}_o \cdot \hat{g}_2 \cdot \underset{\sim}{S}_2] \qquad (1\text{-}11)$$

If the electrons have identical g tensors, we can write

$$\mathcal{H}_{Zeeman} = \beta \underset{\sim}{H}_o \cdot \hat{g} \cdot \underset{\sim}{S} \qquad (1\text{-}12)$$

If the g tensor is isotropic, eq. (1-12) further simplifies to

$$\mathcal{H}_{Zeeman} = \beta H_o g S_z \qquad (1\text{-}13)$$

where $g\beta$ is the scalar isotropic value of the magnetic moment.

C. Dipolar Interaction

The dipolar interaction is the mutual magnetic energy of two coupled magnetic dipoles, averaged over the spatial wavefunctions of the two electrons. The interaction is

represented in the spin Hamiltonian by the term

$$\mathcal{H}_{\text{dipolar}} = \underset{\sim}{S}\cdot\hat{D}\cdot\underset{\sim}{S} \qquad (1\text{-}14)$$

where $\hat{D}$ is the dipole-dipole coupling tensor, or the zero-field splitting tensor. Elements of $\hat{D}$ can be calculated from the spatial wavefunctions ϕ_1 and ϕ_2 of electrons 1 and 2, *e.g.*

$$D_{xy} = \frac{1}{2} g^2\beta^2 \int \phi_1\phi_2 \left(\frac{-3x_{12}y_{12}}{r_{12}^5}\right) d\tau_1 d\tau_2 \qquad (1\text{-}15)$$

where x_{12} and y_{12} are operators for the x and y separations of electrons 1 and 2.

The other elements of $\hat{D}$ can be constructed in analagous fashion by examination of the standard dipole-dipole interaction.

The tensor $\hat{D}$ can be diagonalized by an appropriate coordinate transformation; in this new reference frame, the dipolar interaction becomes

$$\mathcal{H}_{\text{dipolar}} = -XS_x^2 - YS_y^2 - ZS_z^2 \qquad (1\text{-}16)$$

where X, Y, and Z are the principal values of the $\hat{D}$ tensor. It can be shown that $X + Y + Z = 0$; it is therefore possible to simplify eq. (1-16) so that it contains only two energy parameters, D and E;

$$\mathcal{H}_{\text{dipolar}} = D(S_z^2 - \tfrac{1}{3}|\underset{\sim}{S}|^2) + E(S_x^2 - S_y^2) \qquad (1\text{-}17)$$

where

$$D = \frac{1}{2}(X+Y) - Z$$

$$E = -\frac{1}{2}(X-Y)$$

D. Exchange Interaction

The exchange interaction is a consequence of the requirement that the total wave function of a multi-electron system be antisymmetric upon exchange of electron coordinates (Pauli principle). Suppose we write the total wavefunction Φ as

$$\Phi = \phi_{space} \times \psi_{spin} \tag{1-18}$$

The parity of ϕ_{space} will clearly depend on that of ψ_{spin}, so that the overall Φ will be antisymmetric.

For a two-electron system, we can use as a basis set three symmetric functions (triplet states) and one antisymmetric function (singlet). Because of the above considerations, the space part of the triplet manifold will be different from the singlet; this results in a different electronic energy when the space part is evaluated in the molecular Hamiltonian. This energy differential is represented phenomenologically in the spin Hamiltonian by the term

$$\mathcal{H}_{ex} = \underset{\sim}{S}_1 \cdot \hat{J} \cdot \underset{\sim}{S}_2 \tag{1-19}$$

or, by rearrangement

$$\mathcal{H}_{ex} = \underset{\sim}{S} \cdot \hat{J} \cdot \underset{\sim}{S} \tag{1-20}$$

Note that the exchange term is mathematically isomorphic to the dipolar interaction. For isotropic exchange, we obtain

$$\mathcal{H}_{ex} = J \, \underset{\sim}{S}_1 \cdot \underset{\sim}{S}_2$$

and the triplet manifold is split from the singlet by energy 2J. If direct exchange is the dominant mechanism,

$$J = \iint \phi_1(1)\phi_2^*(2) \frac{e^2}{r_1^2} \phi_1(2)\phi_2^*(2)\, d\tau_1 d\tau_2 \qquad (1\text{-}21)$$

the electronic exchange matrix element. However, exchange often is due to superexchange pathways (6,7); in this case it is difficult to write down the exchange energy directly.

E. Hyperfine Interaction

The generalized interaction between the electron and nuclear spins in a molecule with 1 electron can be written as

$$\mathcal{H}_{HF} = \sum_i \underset{\sim}{S} \cdot \hat{A}_i \cdot \underset{\sim}{I}_i \qquad (1\text{-}22)$$

where $\hat{A}_i$ is the hyperfine tensor for nucleus i, and $\underset{\sim}{I}_i$ is the operator for the ith nuclear spin. We shall consider only isotropic hyperfine interactions; then

$$\mathcal{H}_{HF} = \sum_i A_i \underset{\sim}{S} \cdot \underset{\sim}{I}_i \qquad (1\text{-}23)$$

where A_i is now the isotropic hyperfine coupling constant for nucleus i.

This interaction is proportional to the square of the electronic wavefunction at nucleus i, *i.e.*

$$A_i = \frac{8\pi}{3} g\beta g_n \beta_n |\phi(0)|^2 \qquad (1\text{-}24)$$

where g_n is the nuclear g value, g tne electron g value (we assume an isotropic g value here) and $\phi(0)$ the electronic wavefunction at r = 0. At high field the nuclear spin is quantized in the direction of $\underset{\sim}{H}_o$ (z direction); then

$$\mathcal{H}_{HF} = \sum_i A_i I_z S_z \qquad (1\text{-}25)$$

The effect of hyperfine interaction on the EPR energy levels is normally evaluated using first-order perturbation theory. The procedure is to first diagonalize the remaining spin Hamiltonian and obtain energy levels $E_1 \ldots E_n$; then, associated with each transition E_i is a manifold of hyperfine states with energy

$$E_i' = E_i - \sum_i A_1 m_{zi} \qquad (1\text{-}26)$$

where m_{zi} ranges from $\max|I_z|$ to $-\max|I_z|$.. Transitions can now be computed between hyperfine manifolds using the selection rule $\Delta m_{iz} = 0$. For the simple case of two energy levels and one hyperfine nucleus of spin $\frac{1}{2}$ we obtain four energy levels;

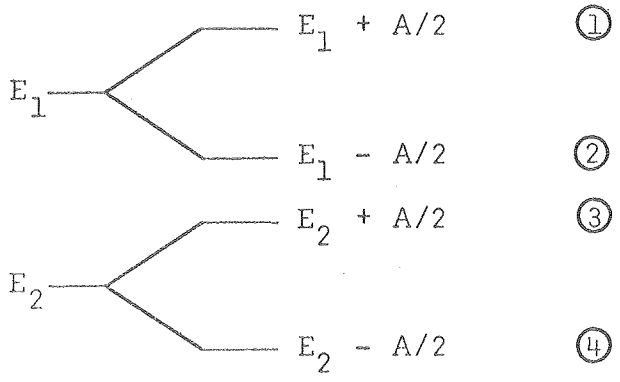

and two transitions,

④ → ① with energy $(E_1 - E_2) + A$

③ → ② with energy $(E_1 - E_2) - A$

The single transition (in the absence of hyperfine interaction) at $(E_1 - E_2)$ is thus split into two transitions separated by 2A.

It is possible to include the hyperfine interaction directly in the Hamiltonian or to go to higher orders of perturbation theory. The above treatment is valid if $[A/(E_1-E_2)]$ is small; otherwise, one may go to higher orders of $A/\Delta E$. In certain cases, it is convenient to treat the hyperfine manifold phenomenologically as an inhomogeneous broadening.

F. Random Perturbations and Motional Averaging

The preceding sections have all been concerned with interactions that are not explicitly time dependent; all involved intramolecular interactions. In a large ensemble (*e.g.* solution, crystal, *etc.*) molecules may be perturbed by magnetic fields from neighboring molecules; these fields will vary in time with molecular motions.

The quantum mechanical treatment of such random dipolar or exchange perturbations is quite complex; interested readers are referred to references (8-10). We shall adopt a phenomenological approach and treat these effects as a broadening of the individual transitions with a Gaussian or Lorentzian function. The width of this function can be estimated from theoretical and empirical considerations. In situations where there are many, closely spaced transitions, this linewidth parameter has little effect on the EPR lineshape.

1.4 Solution to the Spin Hamiltonian

A. General Approach

We shall be considering only Hamiltonians which are explicitly time-independent; the problem is therefore to solve the time-independent Schroedinger equation for the magnetic Hamiltonian $\mathcal{H}_m$;

$$\mathcal{H}_m \psi_i = E_i \psi_i \qquad (1\text{-}27)$$

for the eigenvectors ψ_i and energies E_i.

$\mathcal{H}_m$ is given by

$$\mathcal{H}_m = \mathcal{H}_{zeeman} + \mathcal{H}_{dipolar} + \mathcal{H}_{ex} \qquad (1\text{-}28)$$

(hyperfine interactions are added in afterwards, as explained in sec. 1.3). The general procedure for solving eq. (1-27) for an n-spin system is

(1) Choose a basis set $\{\phi_i\}$ which spans the spin space of the Hamiltonian.

(2) Calculate matrix elements $H_{ij} = \langle \phi_i | \mathcal{H}_m | \phi_j \rangle$ for all i,j.

(3) Diagonalize the Hamiltonian matrix to obtain energies E_i and eigenfunctions $\psi_k = \Sigma\, c_k^i \phi_i$, where the c_i^k are coefficients of the basis functions.

We illustrate this procedure with a paradigmatic example, a molecular state with two unpaired spins.

B. Molecular Two-Spin State

We assume that the g tensor is isotropic, that J is isotropic, and that the molecule under consideration is rigidly fixed at a particular orientation with respect to

the Zeeman field $\underset{\sim}{H}_o$.

Then, the spin Hamiltonian is

$$\mathcal{H}_m = g\beta \underset{\sim}{H}_o \cdot \underset{\sim}{S} + \underset{\sim}{S} \cdot \hat{D} \cdot \underset{\sim}{S} + J\underset{\sim}{S}_1 \cdot \underset{\sim}{S}_2 \qquad (1\text{-}29)$$

We transform to the principal axis system of the zero-field splitting tensor $\hat{D}$; then

$$\mathcal{H}_m = g\beta \underset{\sim}{H}_o \cdot \underset{\sim}{S} - XS_x^2 - YS_y^2 - ZS_z^2 + J\underset{\sim}{S}_1 \cdot \underset{\sim}{S}_2 \qquad (1\text{-}30)$$

where $\underset{\sim}{H}_o$ is no longer along z but may lie in any direction. We take $\underset{\sim}{H}_o$ to be

$$\underset{\sim}{H}_o = (H_x \; H_y \; H_z) = H_o(\sin\theta\sin\phi \;\; \sin\theta\cos\phi \;\; \cos\theta) \qquad (1\text{-}31)$$

If $\underset{\sim}{H}_o$ were equal to zero the solutions to the Hamiltonian would be eigenfunctions of S_x^2, S_y^2, and S_z^2; these states (the zero-field states) are as follows:

(1) $\underset{\sim}{S} = 0$

There is only one solution, the singlet state

$$S = \frac{1}{\sqrt{2}} [\alpha(1)\beta(2) - \alpha(2)\beta(1)] \qquad (1\text{-}32)$$

(2) $\underset{\sim}{S} = 1$

The zero-field triplet manifold is

$$T_x = \frac{1}{\sqrt{2}} [\beta(1)\beta(2) - \alpha(1)\alpha(2)]$$

$$T_y = \frac{1}{\sqrt{2}} \cdot i[\beta(1)\beta(2) + \alpha(1)\alpha(2)] \qquad (1\text{-}33)$$

$$T_z = \frac{1}{\sqrt{2}} [\alpha(1)\beta(2) + \alpha(2)\beta(1)]$$

The energies of these states are

$$\begin{aligned} E_S &= +J \\ E_X &= -J+X \\ E_Y &= -J+Y \\ E_Z &= -J+Z \end{aligned} \tag{1-34}$$

The Zeeman field mixes the three triplet sublevels but not the singlet state. The singlet is therefore still an eigenfunction, with energy +J (since $\underset{\sim}{S} = 0$ for a singlet). The triplet Hamiltonian matrix with the zero-field states as a basis set becomes

$$\mathcal{H} = \begin{array}{c} \\ \langle T_x| \\ \langle T_y| \\ \langle T_z| \end{array} \begin{array}{c} \begin{array}{ccc} |T_x\rangle & |T_y\rangle & |T_z\rangle \end{array} \\ \begin{bmatrix} X-J & -ig\beta H_z & ig\beta H_y \\ ig\beta H_z & Y-J & -ig\beta H_x \\ -ig\beta H_y & ig\beta H_x & Z-J \end{bmatrix} \end{array} \tag{1-35}$$

We set the zero of energy at -J to simplify the ensuing calculations. The eigenvalues of $\mathcal{H}$ are found by setting

$$|\mathcal{H} - \lambda\hat{I}| = 0 \tag{1-36}$$

where λ is the eigenvalue and I the identity matrix. This yields a cubic equation for λ;

$$\begin{aligned} &\lambda^3 - \lambda[g^2\beta^2H_o^2 - (XY + YZ + XZ)] \\ &+ g^2\beta^2H^2(X\sin^2\theta\cos^2\phi + Y\sin^2\theta\sin^2\phi + Z\cos^2\theta) \\ &- XYZ = 0. \end{aligned} \tag{1-37}$$

where we have set

$$H_x = H_o \sin\theta\cos\phi$$
$$H_y = H_o \sin\theta\sin\phi$$
$$H_z = H_o \cos\theta$$

This equation cannot be solved analytically in the general case. We must thus choose one of the following alternatives;

(1) numerical solution

(2) perturbation theory (utilizing the inequality $g\beta H_o \gg X,Y,Z$ in a high-field EPR experiment)

(3) Exact solutions are available when $\underset{\sim}{H}_o$ lies along a principal axis (x,y, or z).

Method (1) is convenient for computer simulations, and is also the most accurate. Method (2) can be used to obtain an approximate analytical expression for the transition energy;

$$E(\theta,\phi) = \delta[3\cos^2\theta - 1 - \eta(\sin^2\theta\cos 2\phi)] + g\beta H_o \qquad (1\text{-}38)$$

where

$$\eta = \left(\frac{Y-X}{Z}\right)$$

and

$$\delta = \frac{\hbar}{g^2\beta^2 \left\langle \frac{1}{r_{12}^3} \right\rangle}$$

This function was used by Bloembergen and Rowland to obtain an orientationally averaged triplet spectrum in analytical

form (11). Method (3) gives some qualitative insight into the behavior of the energy levels as a function of orientation. The subspectra generated when $\underset{\sim}{H}_o \parallel x,y,$ or z are known as the canonical spectra; these orientations are called canonical orientations. The maxima of the observable peaks in the first derivative of the orientationally averaged triplet spectrum lie at the canonical transition energies.

Each canonical orientation yields two transitions, symmetrically positioned on either side of $g\beta H_o$. The splitting between the two canonical energies is, to first order,

$$\begin{aligned} g\beta(H_z^+ - H_z^-) &= 2|D| \\ g\beta(H_x^+ - H_x^-) &= |D| + 3|E| \\ g\beta(H_y^+ - H_y^-) &= |D| - 3|E| \end{aligned} \qquad (1\text{-}39)$$

where $H_z^\pm$, $H_x^\pm$, and $H_y^\pm$ are the resonant field positions for the z, x and y canonical orientations respectively. Figure 1-1 shows a randomly ordered triplet spectrum with the canonical field positions labelled below.

Once the energies are found, the eigenvectors ψ_i are easily obtained from the matrix equation

$$\mathcal{H}\psi_i = \lambda_i\psi_i \qquad (1\text{-}40)$$

At high field, the three energy levels will be close to the high field states, *i.e.* one state will have energy ~ $g\beta H_o$, another ~ 0, and a third ~ $-g\beta H_o$. We designate these 3

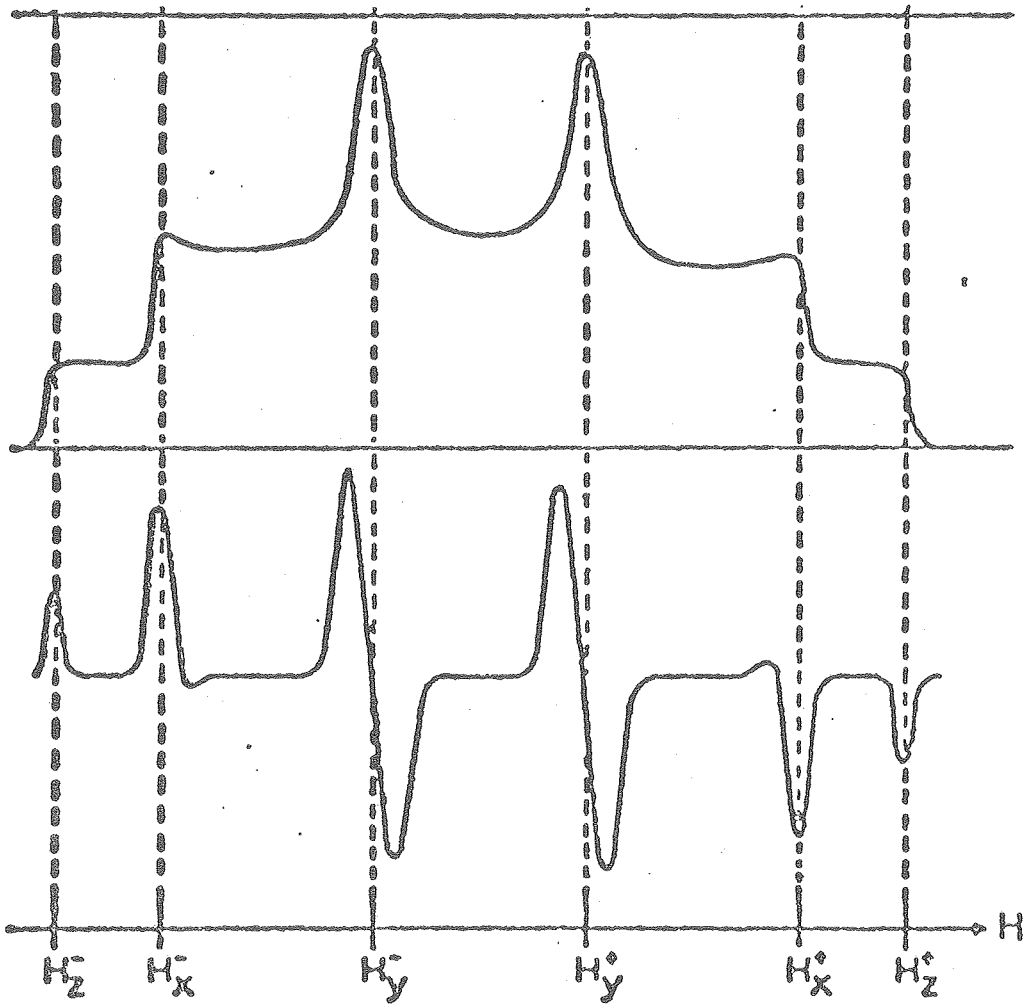

Figure 1-1. Simulated absorption (top) and first derivative (bottom) EPR spectrum of a randomly ordered ensemble of triplet molecules. Figure taken from reference (12).

levels the T_α, T_β, and T_γ states; clearly $T_\alpha \sim T_{+1}$, $T_\beta \sim T_0$, and $T_\gamma \sim T_{-1}$. The variation in energy for the canonical orientations can be determined from eq. (1-39); for the general case, numerical diagonalization or eq. (1-38) can be utilized.

We thus obtain 3 triplet eigenfunctions.

$$|T_\alpha\rangle = \sum_{i=x,y,z} c_i^\alpha |T_i\rangle \qquad \text{energy} = E_\alpha$$

$$|T_\beta\rangle = \sum_{i=x,y,z} c_i^\beta |T_i\rangle \qquad \text{energy} = E_\beta \qquad (1\text{-}41)$$

$$|T_\gamma\rangle = \sum_{i=x,y,z} c_i^\gamma |T_i\rangle \qquad \text{energy} = E_\gamma$$

This constitutes the triplet spin manifold at orientation (θ,ϕ); the coefficients c_i^α, c_i^β, c_i^γ, and energies E_α, E_β, and E_γ will depend upon θ and ϕ.

The allowed transitions are obtained from the oscillator strength equation

$$|\mu_{ij}|^2 = |H_1 \langle \psi_i | S_{1x} + S_{2x} | \psi_j \rangle|^2 \qquad (1\text{-}42)$$

where H_1, the microwave magnetic field, is assumed to be in the x direction. At high field, we obtain

$$|\mu_{\alpha\beta}|^2 \sim |\mu_{\beta\gamma}|^2 \sim \frac{1}{2}$$
$$|\mu_{\alpha\gamma}|^2 \sim 0 \qquad (1\text{-}43)$$

We then have two allowed transitions of approximately equal strength, one at energy $|E_\alpha - E_\beta|$, the other at energy $|E_\beta - E_\gamma|$. For the canonical orientations, these energies are given by eq. (1-39).

Thus, a discrete orientation of the two-spin PMAS yields two lines, broadened as described in sec. 1.3. For a rigid ensemble of such systems, the observed spectrum will be a superposition of all such possible transitions. We discuss this in more detail in sec. 1.5.

1.5. Ensemble Averaging

A. General Discussion

A typical EPR experiment is performed on a macroscopic sample which is placed in an EPR tube. The entire set of paramagnetic entities in this sample which can absorb microwave radiation from the H_1 field constitutes an ensemble of spin systems. The observed EPR lineshape will be determined by an ensemble average of the complex magnetic susceptibility over all elements of the ensemble. We begin by considering only chemically homogeneous ensembles (*i.e.* each member of the ensemble has the same chemical identity). Any ensemble can be partitioned into subsets of such homogeneous ensembles; each of these can be examined separately, and the resultant subspectra superimposed to give the experimental lineshape. The members of such an ensemble will, of course, be variable in other respects.

The most important of these are:

(1) Electronic state of the molecule (including local electronic perturbations),

(2) Magnetic environment (*i.e.* perturbations due to neighboring molecules),

(3) Hyperfine state,

(4) Orientation of the molecule with respect to the Zeeman field.

We shall consider (1) and (2) only by the use of a phenomenological broadening function (see sec. 1.3) for individual transitions. This effectively shifts the transition (with a probability given by the lineshape function) away from the unperturbed value, thus mimicking the effect of environmental electronic and/or magnetic perturbations. The procedure used to average over hyperfine states follows directly from the discussion in sec. 1.3; all possible values of the z component of nuclear spin are considered, and a resulting set of transitions are calculated from the manifold of hyperfine states superimposed on the basic electron spin resonance eigenvalues.

It is item (4), however, which presents the most interesting problem in ensemble averaging in magnetic resonance. In section B below we give an elementary introduction to orientation averaging; in Chapter 3 we develop a sophisticated theory for partially ordered ensembles; in Chapter 4, this theory is applied to a photosynthetic system.

B. Orientation Averaging

The nature of orientation averaging that needs to be performed depends upon the nature of the sample one is working with. If the molecules in the sample are tumbling rapidly in comparison with the inverse of the orientational line-width, each molecule sees a time-averaged Hamiltonian; here the orientational averaging process must be used to compute this average $\bar{\mathcal{H}}_m$ from $\mathcal{H}_m(t)$, *i.e.*

$$\bar{\mathcal{H}}_m = \int \mathcal{H}_m[\theta(t),\phi(t)]dt \qquad (1\text{-}44)$$

where θ and ϕ, the angles specifying the orientation of $\underset{\sim}{H}_o$ in the molecular fixed axis system are now explicit functions of time. If all molecules are in other respects equivalent, an observation on such an ensemble should yield a single set of molecular EPR transitions obtained from solving the Hamiltonian equation

$$\bar{\mathcal{H}}_m \psi_i = E_i \psi_i \qquad (1\text{-}45)$$

We shall be concerned with the opposite extreme, *i.e.* when molecular motion is very slow compared to absorption of a photon. Such an ensemble will exist at low temperature (frozen sample) or when the molecules are bound to membranes which tumble slowly.

In this case, each molecule is effectively frozen in its orientation for the duration of the measurement; the ensemble must now be described by a distribution function $P_{\alpha\beta\gamma}$, giving

the probability that a molecule picked from the ensemble at random would be related to a laboratory-fixed coordinate system by an Euler rotation matrix $A(\alpha\beta\gamma)$. If the spin Hamiltonian contains orientation-dependent terms, the EPR spectrum due to a member of the ensemble will depend upon α,β, and γ; the observed EPR intensity for the ensemble when the Zeeman field has magnitude H_o will be given by the ensemble average

$$\bar{I}(H_o) = \iiint I(\alpha,\beta,\gamma,H_o)\times P(\alpha\beta\gamma)\, d\alpha d\beta d\gamma \qquad (1\text{-}46)$$

where $I(\alpha,\beta,\gamma,H_o)$ is the net EPR absorption at field strength H_o for a molecule with orientation $\alpha\beta\gamma$. If the spin Hamiltonian yields n transitions and these are convoluted with Gaussian broadening functions, we obtain

$$I(\alpha,\beta,\gamma,H_o) \propto \sum_{i=1}^{n} e^{-[H_o - E_i(\alpha,\beta,\gamma)]^2/\delta^2} \times O_i(\alpha\beta\gamma) \qquad (1\text{-}47)$$

where $E_i(\alpha,\beta,\gamma)$ is the orientation-dependent energy of the ith transition, δ is the broadening parameter, and $O_i(\alpha\beta\gamma)$ the oscillator strength of the ith transition.

Orientation will affect the spin energy levels of the molecule through the Zeeman interactions. Thus, a more useful way of describing the orientation is to specify the angles θ and ϕ which orient the Zeeman field in the principal magnetic axis system (PMAS) of the paramagnetic species. The explicit dependence of $\mathcal{H}_m$ on orientation is now apparent;

$$\mathcal{H}_{Zeeman} = H_o \beta \, \hat{g} \cdot \begin{bmatrix} \sin\theta\sin\phi \\ \sin\theta\cos\phi \\ \cos\theta \end{bmatrix} \cdot \underset{\sim}{S} \qquad (1\text{-}48)$$

We can thus rewrite eq. (1-46) as

$$\bar{I}(H_o) = \iint I(\theta,\phi,H_o)\, D(\theta,\phi)\, d\theta d\phi \qquad (1\text{-}49)$$

where $D(\theta,\phi)$ specifies the probability that $\underset{\sim}{H}_o$ has orientation (θ,ϕ) in the PMAS of a randomly chosen member of the ensemble, and

$$I(\theta,\phi,H_o) \propto \sum_{i=1}^{n} e^{-[H_o - E_i(\theta,\phi)]/\delta^2} \times O_i(\theta,\phi) \qquad (1\text{-}50)$$

Full knowledge of $\mathcal{H}_m$ and $D(\theta,\phi)$ permit one to determine $\bar{I}(H_o)$ in straightforward fashion, either analytically (if the integral can be done) or numerically. For two extreme cases $D(\theta,\phi)$ can be written trivially;

(1) For a random ensemble,

$$D(\theta,\phi) = \sin\theta \qquad (1\text{-}51)$$

(angular volume element)

(2) For a single crystal,

$$D(\theta,\phi) = \sum_i \delta(\theta-\theta_i)\delta(\phi-\phi_i) \qquad (1\text{-}52)$$

where the sum runs over all molecules in the unit cell, and δ is the Dirac delta function.

In the general case, when $D(\theta,\phi)$ has an unknown functional form, one usually wishes to work backwards, moving from the experimental EPR lineshape to determination of molecular ordering. This complex problem is the subject of Chapter 3.

REFERENCES

1. A. Carrington and P. McLachlan, Introduction to Magnetic Resonance. Harper and Row, New York, NY (1967).

2. A. Abragam and B. Bleaney, Electron Paramagnetic Resonance of Transition Ions. Clarendon Press, Oxford (1970).

3. C.P. Schlicter, Principles of Magnetic Resonance. Harper, New York, NY (1963).

4. C. Poole and H. Farach, Relaxation in Magnetic Resonance. Academic Press, New York, NY (1971).

5. C. Poole, Electron Spin Resonance. Wiley (Interscience), New York, NY (1967).

6. P.W. Andersen, Phys. Rev. 79, 350 (1956).

7. E.K. Metzner, Ph.D. Thesis. University of California, Berkeley, CA. Lawrence Berkeley Laboratory Report LBL-3356 (September 1974).

8. J.H. Van Vleck, Phys. Rev. 74, 118 (1948).

9. P.W. Andersen and P.R. Weiss, Rev. Mod. Phys. 25, 269 (1953).

10. J.M. Luttinger and L. Tizza, Phys. Rev. 70, 954 (1946).

11. D.N. Bloembergen and T.J. Rowland, Acta. Metallurg. 1, 731 (1953).

12. J. Kleibucker, Ph.D. Thesis. Agricultural University, Wageningen, The Netherlands (1977).

CHAPTER 2

INTRODUCTION TO THE LIGHT REACTIONS OF PHOTOSYNTHESIS

The photosynthetic process has been extensively described in books (1-4) and review articles (5-7), and fundamental knowledge of all but the most recent results is accessible from these sources. The treatment of the subject here will therefore be quite cursory and will focus on the particular features of photosynthesis which are studied in this thesis. Of primary interest will be the early light and electron transfer reactions, and investigation of these events via optical and EPR techniques. Many of the topics presented here are discussed in detail in a review by Sauer (5) of the light reactions in photosynthesis.

2.1 General Overview of Photosynthesis

The net result of all forms of photosynthesis is the conversion of light energy into chemical energy. The chemical energy is normally stored by photosynthetic organisms in the form of starches and sugars. For green plants, the overall reaction can be written

$$6CO_2 + 6H_2O \xrightarrow{h\nu} (CH_2O)_6 + 6O_2 \qquad (2\text{-}1)$$

Bacterial photosynthesis does not involve the splitting of water and evolution of oxygen; the chemical transformation in this case is

$$CO_2 + 2H_2A \xrightarrow{h\nu} H_2O + (CH_2O) + 2A \qquad (2\text{-}2)$$

where H_2A is an appropriate hydrogen donating species (*e.g.* H_2S).

Most of the organic chemistry of the photosynthetic process occurs in the so-called dark reactions, after the light energy has been used to split water and/or been converted to ATP. We shall be concerned exclusively with the initial steps of the production of useful chemical energy from light. In green plants, there are two systems which perform this function; they are referred to as photosystem I (PSI) and photosystem II (PSII). PSI converts light energy to stored chemical energy, while PSII is involved in splitting water into molecular oxygen and reducing equivalents. Bacteria contain only one system which is analagous to PSI.

The initial event in each of these systems is the absorption of a photon by a chlorophyll-containing species, producing an excited state of the chromophore. The excited electron then undergoes a series of electron transfer reactions, residing in turn on a number of acceptors along the photosynthetic electron transfer pathway.

Figures 2-1 and 2-2 display current schemes for this process in bacteria and green plants, respectively; note that PSI and PSII are linked in a "z-scheme". In the following sections we discuss in more detail several of the above components, and investigate the nature of the initial light reaction and charge separation.

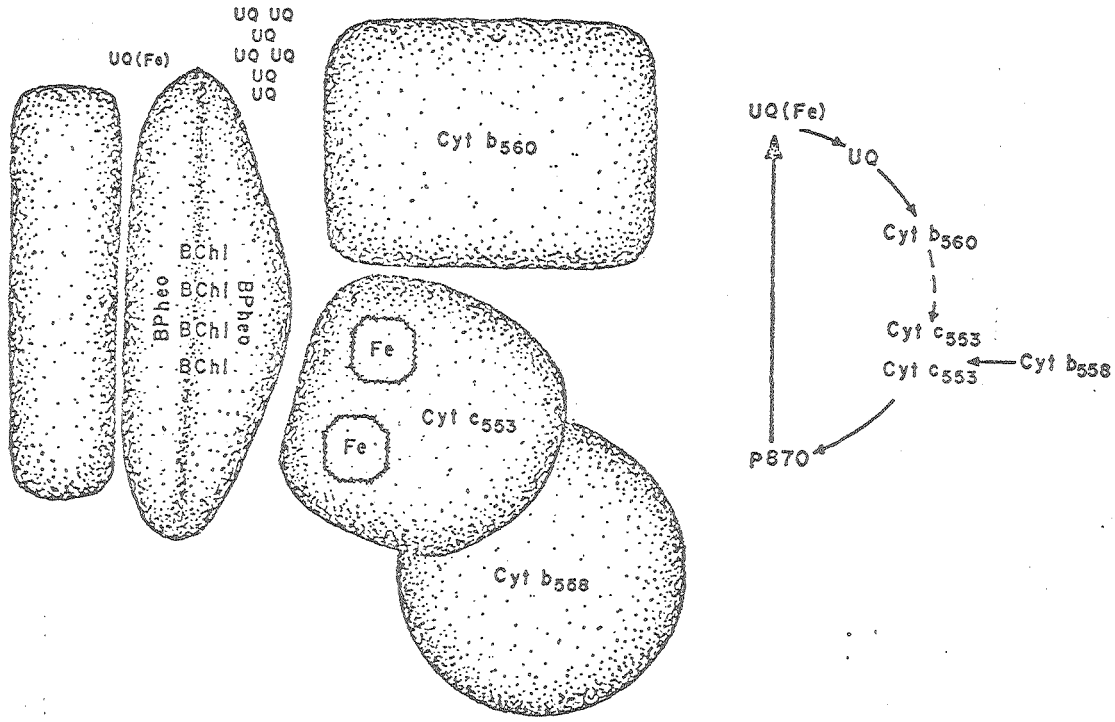

XBL751-5022

Figure 2-1. (a) Overview of electron transfer in bacterial photosynthesis.

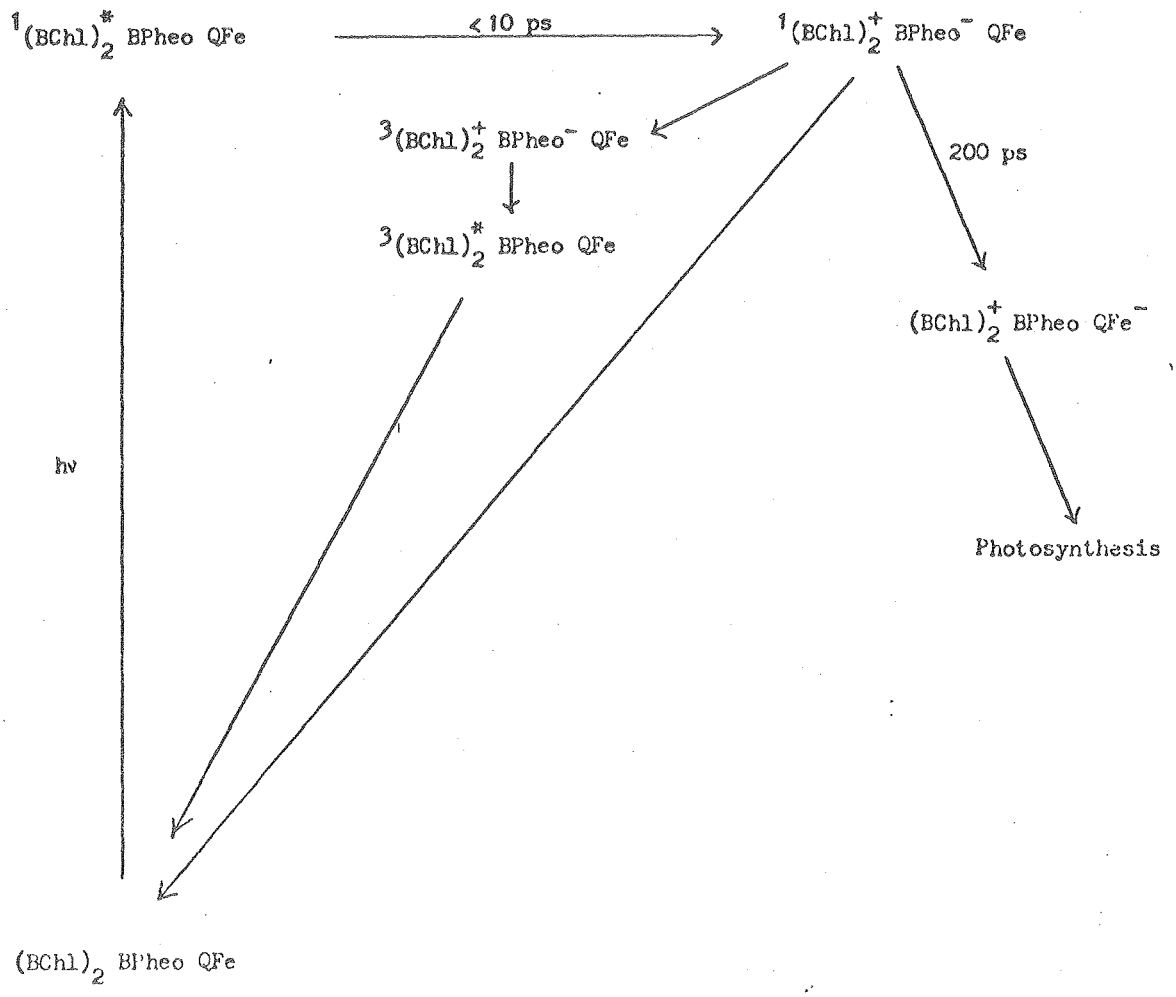

Figure 2-1. (b) Electron transfer scheme for the early events in bacterial photosynthesis. The back reaction to the $(BChl)_2$ triplet occurs when the QFe acceptor is reduced. The $(BChl)_2$ species is designated as P, the BPheo as I, and the QFe as X in the notation currently in use in the literature.

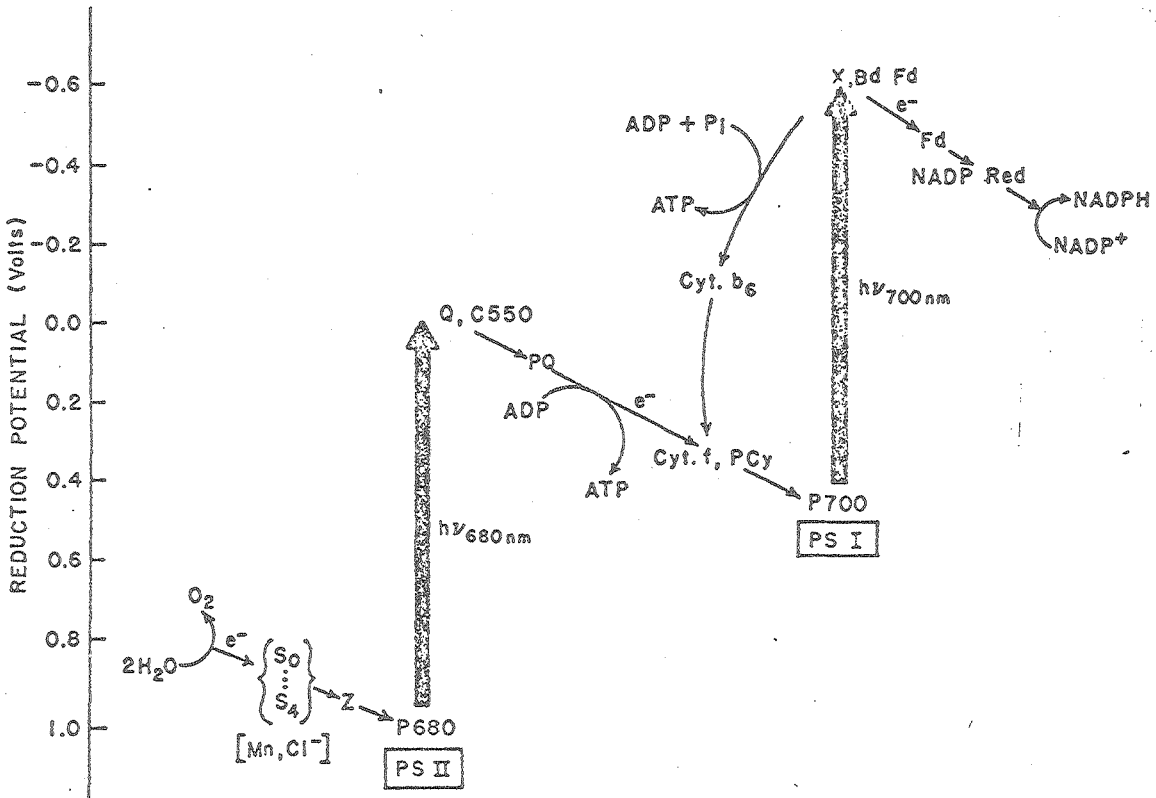

Figure 2-2. Electron transfer scheme for Photosystems I and II in plant photosynthesis.

2.2 Physical Organization of Photosynthetic Systems

A. Organization at the Cellular Level

The photosynthetic light reactions in both bacterial systems and higher plants are localized in membrane structures. In bacteria, the membranes are dispersed throughout the cell, while in green plants they are confined to a discrete organelle, the chloroplast. These membranes can be observed directly by electron microscopy; figures 2-3, 2-4, and 2-5 display micrographs of various fragments of photosynthetic bacteria and chloroplasts.

The membranes in chloroplasts and in some photosynthetic bacteria appear to lie in a regular fashion. In chloroplasts, the thylakoid membranes are stacked in parallel sheets inside the disk-shaped organelle (see fig. 2-5). In the bacteria *Rps. viridis* and *Rps. palustris*, the membranes form concentric sheets in the cylindrical cell (figs. 2-3 and 2-4). This regular arrangement of the membranes allows us to observe orientation effects in photosynthetic systems (Chapters 4 and 5).

The organization of the active components of photosynthesis in the membrane is complex; some aspects of this topic are investigated in the remainder of this thesis. In the next section a general overview consistent with the experimental data to date will be presented.

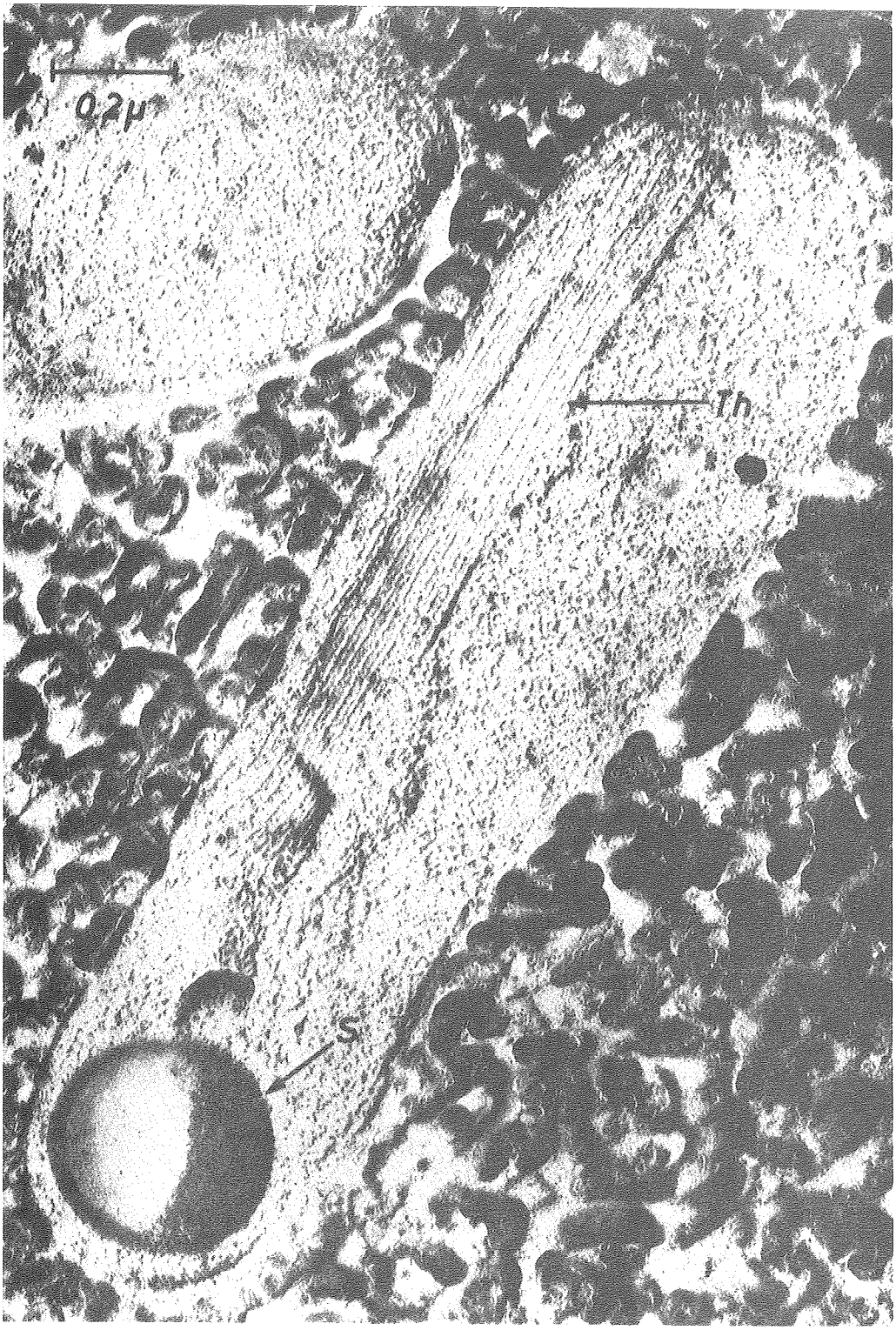

XBB 783-2829

Figure 2-3. (a) Longitudinal view of *Rps. viridis* cell showing ordering of internal photosynthetic membrances (from reference 9).

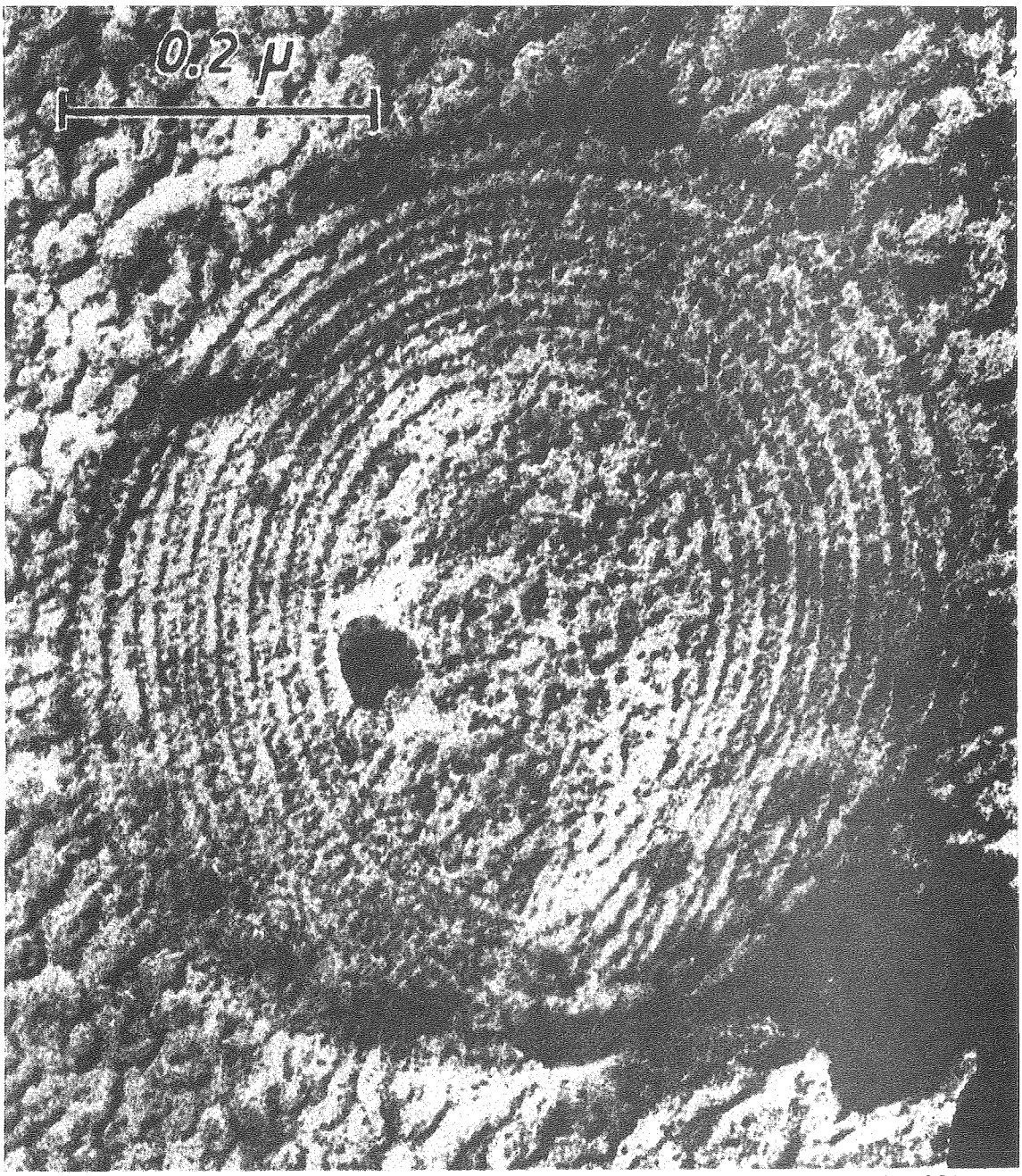

Figure 2-3. (b) Transverse view of *Rps. viridis* (from reference 9).

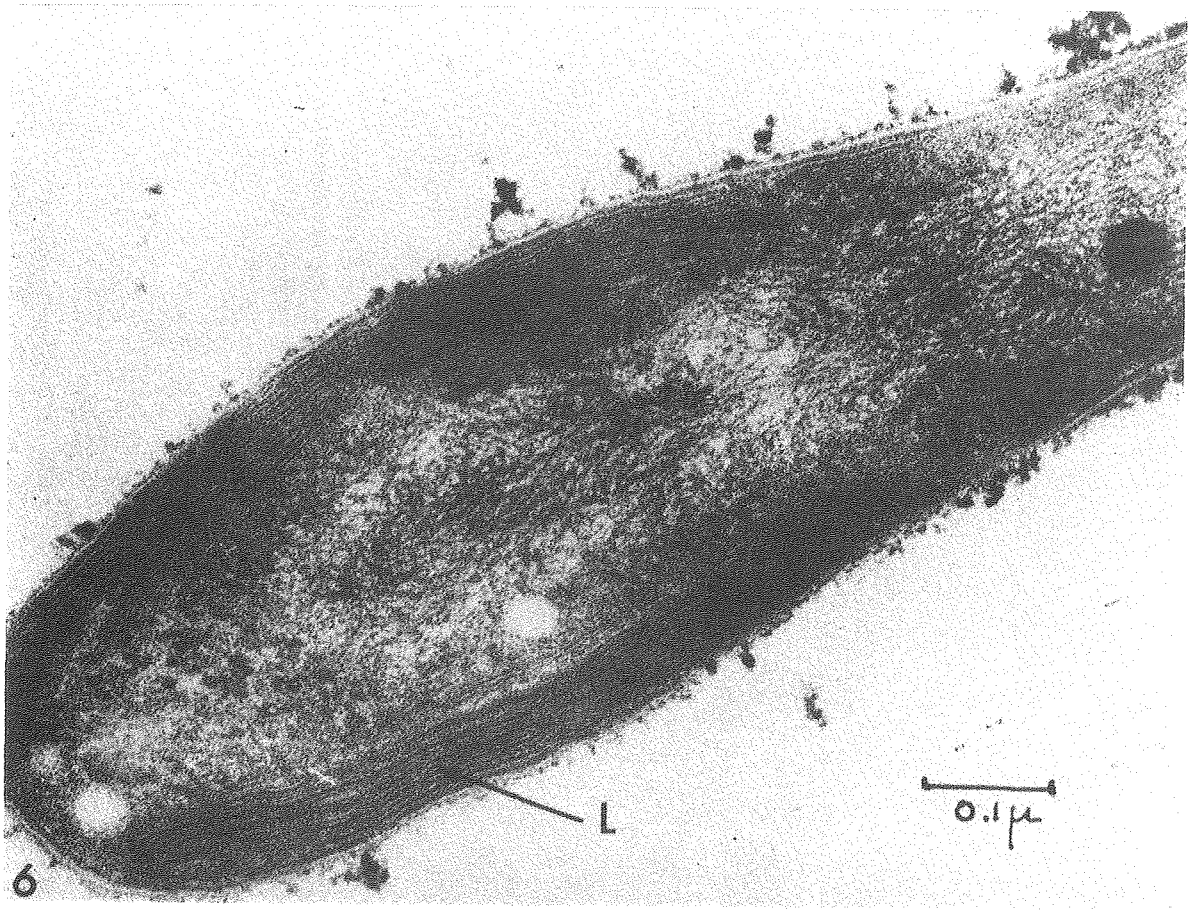

XBB 784-4210

Figure 2-4. (a) Longitudinal view of *Rps. palustris* cell showing ordering of internal photosynthetic membrances (from reference 10).

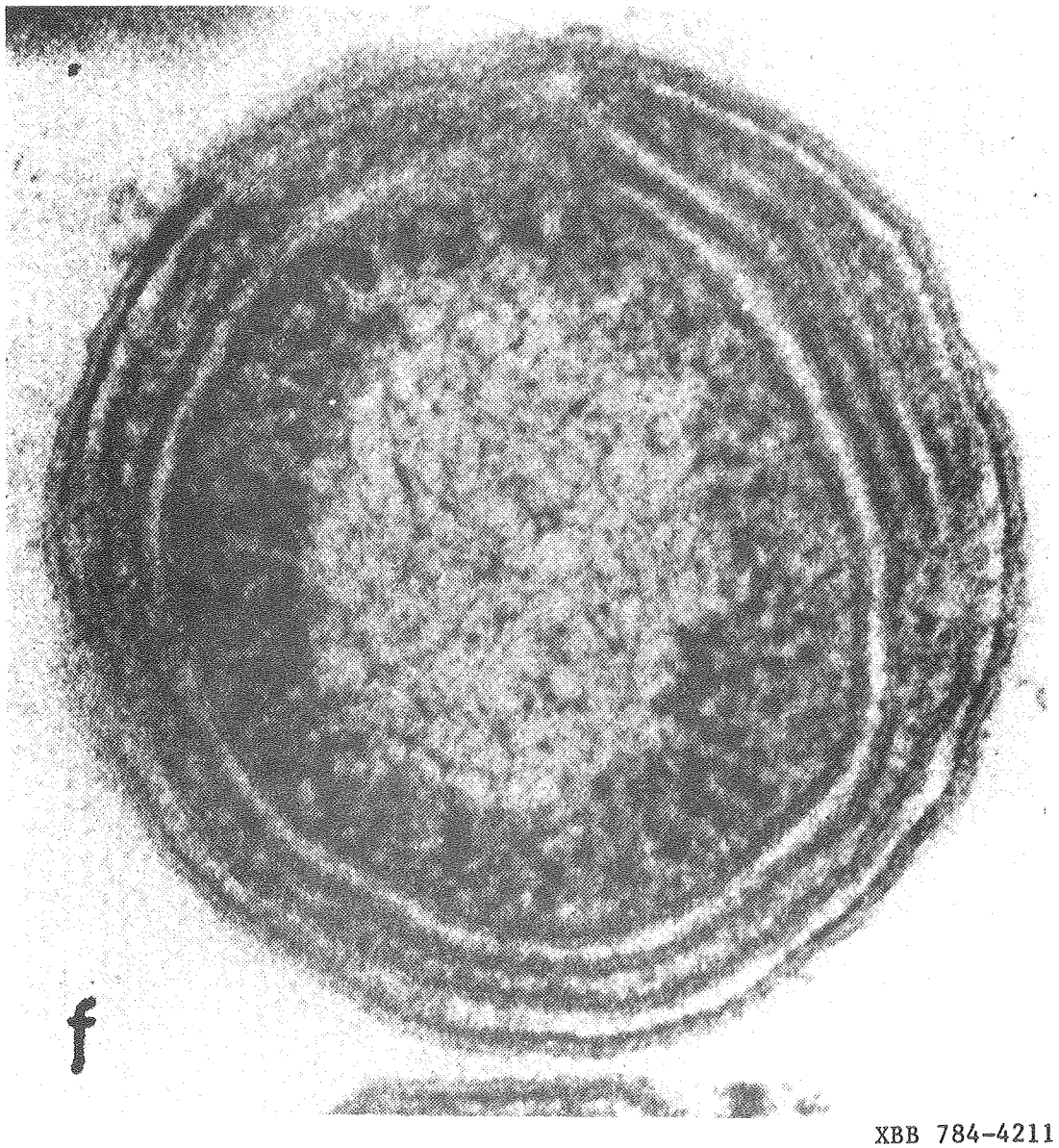

Figure 2-4. (b) Transverse view of *Rps. palustris* (from reference 10).

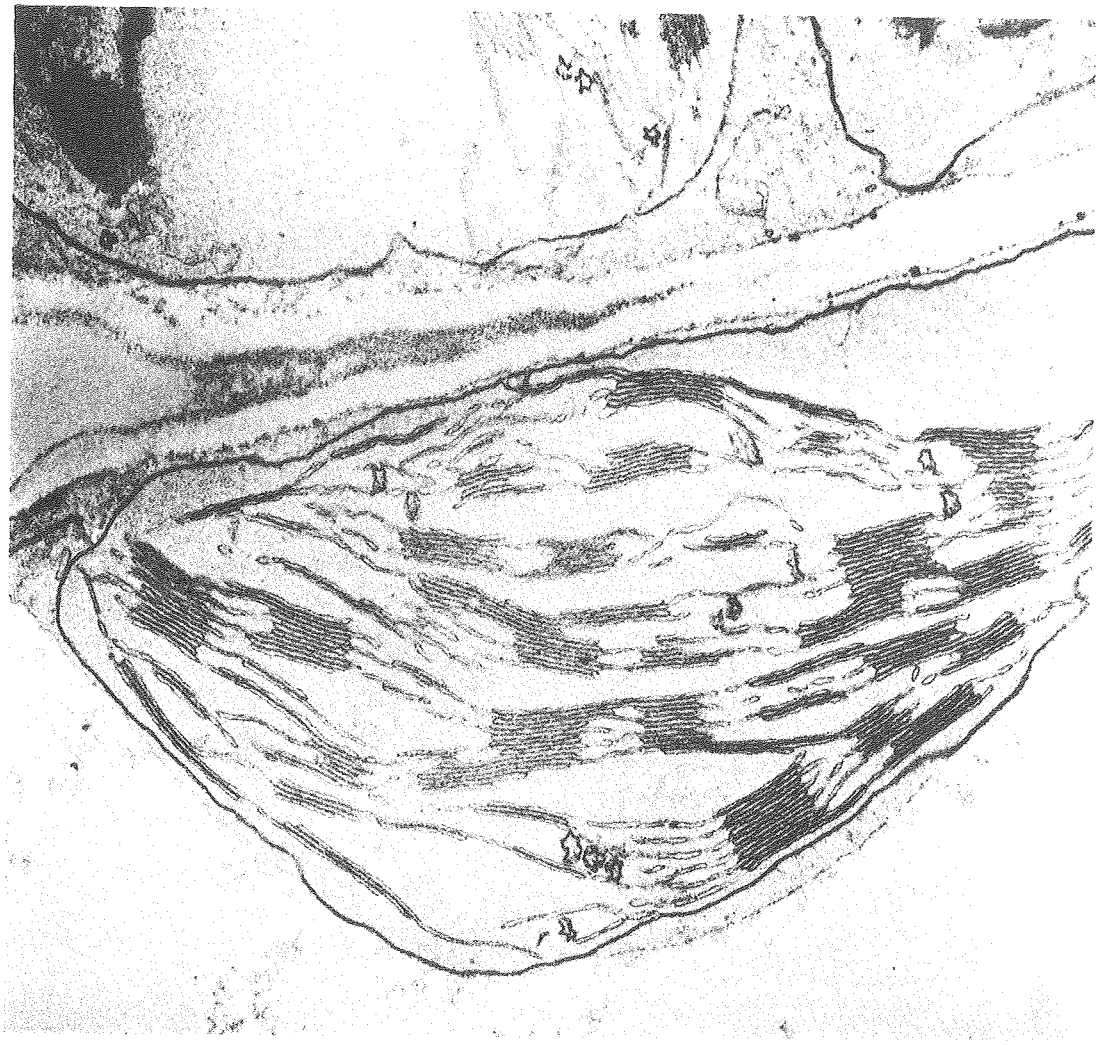

XBB 740-7521

Figure 2-5. Electron micrograph of chloroplast displaying the arrangement of the thylakoid membranes (from reference 8).

B. Structure of Photosynthetic Membranes - The Pebble Mosaic Model

The foundation of the photosynthetic membrane is a lipid bilayer (11). By various chemical treatments (*e.g.* solubilizing with detergent) it is possible to isolate intact components from the membrane. These components include reaction center preparations and antenna (bacterio) chlorophyll-proteins (12-14). The reaction center contains the primary donor and the initial electron acceptors; all photochemistry begins with excitation of the reaction center chlorophyll. The antenna (bacterio) chlorophyll proteins serve as photon absorbers which ultimately donate their energy to the reaction center via an energy transfer mechanism.

The detailed organization of the bulk antenna and its relation to the reaction centers is a subject of controversy (particularly in green plants, where the existence of two types of reaction center, PSI and PSII, complicates the issue), and several models (15-17) have been advanced. However, the general characteristics of most reasonable models have some common features. The antenna proteins are dispersed throughout the membranes; the reaction center particles are associated with groups of antenna molecules. A reaction center plus its group of antenna molecules are designated a photosynthetic unit (PSU). The PSU also contains other molecular species (*e.g.* carotenoids).

Figure 2-6 displays a hypothetical structure for a photosynthetic membrane in green plants - the pebble mosaic model. This model can be taken seriously in terms of general features, but it lacks at present specific structural information about the geometrical arrangement of the most important components. Elucidation of information of this sort is one of the subjects of the chapters which follow.

The reaction centers appear to have some regular orientation with respect to the membrane surface (this is actually demonstrated in the results of Chapters 4 and 5). Figures 2-7 is an electron micrograph of the membrane surface; it seems reasonable to associate the photosynthetic units with the regular array of bumps or protuberances.

C. Description of the Antenna and Reaction Centers

The bulk antenna is composed primarily of chlorophyll (green plants) or bacteriochlorophyll (bacteria) proteins. In general, bacteriochlorophyll-containing aggregates have their long wavelength absorption shifted further to the red, and have different redox potentials. The two chromophores do fill identical roles, and their similarities are more important than their differences. Chlorophyll is present in two forms, chlorophyll a (Chl a) and chlorophyll b (Chl b); bacteriochlorophyll exists in two analogous forms, BChl a and BChl b.

The reaction center is distinguished from the antenna in that it contains the machinery for charge separation. The composition of the reaction center is much better known

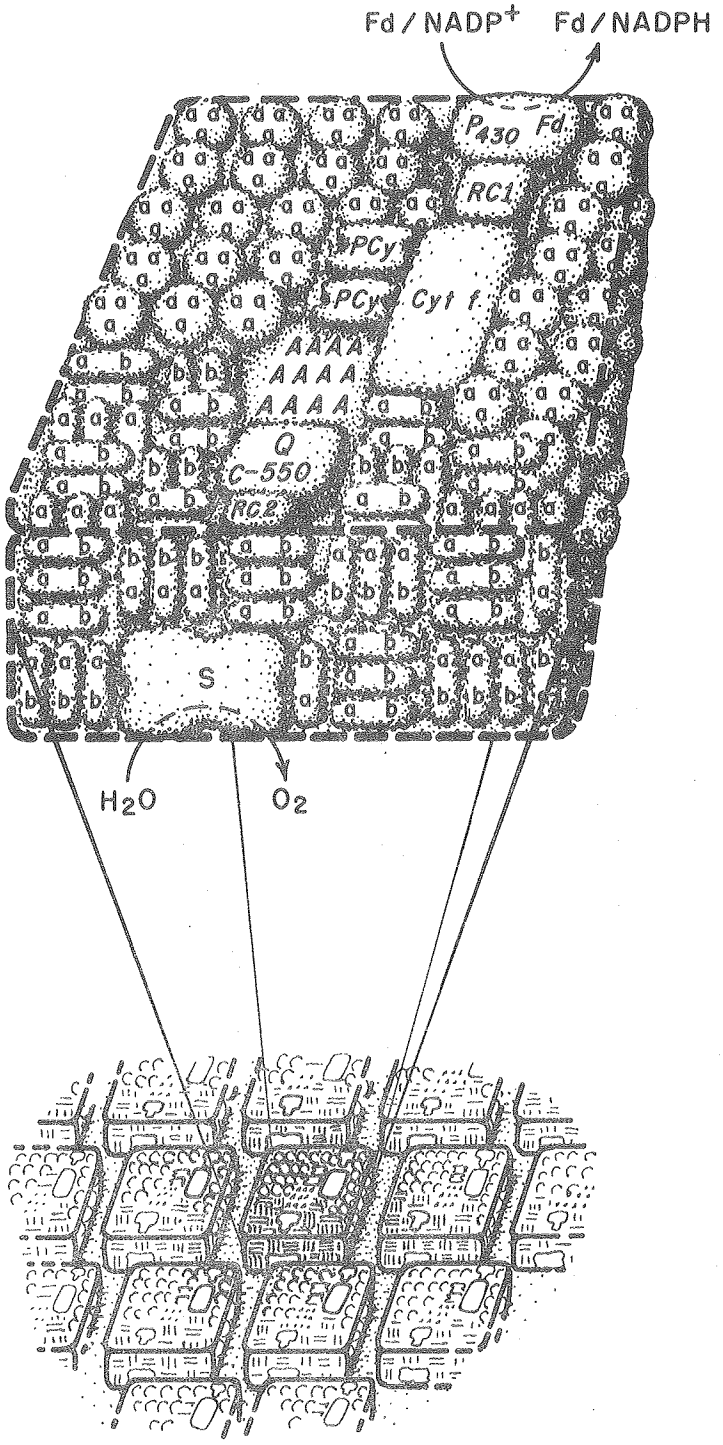

XBL729-4761

Figure 2-6. Hypothetical representation of the pebble mosaic model in green plants (from reference 18).

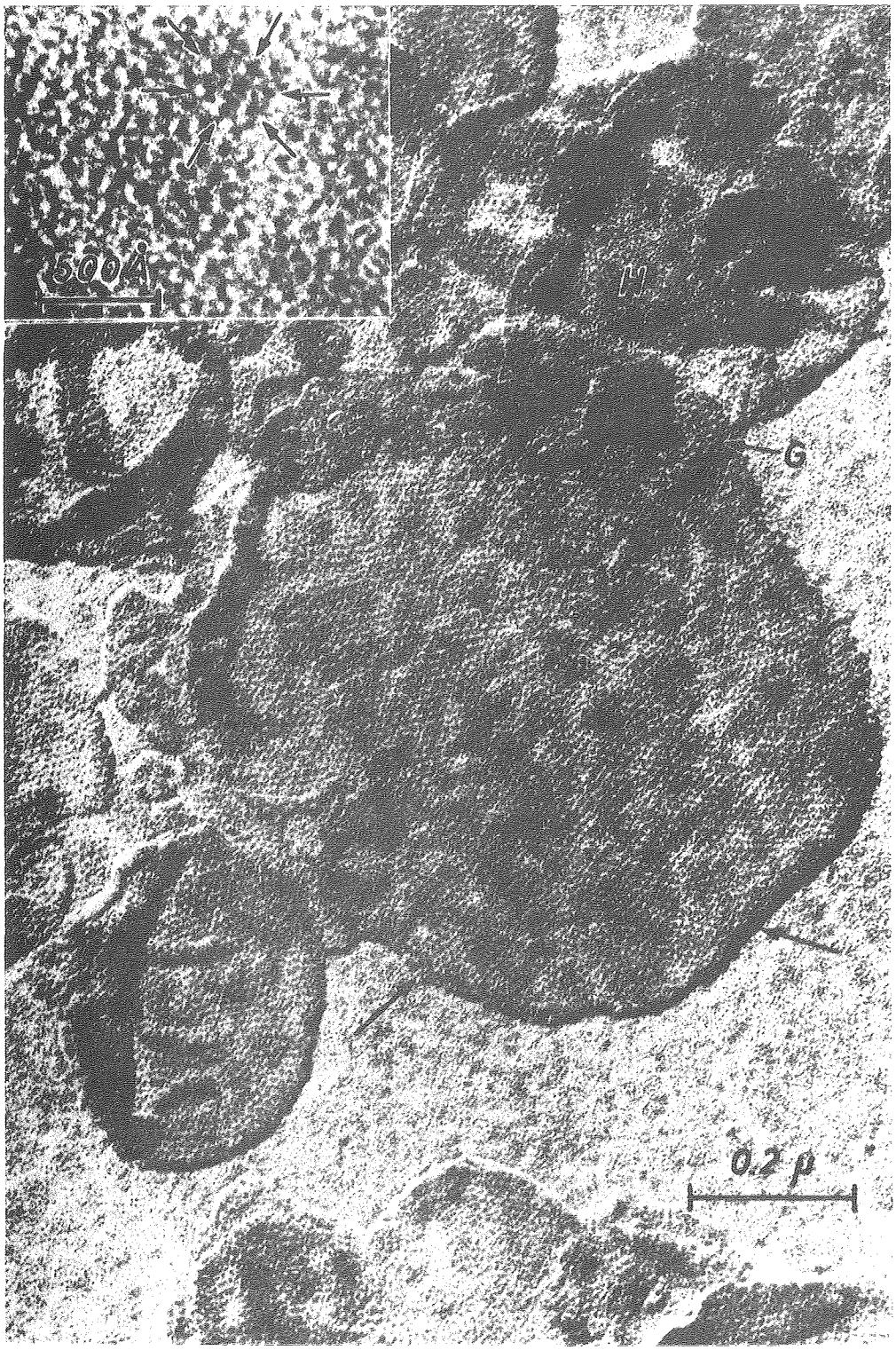

XBB 783-2831

Figure 2-7. Electron micrograph of an *Rps. viridis* membrane showing regular surface features (from refence 9).

for bacteria than green plants (because more "enriched" preparations can be extracted), so we shall discuss only the bacterial reaction center in detail.

The *Rps. spheroides* reaction center, for example, contains 4 BChl a molecules, 2 bacteriopheophytin (BPh), 1 or 2 quinones, iron and peptides of 21, 24, and 28 kdaltons (5). Two of the BChl a molecules form P870, the special pair which is the primary donor in bacterial photosynthesis; they are contained in a protein moiety and presumably are rigidly fixed with respect to each other and to the membrane. The Fe and quinones are part of the acceptor X (see fig. 2-1), and are also organized in a protein structure. One of the BPh is presumably I; the function of the remaining BChl a and BPh molecules is unclear.

It seems logical to suppose that the reaction center components have some particular, fixed orientations with respect to one another so as to facilitate efficient charge separation. The elucidation of the structure and interactions within the reaction center should therefore provide a key to the understanding of how plants convert light energy to chemical energy; this knowledge could be profitably applied to man's attempts to utilize solar power.

2.3 Light Absorption and Electron Transfer in Photosynthesis

A. Bacterial Systems

We shall be concerned with the initial absorption of light and with electron transfer to the two earliest acceptors, I and X.

The normal course of events *in vivo* is simply;

$$PIX \xrightarrow{h\nu} P^*IX \rightarrow P^+I^-X \rightarrow P^+IX^-$$

The primary donor, P, is known to be a BChl dimer (BChl a or BChl b, depending upon the organism). The major optical bleaching upon absorption of light is at 870 nm for BChl a containing species (*e.g. Rps. spheroides*) and 960 nm for BChl b containing species (*e.g. Rps. viridis*). Evidence for strong coupling of the two BChl molecules is provided by EPR linewidth narrowing of ~ $1/\sqrt{2}$ relative to the BChl monomer) (19) and absorption and circular dichroism studies, which show evidence of exciton splitting of the optical transitions (20,21) Figures 2-8 and 2-9 display steady state light-induced EPR signal and optical spectra, respectively, from bacterial reaction centers.

I is a transient acceptor which was first seen by Parsons *et al.* via nanosecond flash spectroscopy in *Rps. spheroides* reaction centers (22). These authors observed the P^+I^- (P_F) state by blocking photochemistry via chemical reduction of the X acceptor with dithionite. Examination of the optical difference spectrum as a function of wavelengtn leads to the conclusion that I is a BPh molecule (23)

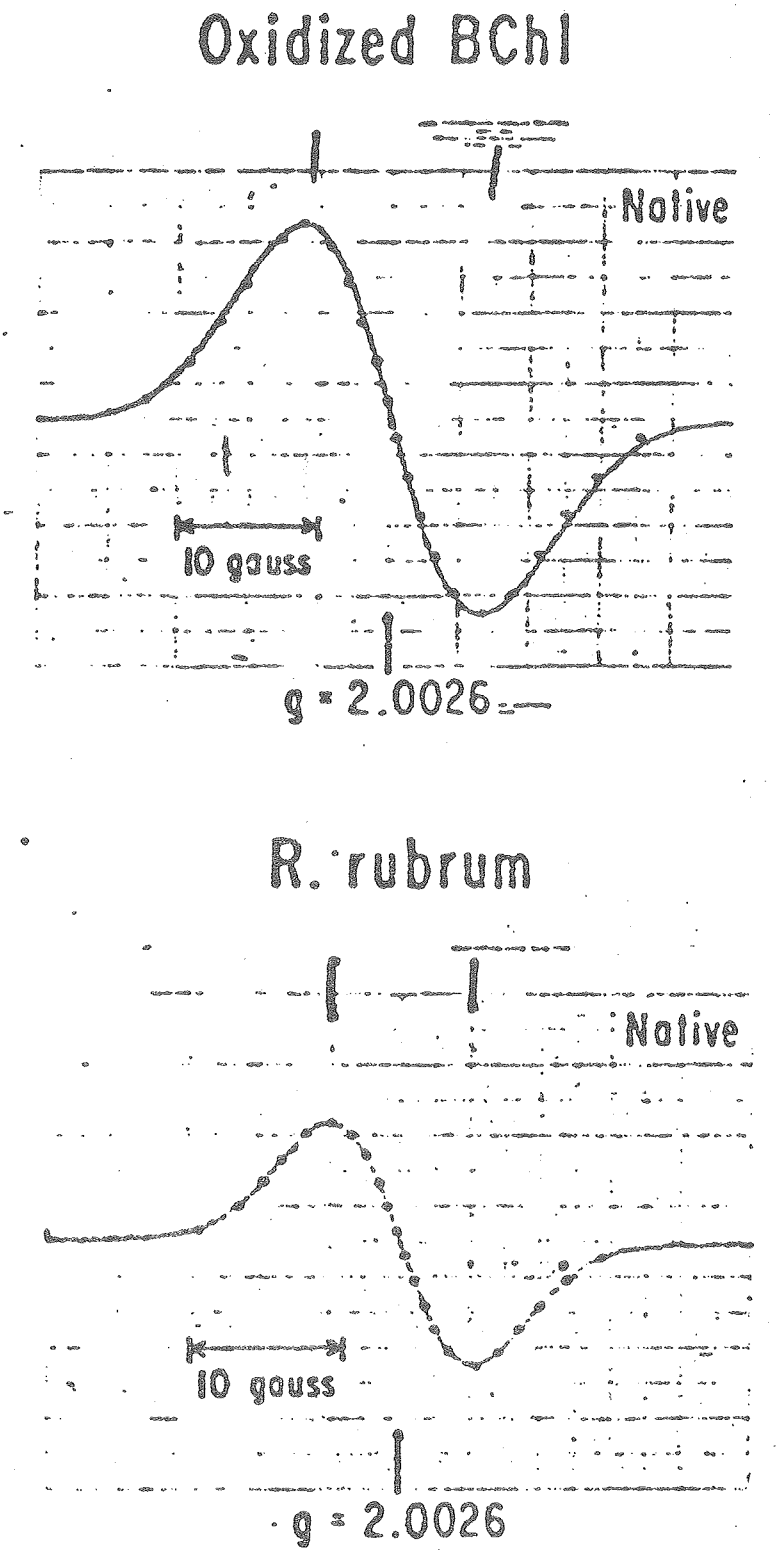

Figure 2-8. Comparison of the EPR spectrum of $BChl^{+}$ with that of the oxidized primary donor of *R. rubrum* (from reference 19).

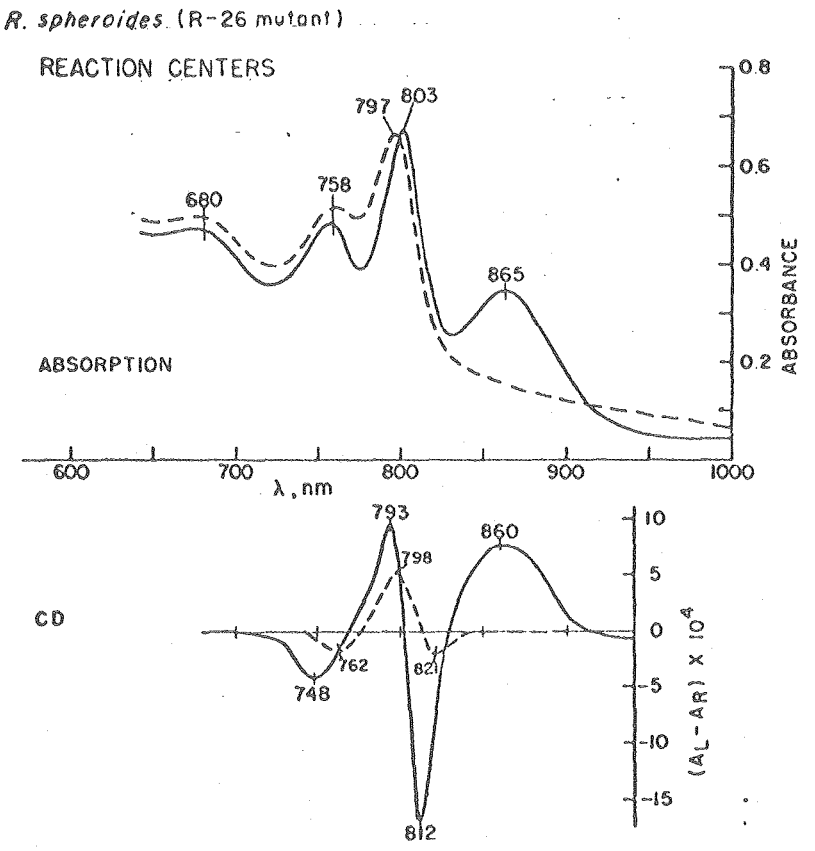

Figure 2-9. Reaction center complexes from *Rps. spheroides*, R-26 mutant, at room temperature. Absorption spectra (top) and CD spectra (bottom) for samples either in the dark (solid curves) or under cross-illumination by an actinic beam (from reference 20).

Picosecond studies show that the P_F state is generated even when photochemistry is not blocked. A value of ~ 200 ns is obtained for the lifetime of the P^+I^- state; the formation of the radical pair occurs less than 10 ps after absorption of a photon by P870 (24,25).

The X acceptor is believed to be an iron-quinone complex (FeQ); iron-ubiquinone in BChl a organisms, iron-menaquinone in BChl b organisms (26). Reduction of X is associated with optical changes and an EPR signal with a first derivative peaks at g = 1.82 (positive) and a higher-field negative peak (26). The precise nature of the QFe complex is unclear. A current hypothesis is that there are two quinones associated with an iron, and that two stable paramagnetic species are formed; first $Q_AFeQ_B^-$, then $Q_A^-FeQ_B^=$. The two states appear to have different locations of the high-field EPR peak; g = 1.75 for $Q_AFeQ_B^-$, and g = 1.67 for $Q_A^-FeQ_B^=$ in *Rps. viridis* (27).

B. Photosystem I

We shall be concerned with the three earliest acceptors in PSI (A_1,A_2,P430) and the primary donor, P700. Both P700 and P430 have been studied for many years and are well characterized. A_1 and A_2 are more recent additions to fig. 2-2; in fact, some of the work presented in Chapter 5 of this thesis has been important in establishing their existence. A full discussion of A_1 and A_2 will therefore be deferred to Chapter 5.

$P700^+$ was first observed by Kok by optical methods (28) and by Commoner (29) via EPR. Figure 5-2 contains a steady-state EPR spectrum of $P700^+$ (signal I) obtained under conditions of continuous illumination. Figure 2-10 is an optical difference spectrum of P700 obtained upon illumination.

Analysis of signal I leads to the conclusion that $P700^+$ is a Chl a dimer in which the unpaired electron is fully delocalized over the two constituent molecules. The peak to peak linewidth of signal I is 7.5 G ± 0.5 G, whereas that of a Chl a monomer is ~ 10 G (30). The reduction in linewidth can be explained by delocalization over more than one molecule; the equation for a dimer is (30)

$$\Delta H \text{ dimer} = \frac{1}{\sqrt{2}} \Delta H \text{ monomer}$$

This equation fits the observed linewidth narrowing within the limits of experimental error.

Evidence for strong coupling between two or more Chl a molecules in the reaction center also is present in optical studies, particularly circular dichroism. Figure 2-10 displays the absorption and circular dichroism spectra of PSI enriched preparations isolated from spinach chloroplasts. A typical exciton circular dichroism bandshape is observed.

P430, the first stable photoreduced species, has been characterized in optical experiments by Ke and co-workers (31). Kinetic analyses have correlated P430 with two light-induced

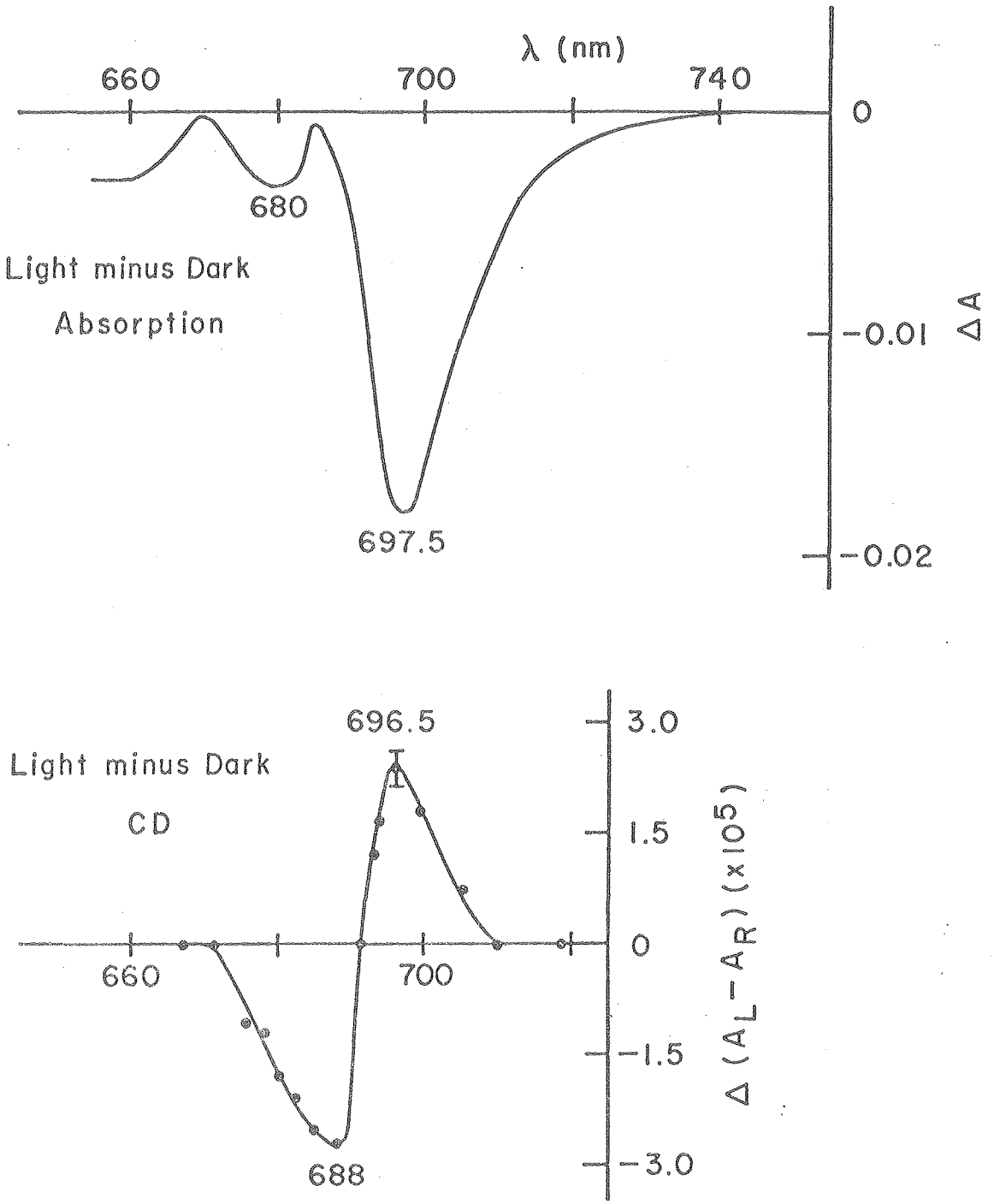

Figure 2-10. Absorption (top) and circular dichroism (bottom) difference spectra of enriched P700 particle preparations isolated from spinach chloroplasts (from reference 38).

EPR signals arising from centers A and B. The two EPR centers are distinguished by their different midpoint potentials in redox titrations (585 mv and 540 mv, respectively) (32).

The evidence to date suggests that this acceptor complex is a bound ferredoxin species (33). Centers A and B appear to be 4Fe - 4S centers which are closely coupled (34). A more detailed discussion of the electrochemical and orientational properties of these species can be found in reference (34).

C. Mechanism of Electron transfer

Electron transfer in the early reactions of photosynthesis appears to proceed via a quantum mechanical tunnelling process. This is suggested by the lack of a dependence of the transfer time on temperature for a wide range of temperatures. The best known experimental results are those of Devault and Chance on electron transfer from cytochrome c 550 to the primary donor in *Chromatium vinosum* (35). More recently, picosecond techniques have allowed measurement of the transfer rates of a variety of photosynthetic processes as a function of temperature (24,25).

The Theoretical treatments by Hopfield (36) and Jortner (37) have attempted to predict the absolute rate and temperature dependence of electron transfer in *Chromatium*; Hopfield employed a model isomorphic to Förster's energy transfer theory, while Jortner used a non-adiabatic multiphonon formalism. Both theories successfully fit the experimental

data by varying adjustable parameters; these results are encouraging but are certainly far from convincing.

The point here that is relevant to this thesis is the non-adiabatic nature of the transfer. This implies, in particular, that the spin state of the electron is unperturbed by the transfer process. We shall assume the validity of this hypothesis in the ensuing chapters.

REFERENCES

1. Govindjee, ed. Bioenergetics of Photosynthesis, Academic Press, New York, NY (1975).

2. E. Rabinowitch and Govindjee. Photosynthesis, Wiley, New York, NY (1969).

3. J. Olson and G. Hind, eds. Brookhaven Symposium in Biology Number 28 (1976).

4. R.K. Clayton and W.R. Sistrom, eds. The Photosynthetic Bacteria; Plenum, New York, NY (1977).

5. K. Sauer, Ann. Rev. Phys. Chem. (1979) in press.

6. H. Levanon and J.R. Norris, Chem. Rev. 78, 185 (1978).

7. A.J. Hoff, Physics Reports (1979) in press.

8. R.B. Park in Plant Biochemistry (J. Bonner and J.E. Varher, eds.). Academic Press, New York, NY, p. 124 (1965).

9. P. Giesbrecht and G. Drews, Arch. Mikrobiol 54, 297 (1966).

10. H.-D. Tauschel and G. Drews, Arch. Mikrobiol. 59, 381 (1967).

11. K. Sauer, Acc. Chem. Res. 11, 257 (1978).

12. L.A. Austin, Ph.D. Thesis. University of California, Berkeley, CA. Lawrence Berkeley Laboratory Report LBL-5512 (August 1976).

13. N. Nelson and T. Bengis, Proc. Third Int. Congress Photosynthesis, 609 (1974).

14. J. Golbeck, S. Lien and A. San Pietro. Arch. Biochem. Biophys. 178, 140 (1977).

15. W. Butler and Kitajama. Biochim. Biophys. Acta 396, 72-85 (1975).

16. W. Butler and R. Strasser. Proc. Nat. Acad. Sci. 74 3382 (1977).

17. J.P. Thornber, R.S. Alberte, J.P. Shiozawa and K.S. Kan. Brookhaven Symp. Biol. 28, 132 (1977).

18. K. Sauer in Bioenergetics of Photosynthesis (Govindjee, ed.). Academic Press, New York, NY p. 115 (1975).

19. J. McElroy, G. Feher and D.C. Mauzerall. Biochim. Biophys. Acta 267, 363 (1972).

20. K. Sauer, E.A. Dratz and L. Coyne. Proc. Nat. Acad. Sci. USA 61, 17 (1968).

21. K. Philipson and K. Sauer. Biochem. 12, 535 (1973).

22. W.W. Parson and T. Menger. Brookhaven Symp. Biol. 28, 195 (1977).

23. J. Fajer, M.S. Davis, D.C. Brune, L.D. Spaulding, D.C. Borg and A. Forman. Brookhaven Symposium Biol. 28, 74 (1977).

24. K.J. Kaufmann, P.L. Dutton, T.L. Netzel, J.S. Leigh and P.M. Rentzepis. Science 188, 1301 (1975).

25. D. Holton, M.W. Windsor, W.W. Parson and J.P. Thornber. Biochim. Biophys. Acta 501, 112 (1978).

26. M.Y. Okamura, R.A. Isaacson and G. Feher. Proc. Nat. Acad. Sci. USA 72, 3491 (1975).

27. G.C. Dismukes, H.A. Frank, R. Friesner and K. Sauer. Biophys. J. 25, 54a (1979).

28. B. Kok, Biochim. Biophys. Acta 48, 527 (1961).

29. B. Commoner, J.J. Heise and J. Townsend. Proc. Nat. Acad. Sci. USA 42, 710 (1956).

30. J.R. Norris, R.A. Uphaus, H.L. Crespie and J.J. Katz. Proc. Nat. Acad. Sci. USA 68, 625 (1971).

31. B. Ke, E. Dolan, K. Sugahara, R.M. Hawkridge and E.R. Shaw, in Photosynthetic Organelles, a special edition of Plant Physiol. No. 3 (Mijachi, Kotch, Fujita and Shibota, eds.) Jap. Soc. Plant. Physiol. Japan. p. 187 (1977).

32. M.C.W. Evans, S.G. Reeves and R. Cammack. FEBS Letters 49, 111 (1974).

33. B. Ke and H. Beinert. Biochim. Biophys. Acta 305, 689 (1973).

34. G.C. Dismukes and K. Sauer, Biochim. Biophys. Acta 504, 431 (1978).

35. D. Devault and B. Chance. Biophys. J. 6, 825 (1966).

36. J.J. Hopfield. Proc. Nat. Acad. Sci. USA 71, 3460 (1974).

37. J. Jortner. J. Chem. Phys. 64, 4860 (1976).

38. K. Philipson, V. Sato and K. Sauer. Biochem. 11, 4591 (1972).

CHAPTER 3

DIRECT CALCULATION OF THE ORIENTATIONAL DISTRIBUTION FUNCTION OF PARTIALLY ORDERED ENSEMBLES FROM THE EPR LINESHAPE

3.1 Introduction

In a recent paper Hentschel *et al.* (1) presented a general method for determining the orientational distribution function of partially ordered ensembles of spin systems. The fundamental equation which is the starting point of such calculations can be written as

$$\bar{I}(H_o) = \iiint P(\alpha\beta\gamma)\ I(\alpha,\beta,\gamma,H_o)\ d\alpha d\beta d\gamma \qquad (3\text{-}1)$$

where $P(\alpha\beta\gamma)$ is the probability that a member of the ensemble can be generated by an Euler rotation with angles α, β, and γ. $I(\alpha,\beta,\gamma,H_o)$ is the EPR intensity at field position H_o for a member of the ensemble specified by $(\alpha\beta\gamma)$, and $\bar{I}(H_o)$ is the experimental intensity observed at H_o.

Hentschel *et al.*, (1) following McBrierty, (2) began by expanding the orientational distribution function $P(\alpha\beta\gamma)$ in terms of the elements of the Wigner rotation matrices.

$$P(\alpha\beta\gamma) = \sum_{\ell}\sum_{m}\sum_{n} P_{\ell mn}\ D^{\ell}_{mn}\ (\alpha,\beta,\gamma) \qquad (3\text{-}2)$$

where

$$P_{\ell mn} = \frac{2\ell+1}{8\pi^2} \int_0^{2\pi}\int_{-1}^{1}\int_0^{2\pi} D^{\ell}_{mn}\ (\alpha,\beta,\gamma)\ P(\alpha\beta\gamma)\ d\alpha d\cos\beta d\gamma$$

is the ℓmn^{th} moment of the distribution function. When equation (3-2) is substituted into equation (3-1), the lineshape is expressed in terms of the moments $P_{\ell mn}$. By lineshape fitting with the moments $P_{\ell mn}$ as adjustable parameters, it is possible to determine these moments.

This method is advantageous for two reasons: [1] If the distribution function is of a suitable form, only a few terms in the expansion need be considered. For example, in an axially symmetric ensemble, $P_{\ell mn}$ is zero if $m \neq 0$ or $n \neq 0$, and we can write

$$P(\alpha\beta\gamma) = \sum_{\ell} P_{\ell 00} D^{\ell}_{00}(0,\beta,0) = \sum_{\ell} P_{\ell 00} P_{\ell}(\cos\beta) \qquad (3\text{-}3)$$

[2] If the EPR intensities $I(\alpha,\beta,\gamma,H_o)$, can be written (or approximated in closed form, the integral of eq. (3-2) now consists of integrals over rotation matrix elements and some angular functions. These integrals can sometimes be evaluated analytically, allowing one to calculate subspectra corresponding to the various moments $P_{\ell mn}$.

In practice, one may encounter distribution functions which do not rapidly converge when expanded in rotation matrix elements. In such a case, the existence of many of the moments $P_{\ell mn}$ would preclude a meaningful lineshape analysis. In addition, some EPR intensities have to be computed numerically for each orientation, which makes consideration

[2] above irrelevant. In other words, it is not possible to calculate subspectra.

Another difficulty arises when the relation between the molecular axes undergoing partial ordering and the principal magnetic axes is not known, (*e.g.* the relation between a partially oriented membrane and the principal magnetic axes of a membrane bound molecule). It is then best to pick trial distribution functions based on a model and attempt to fit the lineshape by treating the relation between axes as an adjustable parameter.

For these reasons, there is a need for a different, albeit equivalent, approach to determining distribution functions of partially ordered ensembles. Our approach is to reduce eq. (3-1) to a double integral over the magnetic variables θ and ϕ, specifying the orientation of the external magnetic field $\underset{\sim}{H}_o$ in the principal magnetic axis system. The form of $\bar{I}$ is then

$$\bar{I}(H_o) = \int\int D(\theta,\phi)\ I(\theta,\phi,H_o)\ d\theta d\phi \qquad (3\text{-}4)$$

where $I(\theta,\phi,H_o)$ is the EPR intensity measured at field position H_o when the orientation of the external magnetic field is given by θ,ϕ. $D(\theta,\phi)$ is a density of states function, giving the probability that the external magnetic field has angular orientation between θ and $\theta+d\theta$, and ϕ and $\phi+d\phi$ in the principal magnetic axis system.

Rather than expanding $D(\theta,\phi)$ in a series of moments, we proceed by calculating the form of $D(\theta,\phi)$ directly from considerations of a physical model. In some cases, this process is trivial, *e.g.* a Gaussian distribution about an axis of symmetry yields

$$D(\theta) = \exp[-\theta^2/\Delta^2] \qquad (3\text{-}5)$$

where Δ is a disorder parameter. In the general case, expression of the distribution function in terms of θ and ϕ is more difficult.

We describe here a general method for calculating the density of states $D(\theta,\phi)$. The partially ordered ensemble is generated by a set of distinct symmetry operations $R_1 \ldots R_n$ with arbitrary weighting functions $g_1 \ldots g_n$; the density of states $D(\theta,\phi)$ is obtained as integrals over the weighting functions which can be evaluated numerically. This method is appropriate for any functional form of the distribution function and for any type of magnetic Hamiltonian. It also explicitly provides for the determination of geometrical information (*e.g.* the relation between the molecular axes undergoing partial ordering and the magnetic axes) if this information is not known. In Chapter 4, the method is applied to the particular case of a polarized triplet signal observed in the photosynthetic bacterium *Rhodopseudomonas viridis*, whole cells of which have been aligned by magnetic field orientation.

3.2 Theory

A: General Form of the Distribution Function

We first define a set of coordinate systems needed for the ensuing derivation. Our approach is essentially the same as that of Hentschel *et al.* (1) The only difference is that we do not define an axis system equivalent to their "laboratory system" which has the external magnetic field, $\underset{\sim}{H}_o$, along its z axis. We instead define a "laboratory axis system" equivalent to their "sample system". In our "laboratory axis system", $\underset{\sim}{H}_o$ is a constant vector.

The three coordinate systems are then given as follows:

1) The laboratory axis system is a coordinate system with its z axis defined by the direction of the external forces that have produced orientation in the sample. In magnetic field alignment, the alignment field $\underset{\sim}{H}_a$, is along the z axis. The orientation of various members of the ensemble of spin systems is specified with respect to this fixed reference frame.

2) The principal magnetic axis system is the coordinate system in which the dipolar Hamiltonian $\mathcal{H} = \underset{\sim}{S} \cdot \underset{\sim}{D} \cdot \underset{\sim}{S}$ is diagonal. It is related by a fixed set of Euler angles, α', β' and γ', to the intermediate axis system.

3) The intermediate axis system serves as a bridge between the laboratory frame and the magnetic axis system. One can think of the magnetic system as being enclosed in a cube; the unit vectors of the intermediate axis system ($\underset{\sim}{x}'$,$\underset{\sim}{y}'$,$\underset{\sim}{z}'$) lie

is applied to $\hat{\underset{\sim}{x}}'$, $\hat{\underset{\sim}{y}}'$ and $\hat{\underset{\sim}{z}}'$, the result is

$$\begin{aligned}
\hat{\underset{\sim}{x}}' &= R_n^{-1}(\alpha_n) \ldots R_1^{-1}(\alpha_1)(1,0,0) \\
\hat{\underset{\sim}{y}}' &= R_n^{-1}(\alpha_n) \ldots R_1^{-1}(\alpha_1)(0,1,0) \\
\hat{\underset{\sim}{z}}' &= R_n^{-1}(\alpha_n) \ldots R_1^{-1}(\alpha_1)(0,0,1)
\end{aligned} \tag{3-7}$$

The external magnetic field in the intermediate axis system, H', is now easily found to be

$$\underset{\sim}{H}' = (\hat{\underset{\sim}{x}}' \cdot \underset{\sim}{H}_o, \hat{\underset{\sim}{y}}' \cdot \underset{\sim}{H}_o, \hat{\underset{\sim}{z}}' \cdot \underset{\sim}{H}_o) \tag{3-8}$$

Rearrangement using equations (3-7) yields

$$\begin{aligned}
\underset{\sim}{H}' &= [R_n^{-1}(\alpha_n) \ldots R_1^{-1}(\alpha_1)]^T \underset{\sim}{H}_o \\
&= R_1(\alpha_1) \ldots R_n(\alpha_n) \underset{\sim}{H}_o
\end{aligned} \tag{3-9}$$

We denote the coordinates of $\underset{\sim}{H}'$ by the following functions

$$\begin{aligned}
H'_x &= F_x(\alpha_1 \ldots \alpha_n) \\
H'_y &= F_y(\alpha_1 \ldots \alpha_n) \\
H'_z &= F_z(\alpha_1 \ldots \alpha_n)
\end{aligned} \tag{3-10}$$

The external magnetic field in the magnetic axis system, $\underset{\sim}{H}''$, is then

$$\underset{\sim}{H}'' = A(\alpha', \beta', \gamma') \cdot \underset{\sim}{H}' \tag{3-11}$$

where α', β' and γ' are constants, perhaps unknown.

Now we can write down the EPR intensity at magnetic field H_o directly as an integral over the variables $\alpha_1 \ldots \alpha_n$.

$$\bar{I}(H_o) = \frac{1}{N} \int_{\alpha_1} \ldots \int_{\alpha_n} I(H''_x, H''_y, H''_z) g_1(\alpha_1) \ldots g_n(\alpha_n) \times d\alpha_1 \ldots d\alpha_n \qquad (3\text{-}12)$$

where N is a normalization constant, and H''_x, and H''_y are functions of $\alpha_1 \ldots \alpha_n$, α', β', and γ'.

The set of points $\{(\alpha_i)$ such that $H''^2_x + H''^2_y + H''^2_z = H_o^2\}$ is a two dimensional manifold in (n+1) space. We therefore transform to a new set of variables in which H''_x, H''_y, and H''_z are functions of only two variables θ and ϕ. This transformation involves mapping the old manifold into a two dimensional manifold in three space.

This transformation can be accomplished by defining a new set of variables $v_1 \ldots v_{n-2}$ to complement θ and ϕ; θ and ϕ are defined to be the magnetic variables giving the location of H_o in the principal magnetic axis system; $v_1 \ldots v_{n-2}$ must be chosen to satisfy the formal requirements of the coordinate transformation. We thus perform the transformation

$$(H_o, \alpha_1, \ldots \alpha_n) \rightarrow (H_o, \phi, v_1 \ldots v_{n-2}, \theta) \qquad (3\text{-}13)$$

under the constraints

$$\begin{aligned} H''_x &= \sin\theta\cos\phi \\ H''_y &= \sin\theta\sin\phi \\ H''_z &= \cos\theta \end{aligned} \qquad (3\text{-}14)$$

and θ and ϕ are determined by the rotation angles $\alpha_1, \ldots \alpha_n$, α', β', and γ'. Application of the n-dimensional-change-of-variable theorem to equation (3-12) yields an integral in terms of the new variables

$$\bar{I}(H_o) = \frac{1}{N} \iint_{\theta\phi} I[H''_x(\theta,\phi), H''_y(\theta,\phi), H''_z(\theta,\phi)]d\theta d\phi$$

$$\times \int_{v_1} \cdots \int_{v_{n-2}} \prod_{i=1}^{n} g_i[\alpha_i(\phi, v_1 \cdots v_{n-2}, \theta)]$$

$$\times \left| \frac{\partial \alpha_1 \cdots \alpha_n}{\partial \phi, v_1 \cdots v_{n-2}, \theta} \right| dv_1 \cdots dv_{n-2} \qquad (3\text{-}15)$$

where $(\partial\alpha_1 \cdots \alpha_n / \partial\phi, v_1 \cdots v_{n-2}, \theta)$ is the Jacobian of the coordinate transformation.

By inspection, we can set

$$D(\theta,\phi) = \frac{1}{N} \int_{v_1} \cdots \int_{v_{n-2}} \prod_{i=1}^{n} g_i[\alpha_i(\phi, v_1 \cdots v_{n-2}, \theta)]$$

$$\times \left| \frac{\partial \alpha_1 \cdots \alpha_n}{\partial \phi, v_1 \cdots v_{n-2}, \theta} \right| dv_1 \cdots dv_{n-2} \qquad (3\text{-}16)$$

Equation (3-16) is the key result of this Chapter. This equation expresses the distribution function of $\underset{\sim}{H}_o$ in any axis system that has a fixed relation to the intermediate axis system (*e.g.* Euler rotation angles α', β', and γ'). In particular, it gives the distribution of $\underset{\sim}{H}_o$ in the intermediate axis system when $\alpha' = \beta' = \gamma' = 0$. For use in equation (3-4), one specifically needs $D(\theta,\phi)$ for the distribution of H_o in the principal magnetic axis system.

B. Generalized Coordinate Transformation

Our procedure will be to use equation (3-16) to calculate a distribution function in the intermediate axis system, $D'(\theta',\phi')$, where θ' and ϕ' specify the orientation of $\underset{\sim}{H}_o$ in the intermediate axis system, and then construct $D(\theta,\phi)$ for the principal magnetic axis system by use of the Euler rotation matrix $A(\alpha', \beta', \gamma')$. This approach is advantageous because one does not have to worry about the angles α', β', and γ' when calculating $D'(\theta',\phi')$. Also, careful choice of an intermediate axis system simplifies the calculations. In particular, one should choose an intermediate axis system such that the first rotation (α_1) is about the laboratory z axis. Then, from equation (3-9)

$$H' = \begin{pmatrix} \cos\alpha_1 & \sin\alpha_1 & 0 \\ -\sin\alpha_1 & \cos\alpha_1 & 0 \\ 0 & 0 & 1 \end{pmatrix} R_2(\alpha_2) \ldots R_n(\alpha_n)H_o \qquad (3\text{-}17)$$

More explicitly

$$H'_x = \sin\theta'\cos\phi' = F_x^{n-1}\cos\alpha_1 + F_y^{n-1}\sin\alpha_1$$

$$H'_y = \sin\theta'\sin\phi' = -F_x^{n-1}\sin\alpha_1 + F_y^{n-1}\cos\alpha_1 \qquad (3\text{-}18)$$

$$H'_z = \cos\theta' = F_z^{n-1} = F_z(\alpha_2 \ldots \alpha_n)$$

where

$$R_2(\alpha_2) \ldots R_n(\alpha_n)\underset{\sim}{H}_o = (F_x^{n-1}, F_y^{n-1}, F_z^{n-1}) \qquad (3\text{-}19)$$

and F_x^{n-1}, F_y^{n-1}, and F_z^{n-1} are functions of $\alpha_2 \ldots \alpha_n$.

The following transformation is convenient.

$$\begin{aligned}
\alpha_1 &= f_1(\phi', v_1 \cdots v_{n-2}, \theta') \\
\alpha_2 &= v_1 \\
&\bullet \\
&\bullet \\
&\bullet \\
\alpha_{n-1} &= v_{n-2} \\
\alpha_n &= f_2(v_1 \cdots v_{n-2}, \theta')
\end{aligned} \tag{3-20}$$

where α_n is defined by solving the equation

$$\cos\theta' = F_z(\alpha_2 \cdots \alpha_n) \tag{3-21}$$

for α_n and setting $\alpha_2 \cdots \alpha_{n-1}$ equal to $v_1 \cdots v_{n-2}$.

Clearly,

$$\frac{\partial \alpha_i}{\partial v_j} = \delta_{i,j+1} \qquad 2 \leq i \leq n-1 \tag{3-22}$$

and

$$\frac{\partial \alpha_i}{\partial \phi'} = 0 \qquad i \neq 1 \tag{3-23}$$

Then, from equation (3-18)

$$\frac{\partial \sin\theta' \cos\phi'}{\partial \phi'} = -\sin\theta' \sin\phi' = (-F_x^{n-1} \sin\alpha_1 + F_y^{n-1} \cos\alpha_1) \times \frac{\partial \alpha_1}{\partial \phi'} \tag{3-24}$$

$$-\sin\theta'\sin\phi' = \sin\theta'\sin\phi'\left(\frac{\partial\alpha_1}{\partial\phi'}\right) \tag{3-25}$$

or

$$\frac{\partial\alpha_1}{\partial\phi'} = -1 \tag{3-26}$$

$$\alpha_1 = -\phi' + f_3(v_1, \ldots v_{n-2}, \theta') \tag{3-27}$$

Using equations (3-22), (3-23), and (3-26), the Jacobian, J, simplifies to

$$|J| = \frac{\partial\alpha_n}{\partial\theta'} \tag{3-28}$$

which can be obtained from (3-18) by differentiating both sides with respect to θ',

$$-\sin\theta' = \frac{\partial F_z}{\partial\alpha_n}\frac{\partial\alpha_n}{\partial\theta'} \tag{3-29}$$

or,

$$|J| = \frac{\sin\theta'}{\left|\frac{\partial F_z(\alpha_2 \ldots \alpha_n)}{\partial\alpha_n}\right|} \tag{3-30}$$

with $\alpha_2 \ldots \alpha_n$ replaced by their transformed variables $v_1 \ldots v_{n-2}, f_2(v_1 \ldots v_{n-2}, \theta')$. Substitution into equation (3-16) yields

$$D'(\theta',\phi') = \frac{\sin\theta'}{N'}\int_{v_1}\cdots\int_{v_{n-2}} g_1[-\phi+f_3(v_1 \ldots v_{n-2},\theta)]$$

$$\times\, g_n[f_2(v_1 \ldots v_{n-2},\theta')]$$

$$\times \frac{\prod_{i=1}^{n-2} g_i(v_i)\, dv_i}{\left|\frac{\partial F_z[v_1 \ldots v_{n-2}, f_2(v_1 \ldots v_{n-2},\theta')]}{\partial\alpha_n}\right|} \tag{3-31}$$

If $g_1(\alpha_1) = 1$, we have an axially symmetric distribution function [*i.e.* $D'(\theta',\phi')$ is a function only of θ']. If we have a randomly oriented system, it can be shown that

$$D'(\theta',\phi') = \text{constant} \times \sin\theta' \qquad (3\text{-}32)$$

Clearly, one has some choice about which variables to set equal to the v_i's, which to set equal to ϕ' and which to set equal to a function of $v_1 \ldots v_{n-2}$, and θ'. Intelligent decisions in this regard can be used to simplify equation (3-31).

It is now necessary to transform the distribution of $\underset{\sim}{H}_o$ in the intermediate axis system to one in the principal magnetic axis system. The Euler rotation matrix $A(\alpha',\beta',\gamma')$ in equation (3-11) establishes the transformation from θ' and ϕ' to θ and ϕ. Since $A(\alpha',\beta',\gamma')$ is a constant rotation matrix, $\sin\theta/\sin\theta'$ is the Jacobian for the transformation. Therefore

$$D(\theta,\phi) = \frac{\sin\theta}{\sin\theta'} D'(\theta',\phi')$$

where

$$\theta = \cos^{-1}(H''_z/H_o)$$

and

$$\phi = \tan^{-1}(H''_x/H''_y)$$

specify the orientation of $\underset{\sim}{H}''$ in the principal magnetic axis system. H''_x, H''_y, and H''_z are found from equation (3-11). The angles α', β', and γ', which establish the relation between the intermediate axis system and the principal magnetic axis system

can be treated as adjustable parameters if they are not known. In conclusion, in this section, we have outlined a prescription for computing $D(\theta,\phi)$ for all values of θ and ϕ.

3.3 Conclusion

Our method of determining the orientational distribution function of a partially ordered system from the EPR lineshape is, in a sense, conceptually different from that of Hentschel *et al.* (1) This latter treatment makes no physical assumptions about the form of the distribution function other than that it can be conveniently expanded in the Wigner rotation matrix elements, and the effectiveness of their parametrization of the distribution function is thus dependent upon how rapidly the series of moments $P_{\ell mn}$ converges. Furthermore, no explicit prescription is given for extracting geometrical information (*i.e.* relation of the principal axis system to the preferred alignment direction), although presumably it would be possible to introduce parameters specifying these quantities.

Our method is based on constructing a distribution function which from the first takes into account the mathematical nature of the ordering in the system, and the symmetry properties of the ensemble. The choice of fitting parameters can thus be tailored to one's physical intuition about the ordering of the system and not restricted to a rigidly prescribed expansion. In the problem described in Chapter 4, for example, the distribution function was fit to a single

Gaussian parameter, Δ, whereas expansion in angular functions could require many terms (and thus require fitting many parameters) to insure convergence. We were also able to fit two geometrical parameters specifying the orientations of the normal to the membrane in the principal magnetic axis system of the triplet (see reference 3). The fit was relatively sharp when compared to experimental error, *i.e.* only a small set of values of the three above parameters gave an adequate fit of the theoretical spectra to the experimental EPR intensity measured parallel and perpendicular to the alignment field.

It was also possible to include in our calculation orientation-dependent intersystem crossing to the ground state singlet (see reference 3). This phenomenon makes a moment analysis very difficult, because analytical "subspectra" cannot be easily worked out for this case.

Our approach has particular appeal in applications to biological problems. In many simpler systems (*e.g.* crystals, liquid crystals) high degrees of ordering are common, and typical distribution functions are trigonometric terms with little random variation; here, expansion in Wigner functions is straightforward and fruitful. Our method would probably yield equivalent results, but would be unlikely to produce a significant saving in computer time or gain in conceptual understanding.

Biological systems, however, are complex heterogeneous structures and often contain inhomogeneous ensembles which have small but significant statistical variations. Such variations blur the observation of orientation effects, making the oriented EPR spectra look more like a random spectrum and less like that of a single crystal.

The resulting smaller and less sharp effects make it difficult to extract meaningful quantitative information about such systems. It is in this regard that we hope that our formulation will prove valuable. We have shown that it is possible to take into account the random disorder that is characteristic of biological ensembles and still extract sharp values for the relatively invariant properties of the ensemble members; we have also obtained a good estimate of the degree of disorder present. These results (3) were achieved with a modest amount of computer time, and from a conceptual viewpoint that is perhaps more intuitive and easily understandable than the Wigner rotation matrix formalism.

The method described here can be applied to calculation of other properties of partially ordered ensembles. For example, optical properties like linear dichroism can be determined if the distribution function can be modeled effectively.

REFERENCES

1. R. Hentschel, J. Schlitter, H. Sillescu and H.W. Spiess, J. Chem. Phys. 68, 56 (1978).

2. V.J. McBrierty, J. Chem. Phys. 61, 872 (1974).

3. H.A. Frank, R. Friesner, J.A. Nairn, G.C. Dismukes and K. Sauer, Biochim. Biophys. Acta, (1979) in press.

CHAPTER 4

STUDIES OF ORIENTED TRIPLET SIGNALS FROM PHOTOSYNTHETIC BACTERIA

4.1 Introduction

It is possible to block photochemistry in bacterial systems by chemically reducing the X (QFe) acceptor (see fig. 2-1). If this is done, an illuminating flash of light will result in formation of the radical pair P^+I^-, followed by a back reaction to the neutral state PI. It is observed that a substantial fraction of the primary donors, P, in such an experiment are prepared in a triplet state.

The high triplet yield of the radical recombination is due to the time evolution of the spin wavefunction of the radical pair P^+I^- via the radical pair mechanism (RPM). At high field (*i.e.* $g\beta H_o \gg$ hyperfine energies or g anisotropy) the RPM leads to $S\text{-}T_o$ mixing exclusively, and thus populates only the middle triplet energy level of P.

EPR signals due to the above triplet species (known as the P_R state) can be observed using a light modulation technique. The instrumental configuration for this experiment is shown in fig. 4-1. Light from either a tungsten lamp or a Spectra Physics argon-ion pumped dye laser is modulated with a 33.5 Hz chopper. The resultant EPR signal is compared with a reference

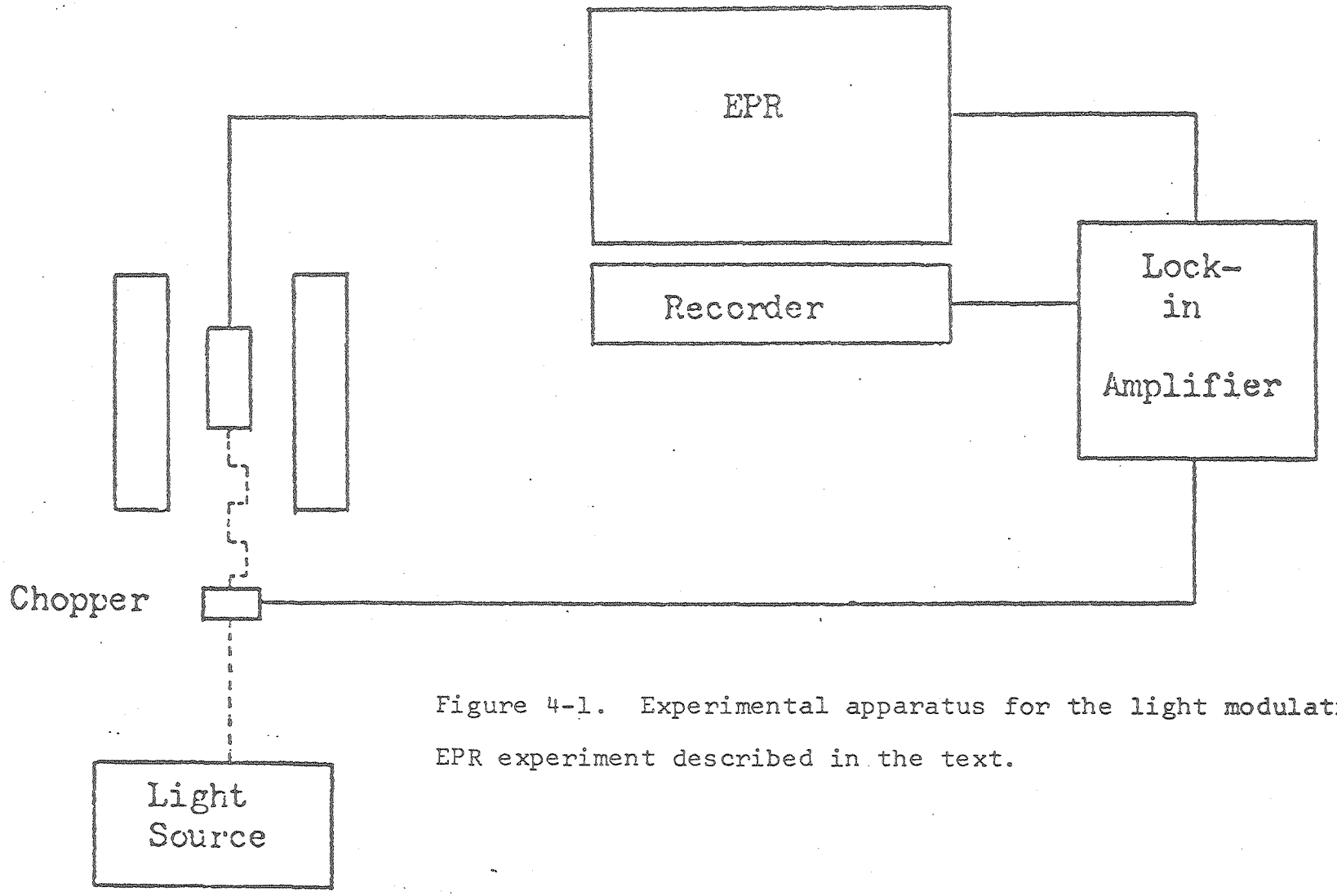

Figure 4-1. Experimental apparatus for the light modulation EPR experiment described in the text.

signal (*i.e.* phase-sensitive detection is employed); thus, only the light-induced component of the signal is measured.

Observation of the triplet signal with this technique is straightforward and can provide information about the D and E values and intersystem crossing rates of the bacteriochlorophyll special pair. However, we are also interested in obtaining geometrical information about the primary donor. As outlined in Chapter 1, the triplet state EPR spectrum is sensitive to the orientation of the applied field $\underset{\sim}{H}_o$ with respect to the PMAS of the triplet. The generation of a partially ordered ensemble of triplets therefore results in an altered light-induced signal; use of the theory of Chapter 3 then allows us to obtain geometrical parameters from a lineshape analysis.

Two types of experiments were performed. The first, on *Rps. viridis* and *Rps. palustris*, involves aligning whole cells of these bacteria in a 21 kg magnetic field. These experiments were conceived of and carried out by Dr. Harry Frank, and it is safe to say that both this and the preceding chapters would never have been written without his original insights and careful experimental work. The second, magnetophotoselection, uses polarized light to generate a partially ordered population of triplet molecules. These experiments were done with *Rps. spheroides* reaction centers by Harry Frank and John Bolt.

4.2 Randomly Ordered Triplet Spectra-Extraction of D, E, k_x/k_z, and k_y/k_z Values

A. Derivation of Steady-State Population Levels as a Function of Orientation

The light-induced triplet signals from randomly ordered ensembles of *Rps. viridis*, *Rps. palustris*, and *Rps. spheroides*, are shown in fig. 4-3. A comparison with the standard random triplet spectrum (fig. 1-1) reveals significant lineshape differences. These are due to the spin polarization of the P_R state, a consequence of the unequal populating rates of the three triplet sublevels by the radical pair mechanism. We employ a simple model which assumes light-induced population of only the T_β level (see eq. 1-41); this is consistent with the qualitative features of the signal polarization (1).

The observed amplitude of the signal at a particular orientation (θ,ϕ) depends upon the steady-state population differences of the triplet sublevels. Following the approach of Levanon and Vega (2) and Winscom (3) we construct a set of differential equations for the populations n_α, n_β, and n_γ;

$$\frac{d\underset{\sim}{n}}{dt} = -\hat{k}\cdot\underset{\sim}{n} + \underset{\sim}{A} \qquad (4\text{-}1)$$

where $n = [n_\alpha \; n_\beta \; n_\gamma]$ describes the populations of the T_α, T_β, and T_γ levels (see sec. 1-4), $\underset{\sim}{A}$ represents the light-induced populating rates, and $\hat{k}$ incorporates the effects of spin-lattice relaxation and intersystem crossing on the population levels.

The $\hat{k}$ matrix is given by

$$\hat{k} = \begin{bmatrix} k_\alpha + W_{\alpha\beta} + W_{\alpha\gamma} & W_{\alpha\beta} & W_{\alpha\gamma} \\ W_{\beta\alpha} & k_\beta + W_{\beta\gamma} + W_{\beta\alpha} & W_{\beta\gamma} \\ W_{\gamma\alpha} & W_{\gamma\beta} & W_{\gamma\alpha} + W_{\gamma\beta} + k_\gamma \end{bmatrix} \quad (4\text{-}2)$$

where k_α, k_β, and k_γ are the intersystem crossing rates for the T_α, T_β, and T_γ levels to the ground singlet, and the W_{ij} are spin-lattice relaxation rates between the triplet sublevels.

Because our experiments are performed at very low temperatures (11.0°K), we expect spin-lattice relaxation to be very slow. This hypothesis is confirmed by two experimental observations;

(1) A variation of the temperature in the range 10°-20° K produces no measurable effect on the signal amplitudes.

(2) Substantial spin polarization (*i.e.* non-Boltzmann distribution of the ensemble) is observed; rapid, efficient spin-lattice relaxation would tend to eliminate polarization of the ensemble.

We therefore set the W_{ij} in eq. (4-2) equal to zero for all i,j. Furthermore, our assumption concerning the populating rates requires that

$$\underset{\sim}{A} = \begin{bmatrix} 0 \\ A_o \sin\omega t \\ 0 \end{bmatrix} \quad (4\text{-}3)$$

where ω is the chopper frequency.

We therefore obtain a set of simplified differential equations which are separable;

$$\frac{dn_\alpha}{dt} = -k_\alpha n_\alpha \qquad (a)$$

$$\frac{dn_\beta}{dt} = -k_\beta n_\beta + A_o \sin\omega t \qquad (b) \qquad (4\text{-}4)$$

$$\frac{dn_\gamma}{dt} = -k_\gamma n_\gamma \qquad (c)$$

These are easily solved to give steady-state solutions

$$n_\alpha = n_\gamma = 0 \qquad (a)$$

$$n_\beta = A_o \sin(\omega t+\phi)/(\omega^2+k_\beta^2)^{1/2} \qquad (b) \qquad (4\text{-}5)$$

where $\phi = \tan^{-1}(\omega/k_\beta)$. The population differences are then

$$\Delta n_+ = n_\beta - n_\alpha = \Delta n_- = n_\beta - n_\gamma = \frac{A_o \sin(\omega t+\phi)}{(\omega^2+k_\beta^2)^{1/2}} \qquad (4\text{-}6)$$

Further analysis of this equation requires examination of the rate k_β. The intersystem crossing rate for the T_β level can be found from the rate constants k_x, k_y, and k_z for the zero-field levels and the coefficients c_β^i in the expansion of the T_β wavefunction (eq. 1-41). Felix and Weissman (4) showed that the phase relations between coefficients are incoherent so that

$$k_\beta = \sum_{i=x,y,z} |c^i|^2 \, k_i \qquad (4\text{-}7)$$

A more detailed discussion of the intersystem crossing rates in photosynthetic bacteria will follow our analysis of the triplet lineshape. At this point, we establish only that the value of any level crossing rate for all three organisms is greater than 1000 sec^{-1}; this follows from the monomer bacteriochlorophyll rates (the dimer rate can never be less than the slowest monomer rate) which exceed 1000 sec^{-1} in all cases (5). Then, $k_\beta > 1000\ sec^{-1} \gg \omega$ (33.5 Hz). We can therefore neglect ω in the denominator of eq. (4-6); we can also set

$$\phi = \tan^{-1}(\omega/k) \approx 0 \qquad (4\text{-}8)$$

then, we obtain

$$\Delta n_+ = \Delta n_- = \frac{A_o \sin\omega t}{k_\beta} \qquad (4\text{-}9)$$

The EPR intensity due to the ensemble members at (θ,ϕ) is given by the average of Δn_+ and Δn_- over the phase-sensitive detection cycle, *i.e.*

$$I_\pm = \int_0^{2\pi/\omega} \Delta n_\pm \, \beta \sin\omega t \, dt \qquad (4\text{-}10)$$

$$= c/k_\beta$$

where c is a proportionality constant which is uniform for all orientations. Thus, the contribution of each orientational subspectrum is weighted by the inverse of the intersystem crossing rate for that orientation.

B. Computer Simulations of the Random Spectra

Our fitting procedure determines four parameters of the polarized triplet spectrum; D, E, k_x/k_z, and k_y/k_z. We fit only the lineshape (*i.e.* the relative peak amplitudes) and scale the theoretical spectrum to the experimental one. The numerical method of generating the spectrum is summarized in the flow chart in fig. 4-2.

The method of fitting the parameters is as follows;

(1) Set D so that the $Z^{\pm}$ peaks lie at the correct field positions.

(2) Set E so that the $X^{\pm}$, $Y_1^{\pm}$, and $Y_2^{\pm}$ peaks lie at the correct field positions

(3) Adjust k_x/k_z, k_y/k_z so that the ratios Z/X, Z/Y_1, and Z/Y_2 are within the error limits of the experimental ratios (see fig. 4-3 for labelling of the $Z^{\pm}$, $X^{\pm}$, $Y_1^{\pm}$ and $Y_2^{\pm}$ peaks).

We found that division of the θ and ϕ intervals (of $\pi/2$ each) into 50 points each is sufficient to generate a smooth and accurate spectrum. Note that all integrations need be performed only in the first quadrant (*i.e.*, $\theta,\phi \leq \pi/2$) because the other quadrants contain identical subspectra.

Table 4-1 lists the experimental field positions and peak amplitude ratios for the triplet signals from *Rps. viridis*, *Rps. palustris*, and *Rps. spheroides*. These numbers were obtained by locating the spectral maxima via a slow field sweep and sitting on this field position, allowing

TABLE 4-1. EXPERIMENTAL AMPLITUDE RATIOS FOR THE RANDOM SPECTRA

$Z^{\pm}$, $X^{\pm}$, $Y_1^{\pm}$, and $Y_2^{\pm}$ refer to amplitudes (in arbitrary units) of the triplet peaks as defined in the text. The errors represent a range of possible values for the ratios as deduced from the repeatability of amplitude measurements.

	$Z^{\pm}/X^{\pm}$	$Z^{\pm}/Y_1^{\pm}$	$Z^{\pm}/Y_2^{\pm}$
Rps. viridis	-1.6 ± .1	5.8 ± 1.0	5.8 ± 1.0
Rps. palustris	-2.1 ± .1	3.6 ± .3	4.2 ± .4
Rps. spheroides	-2.4 ± .3	-4.0 ± .6	6.2 ± 1.5

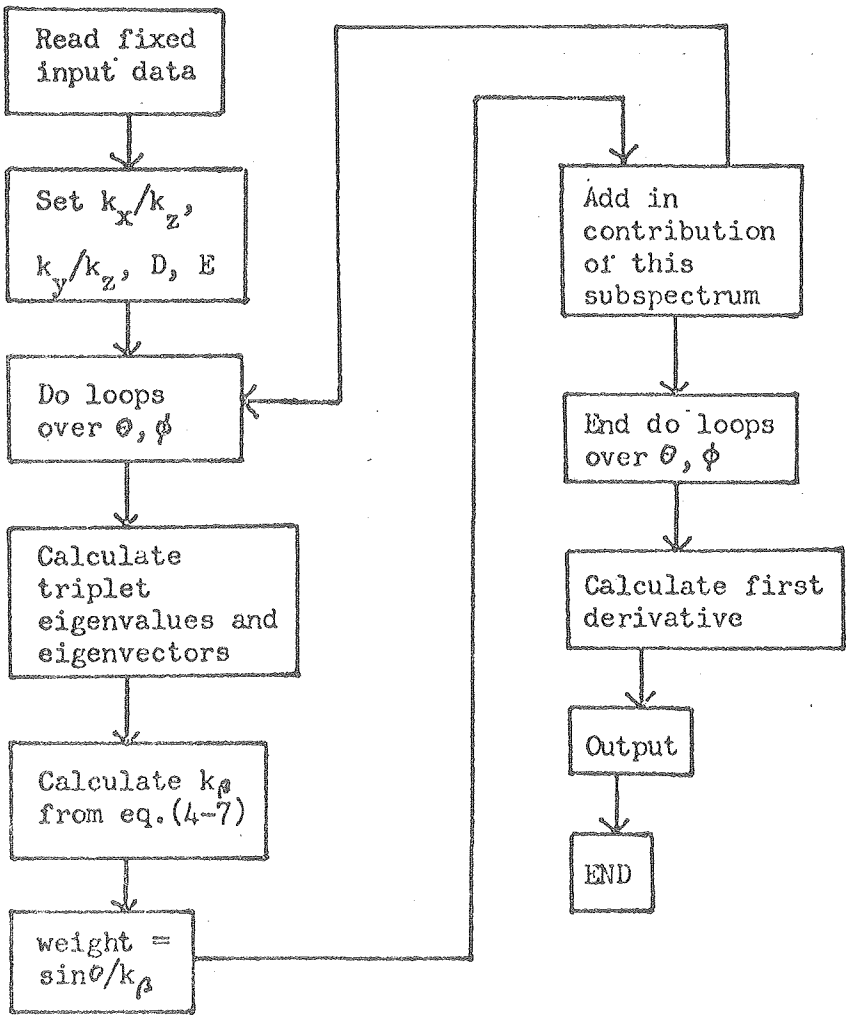

Figure 4-2. Flow chart for computer program to calculate random triplet EPR spectra.

the chart recorder pen to equilibrate. The necessity for this procedure is illustrated in fig 4-3(a), which displays the entire random spectra for the three organisms. These spectra are substantially distorted by sweep artifacts (note the large differences in the high- and low-field parts of the spectrum, which should be nearly symmetric). A slow sweep of the entire spectrum is impractical as it would risk sample deterioration.

Table 4-2 gives the calculated peak ratios and D, E, k_x/k_z, and k_y/k_z values for the three bacteria. The D and E values agree well with those determined by other groups. The k_x/k_z and k_y/k_z ratios are more interesting. Absolute relaxation rates have been measured for *R. spheroides* reaction centers by Clarke *et al.* (6) and Hoff (7). The reported rate constants (see table 4-2) differ drastically; this discrepancy has been the subject of considerable controversy. As can easily be seen by calculating ratios, our data supports Hoff's results, lying within the limits of his experimental error.

Figure 4-3 displays the simulated random spectra for the three species. The qualitative features of the experimental spectra are reproduced with reasonable accuracy (a direct quantitative comparison must be done with peak amplitudes, because the experimental spectra are distorted).

TABLE 4-2. ZERO-FIELD SPLITTING PARAMETERS AND RELATIVE RATE CONSTANTS FOR INTERSYSTEM CROSSING

The |D| and |E| zero-field splitting parameters are given in cm^{-1} units. k_x, k_y and k_z refer to rate constants for depopulation of the triplet spin sublevels associated with the $X^{\pm}$, $Y^{\pm}$ and $Z^{\pm}$ triplet peaks as defined in the text. The errors in the |D| and |E| values are calculated from the repeatability of the signal position determinations. The errors in the rate constants amount to no more than .5 and arise from the range of acceptable k values which fit the random spectra. For *Rps. spheroides* a comparison of the present results with published values is given.

	|D|	|E|	$k_x:k_y:k_z$
Rps. viridis	0.0153 ± 0.0002	0.0037 ± 0.0002	7.5:10.0:1.0
Rps. palustris	0.0183 ± 0.0002	0.0035 ± 0.0002	9.0:6.0:1.0
Rps. spheroides	0.0187 ± 0.0002	0.0031 ± 0.0002	8.3:7.1:1.0
Reference 6	0.0187 ± 0.0002	0.0031 ± 0.0001	1.7:2.0:1.0
Reference 7	0.01872± 0.0002	0.00312± 0.00002	6.4:5.7:1.0

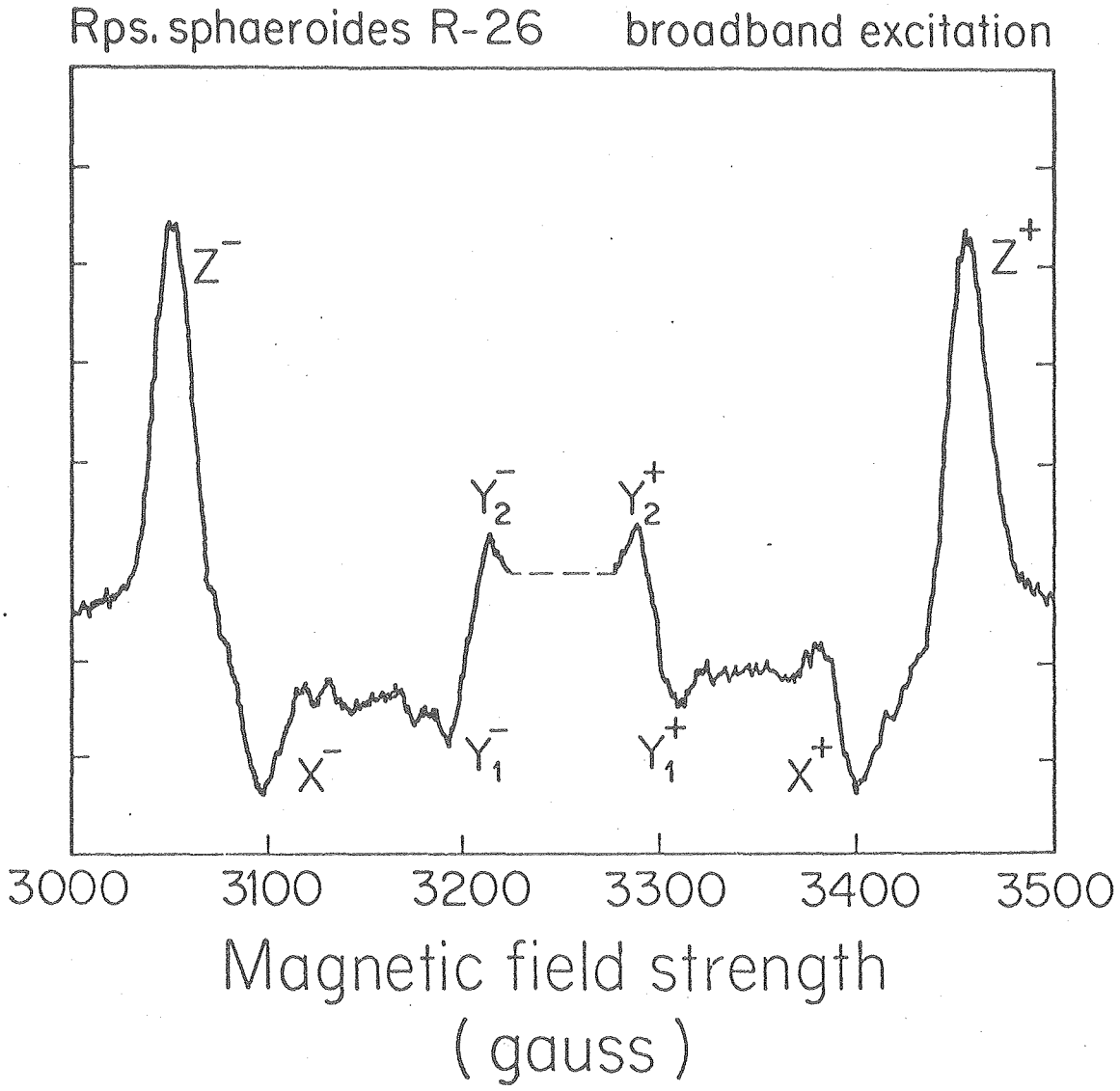

XBL 7812-13056

Figure 4-3. (a) Experimental random triplet spectrum for *Rps. spheroides* determined in the magnetophotoselection experiment.

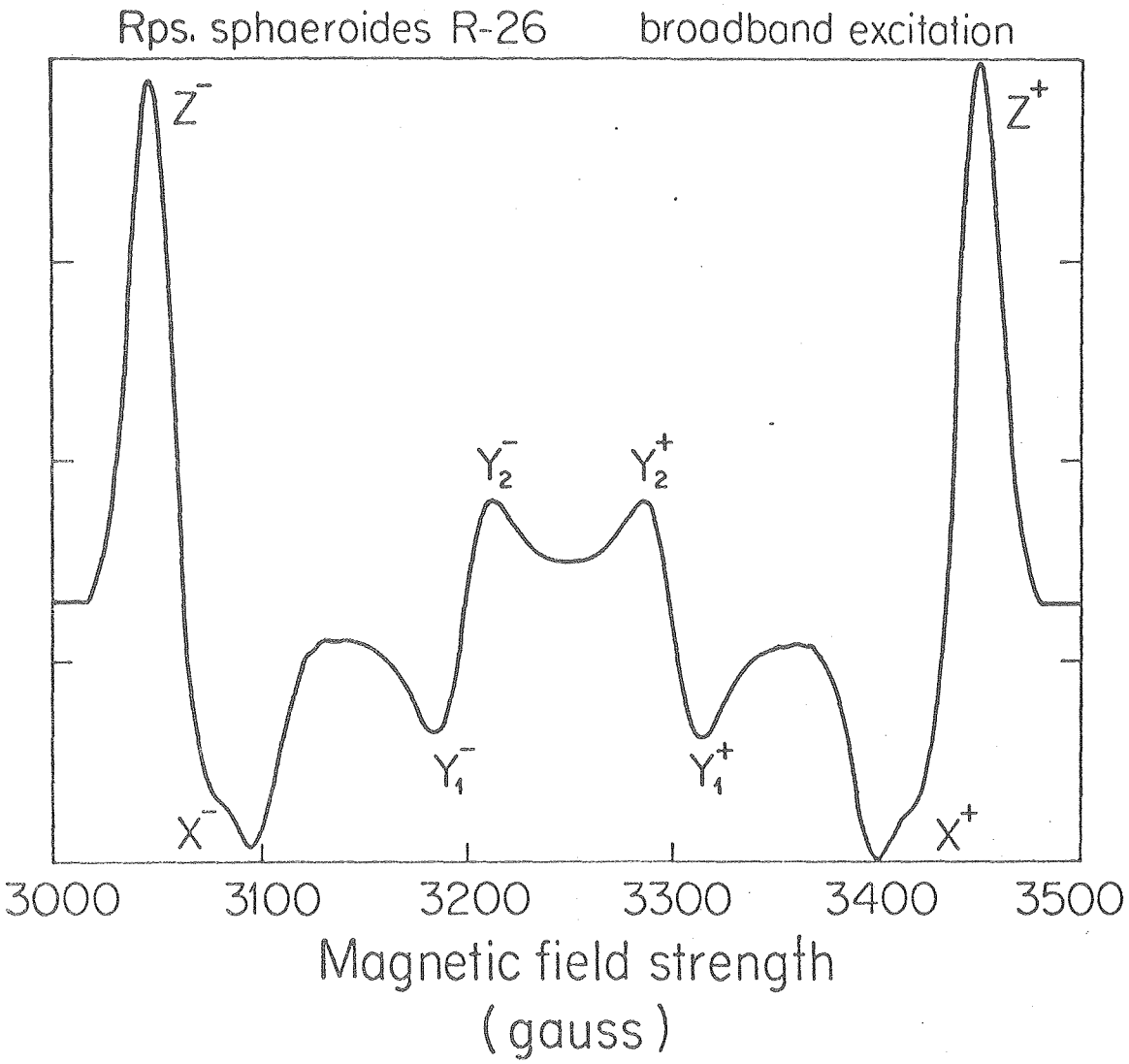

Figure 4-3. (b) Simulated spectrum for 4-3(a).

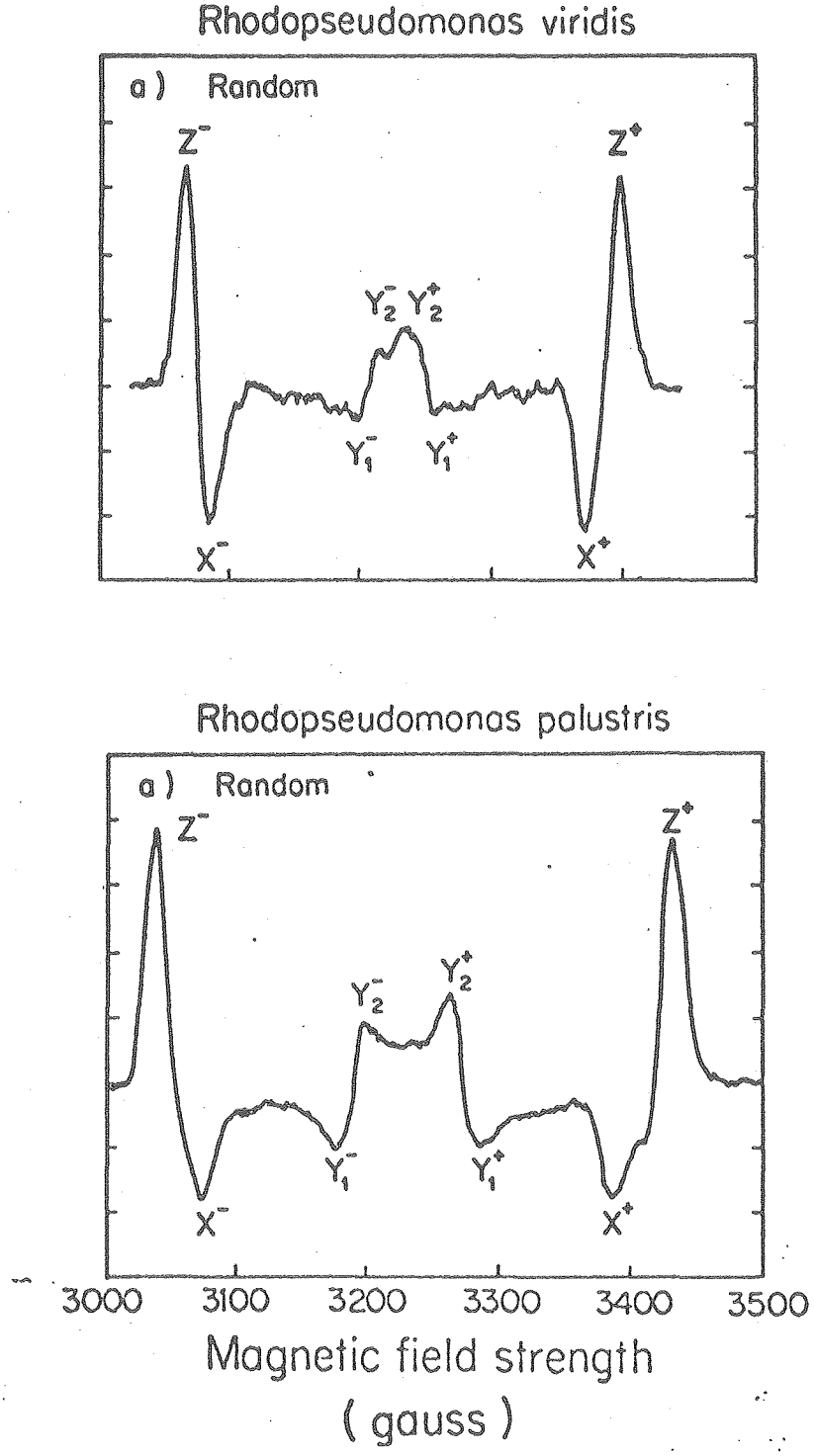

Figure 4-3. (c) Experimental random triplet spectra for *Rps. viridis* and *Rps. palustris*.

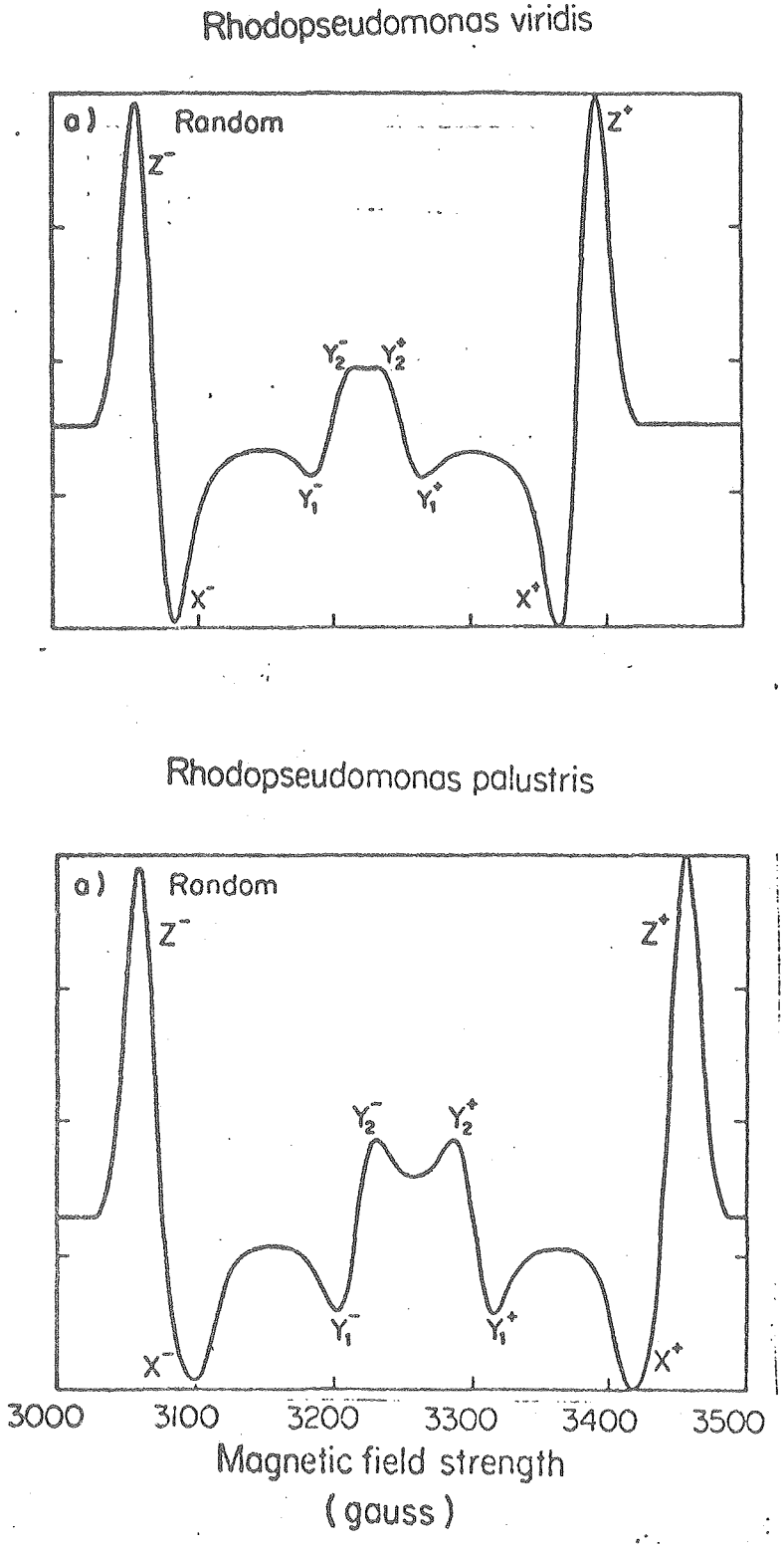

Figure 4-3. (d) Simulated spectra for 4-3(c).

4.3 Experiments Using Magnetically Aligned Whole Cells of *Rps. viridis* and *Rps. palustris*

A. Introduction

Suspension of a solution of whole cells of *Rps. viridis* or *Rps. palustris* in a strong (21 kG) magnetic field, followed by freezing the aligned sample, creates a partially ordered ensemble of special pair dimers. One can then perform the light modulated EPR experiment described above with the Zeeman field parallel to or perpendicular to the alignment field direction; these directions correspond to sampling different partially ordered ensembles of polarized triplets. The resultant spectra can be simulated using the theory of Chapter 3; this procedure allows determination of the orientation of the bacteriochlorophyll special pair with respect to the membrane normal and the degree of ordering of the ensemble.

The development of the theoretical model proceeds as follows;

(1) Determination of $D'(\theta')$, the distribution function for the Zeeman field in the intermediate axis system. A parameter, Δ, is defined which gives a measure of the disorder of the ensemble.

(2) Conversion of $D'(\theta')$ to $D(\theta,\phi)$, the distribution function in the principal magnetic axis system of the triplet. This introduces the parameters X_n, Y_n, and Z_n, the projection of the unit membrane normal on the triplet

magnetic axes. Note that since $X_n^2+Y_n^2+Z_n^2 = 1$, only two of these parameters (we choose X_n and Z_n) are independent.

(3) Computer simulation of the relative peak amplitudes of the parallel and perpendicular spectra. The D, E, k_x/k_z, and k_y/k_z values are fixed by the random simulation; X_n, Z_n, and Δ are treated as unknown parameters. A region of solution of X_n, Z_n and Δ values satisfying the experimental results is obtained.

B. Calculation of $D'(\theta')$ for the Magnetically Ordered Ensemble

Figures 2-4 and 2-5 display electron micrographs of the *Rps. viridis* and *Rps. palustris* photosynthetic membranes. The symmetrical arrangement of these membranes with respect to the long axis of the cell suggest that an alignment of the cells in regular fashion would also align the membranes (and their constituent components). The analysis that follows is based on an incorporation of these assumptions into a mathematical model.

The *Rps. viridis* cell can be represented as a prolate ellipsoid. We shall for the moment ignore end effects (they are indistinguishable from another sort of imperfection in ordering, as will be explained later), and consider the cell to be a perfect cylinder. Inside the cell are membranes rolled into concentric cylindrical sheets having a common axis with the long axis of the cell. Embedded in the membranes are reaction center particles, which contain the

paramagnetic species that gives rise to the observed light induced triplet signal. We assume that the principal axis system of the triplet is fixed with respect to the reaction center particle.

Linear dichroism (8) and photoselection (9) experiments suggest that there is a unique axis of the reaction center particle which is normal to the membrane surface. Our ensemble of intermediate axis systems is then a set of reaction center particles, randomly distributed in the cylindrical membrane structure, each of which has the designated axis normal to the membrane at that point.

A 21 kg magnetic field orients the *Rps. viridis* so that the long axis of the cylinder tends to lie in the plane normal to the orienting field. One can then freeze the sample and perform EPR experiments with the external magnetic field either parallel to, or perpendicular to, the alignment field $\underset{\sim}{H}_a$.

C. Symmetry Operations in the *Rps. viridis* Ensemble

We choose the $\hat{z}'$ intermediate axis to be the unique axis of the reaction center particle. This choice fits the guideline of sec. II, because we assume that an unrestricted rotation of the particle around this axis is possible. This operation is then our first rotation, and we designate the angular variable as λ.

Two further symmetry operations are possible in the laboratory frame; rotation of the cylindrical cell about its long axis, and its rotation around the direction of the alignment field. We arrange the laboratory coordinate system so that the z axis coincides with the alignment field axis. Then the rotation about $\underset{\sim}{H}_a$ corresponds to a rotation about the laboratory z axis; the magnitude of this rotation is specified by the angle, χ, that the long axis of the cell makes with the laboratory y axis. Rotation about the cylinder axis is given by an angle, μ, that a designated normal to the cylinder surface makes with $\underset{\sim}{H}_a$ (see fig. 4-4).

It remains only to take into account imperfections in ordering. The major source of this is deviation of the cell surface from a perfect cylinder (resulting in curvature of the membranes). The effect of this curvature is to produce a non-zero angle between the membrane normal and a normal to the long axis of the cell constructed in a plane defined by the membrane normal and the long axis [see fig. 4-4(b)]. We designate this angle to be the wobble angle, ω.

We further assume that deviations of ω from 0° are random fluctuations, and thus set the probability distribution in ω to be

$$g_\omega(\omega) = \cos\omega \exp[-\omega^2/\Delta^2] = \cos\omega\ h(\omega) \qquad (4\text{-}11)$$

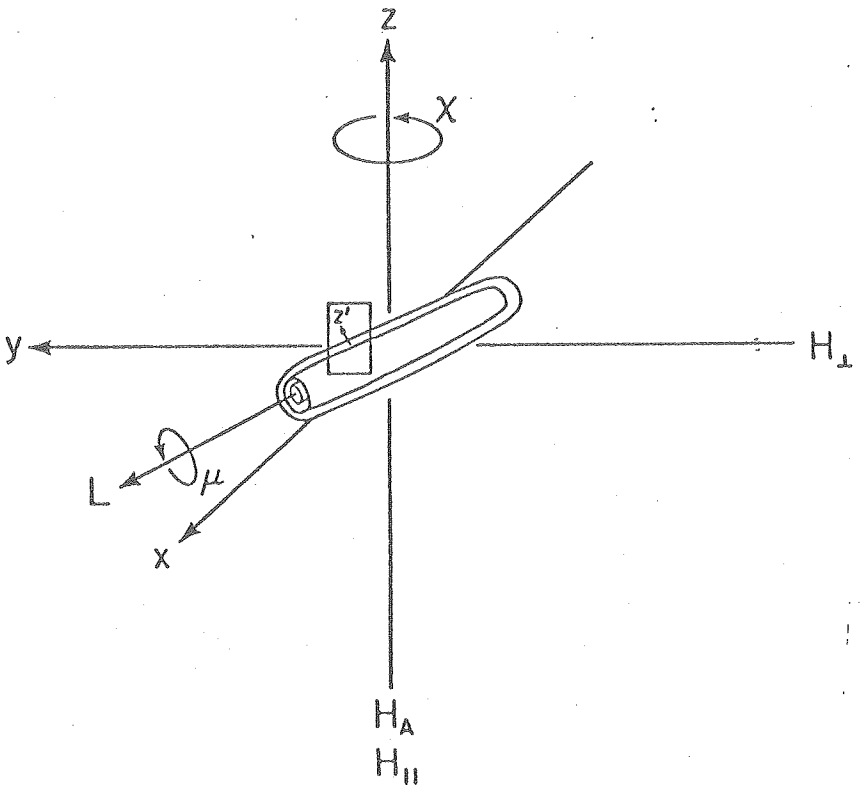

XBL7811-4398

Figure 4-4. (a) Axis system and symmetry operation definitions. x, y and z define the laboratory axis system; x', y' and z' the intermediate axis system; x", y" and z" the principal magnetic axis system. L is the long axis direction of the cell. χ, ν and λ are rotations about the indicated axes. H_A is the alignment field direction, and $H_{\parallel}$ and $H_{\perp}$ show the static EPR field directions used in the present experiments.

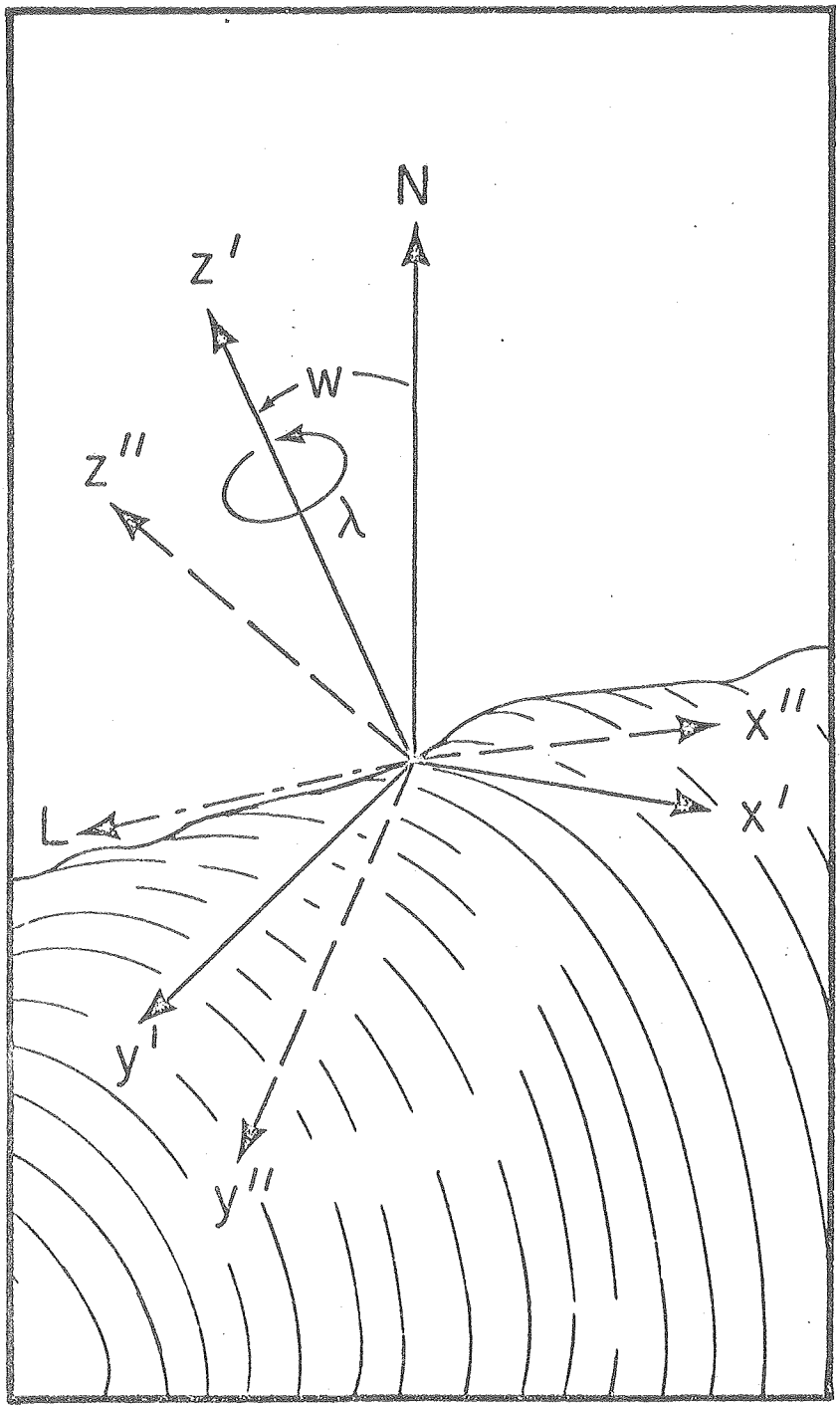

Figure 4-4. (b) A section of the cylindrical membrane surface. The wobble angle, w, is defined as the angle between the membrane normal, z', and the perfect cylinder normal, N, (*i.e.* N ⊥ L).

where Δ is the "disorder parameter" giving the standard deviation of ω, and $\cos\omega$ is the proper angular volume element, corresponding to the arc length swept out by a vector inclined at angle ω when the cell is rotated around its long axis.

We introduce the "wobble" into the density of states calculation as a rotation around the axis perpendicular to the long axis of the cell. A careful choice of the order of operations then allows us to represent every symmetry operation as one rotation in the laboratory coordinate system (λ about the z axis, ω about the x axis, μ about the y axis, and χ about the z axis. The final result for the external magnetic field in the intermediate axis system, $\underset{\sim}{H}'$, is given by

$$\underset{\sim}{H}' = [R_4^{-1}(\chi)\ R_3^{-1}(\mu)\ R_2^{-1}(\omega)\ R_1^{-1}(\lambda)]^T \underset{\sim}{H}_o \qquad (4\text{-}12)$$

$$= R_1(\lambda)R_2(\omega)R_3(\mu)R_4(\chi)\ \underset{\sim}{H}_o$$

D. $\underset{\sim}{H}_o$ Parallel to $\underset{\sim}{H}_a$

We set $\underset{\sim}{H}_o = (0,0,1)$, *i.e.* along the alignment field direction. Then, the rotation $R(\chi)$ is unnecessary, since the projection of (0,0,1) on the $\hat{x}'$, $\hat{y}'$, and $\hat{z}'$ axis is unaffected by a final rotation around the z axis. Following Chapter 3, we obtain

$$\begin{aligned} \alpha_1 &= \lambda \rightarrow -\phi' + f_3(v_1,\theta') \\ \alpha_2 &= \omega \rightarrow v_1 \\ \alpha_3 &\quad \mu \rightarrow f_2(v_1,\theta') \end{aligned} \qquad (4\text{-}13)$$

From (4-12) without $R(\chi)$,

$$F_z = \cos\theta' = \cos\mu \cos v_1$$

or

$$\cos\mu = \cos\theta'/\cos v_1 \qquad (4\text{-}14)$$

Evaluation of $\partial F_z/\partial\mu$ and substitution into equation (3-31) results in

$$D_{\parallel}'(\theta') = \frac{\sin\theta'}{N_{\parallel}'} \cdot \int_{\cos v_1 = 1}^{\cos v_1 = \cos\theta'} \frac{g_\omega(v_1)}{(1 - \frac{\cos^2\theta'}{\cos^2 v_1})^{1/2}} \cdot \frac{1}{\cos v_1}\, dv_1 \qquad (4\text{-}15)$$

Substituting for v_1, we transform the above integral (see Appendix B) to

$$D_{\parallel}'(\theta') = \frac{\sin\theta'}{2N_{\parallel}'} \int_0^{\pi} h(v_1)du \qquad (4\text{-}16)$$

where $v_1 = \cos^{-1}[\frac{1}{2}(1 + \cos^2\theta' + \cos u \sin^2\theta')]^{1/2}$.

This integral has no singularities, and can be easily evaluated numerically. Figure 4-5 plots $D_{\parallel}'(\theta')$ *vs.* θ' for several values of the disorder parameter, Δ.

E. $\underset{\sim}{H}_o$ Perpendicular to $\underset{\sim}{H}_a$

We now set $\underset{\sim}{H}_o = (0,1,0)$ [a choice of (1,0,0) would be equivalent)]. Proceeding as before, we obtain

$$\underset{\sim}{H}' = R_1(\lambda)R_2(\omega)R_3(\mu)R_4(\chi) \cdot \begin{vmatrix} 0 \\ 1 \\ 0 \end{vmatrix} \qquad (4\text{-}17)$$

This yields

$$\begin{aligned} \alpha_1 &= \lambda \rightarrow -\phi' + f_3(v_1, v_2, \theta') \\ \alpha_2 &= \omega \rightarrow v_1 \\ \alpha_3 &= \chi \rightarrow v_2 \\ \alpha_4 &= \mu \rightarrow f_2(v_1, v_2, \theta') \end{aligned} \tag{4-17}$$

From equation (39)

$$F_z = \cos\theta' = \cos\mu\cos\omega\cos\chi + \sin\omega\sin\chi$$

or

$$\cos\mu = (\cos\theta' - \sin v_1 \sin v_2)/(\cos v_1 \cos v_2) \tag{4-19}$$

Evaluation of $\partial F_z/\partial\mu$, substitution into equation (3-31) and evaluation of the v_2 integral yields (see Appendix C for details)

$$D_1'(\theta') = \frac{\sin\theta'}{N'} \cdot \int_0^{\pi/2} h(v_1)\, G(\theta', v_1)\, dv_1 \tag{4-20}$$

where

$$G(\theta', v_1) = 2K(k)\{[1\pm\sin(\theta'+v_1)][1\pm\sin(\theta'-v_1)]\}^{-1/2} \tag{4-21}$$

Figure 4-6 plots $D_1'(\theta')$ *vs.* θ' for several values of Δ.

F. Conversion to the Principal Magnetic Axis System

The computer calculations are performed by generating all possible subspectra, multiplying each one by the appropriate weighting factor, and adding the results. It is convenient to carry out the orientational averaging in the PMAS so as to facilitate calculation of subspectra. The

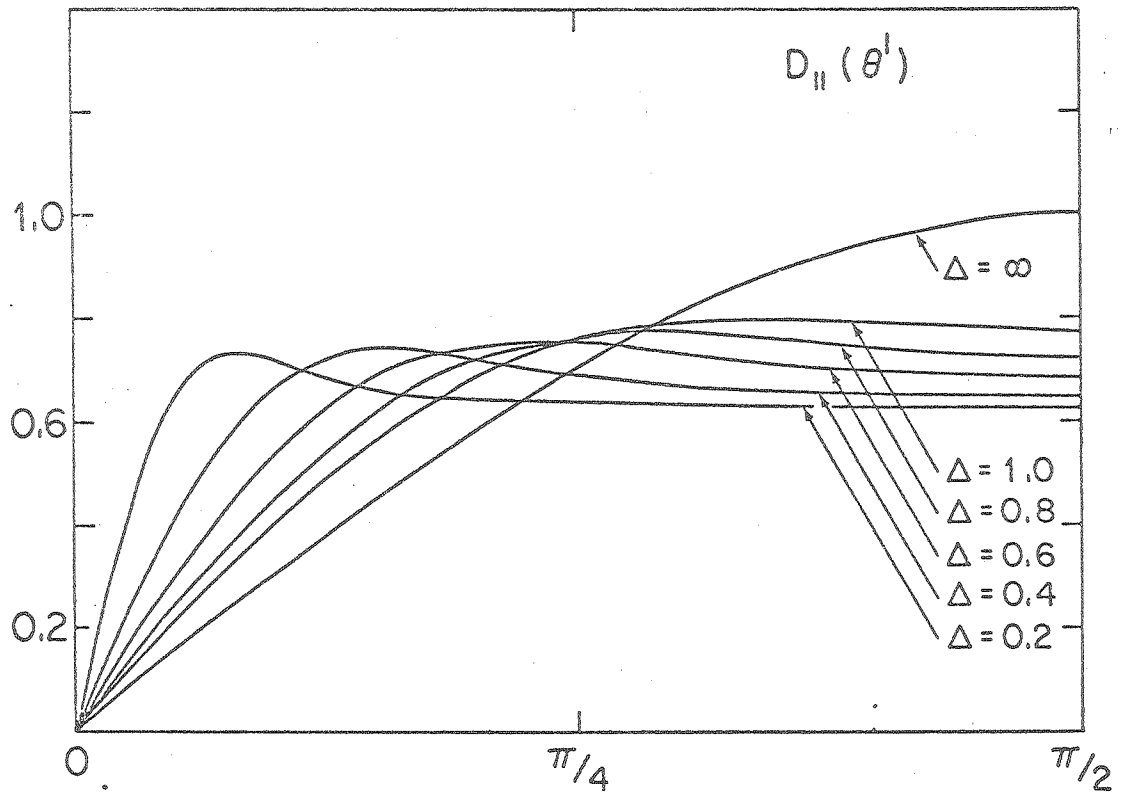

Figure 4-5. (a) Distribution function $[\mathcal{D}'_{\parallel}(\theta')]$ for $\underset{\sim}{H}_o$ parallel to $\underset{\sim}{H}_a$; plot of $\mathcal{D}'_{\parallel}(\theta')$ for several values of the disorder parameter Δ in radians.

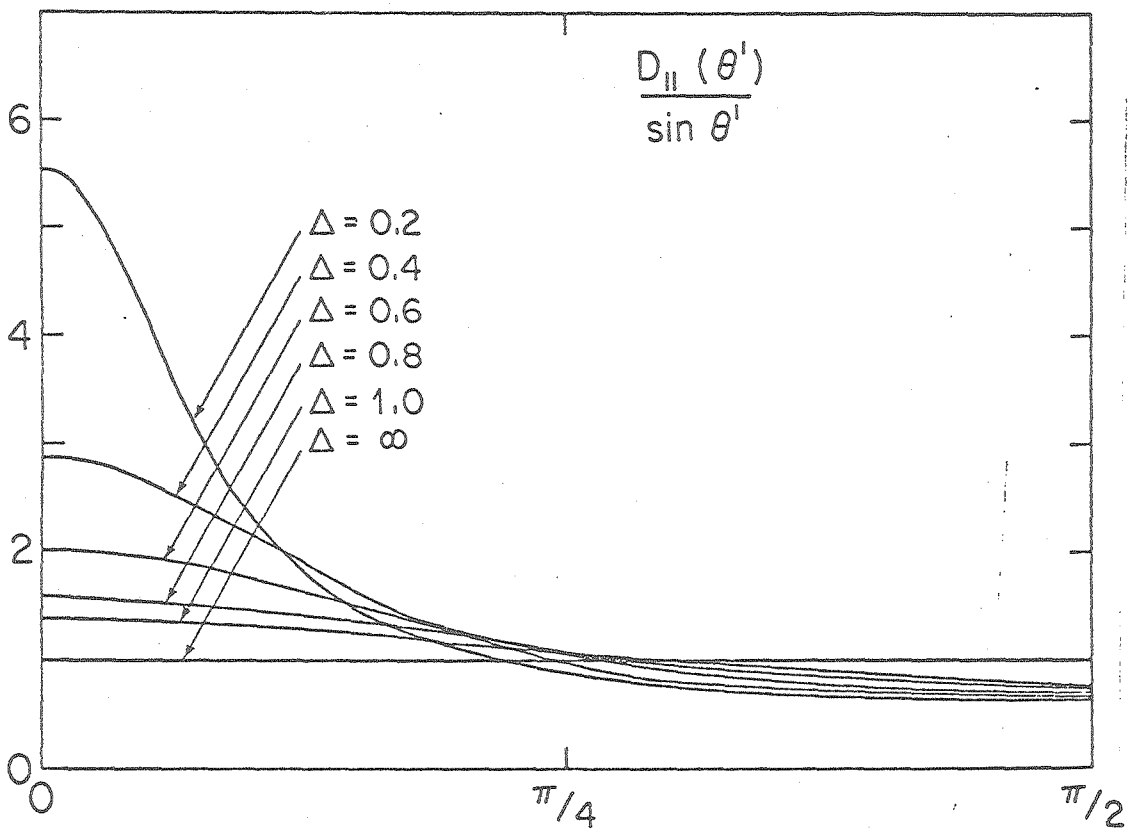

Figure 4-5. (b) Distribution function [$\mathcal{D}'_{\parallel}(\theta')$] for $\underset{\sim}{H}_o$ parallel to $\underset{\sim}{H}_a$; plot of $\mathcal{D}'_{\parallel}(\theta')/\sin\theta'$ versus θ' for several values of the disorder parameter Δ in radians. Note that $\mathcal{D}'_{\parallel}(\theta')/\sin\theta'$ must approach a constant as Δ approaches ∞ ($\Delta = \infty$ corresponds to a random sample).

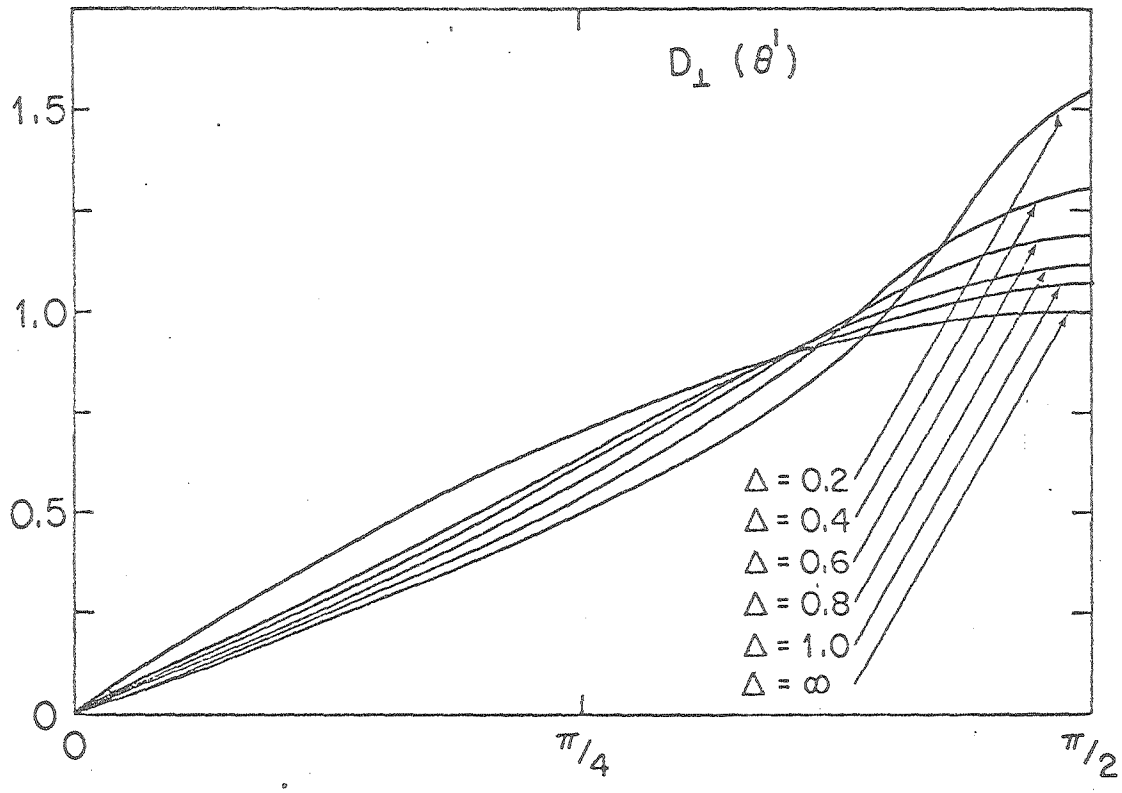

Figure 4-6. (a) Distribution function [$\mathcal{D}_1(\theta')$] for $\underset{\sim}{H}_o$ perpendicular to $\underset{\sim}{H}_a$; plot of $\mathcal{D}_1(\theta')$ versus θ for several values of the disorder parameter Δ in radians.

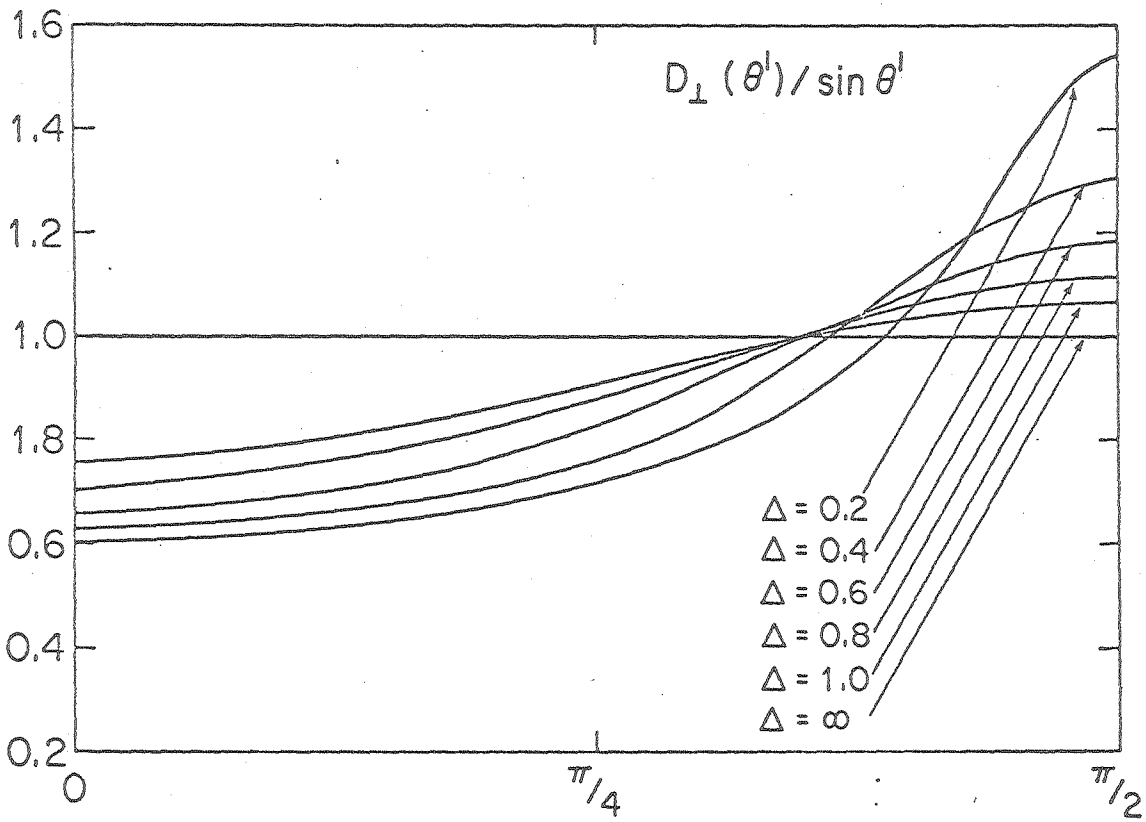

Figure 4-6. (b) Distribution function [$\mathcal{D}_\perp(\theta')$] for $\underset{\sim}{H}_o$ perpendicular to $\underset{\sim}{H}_a$; plot of $\mathcal{D}_\perp(\theta')/\sin\theta'$ versus θ for several values of the disorder parameter Δ in radians. Note that $\mathcal{D}_\perp(\theta')/\sin\theta'$ must approach a constant as Δ approaches ∞ ($\Delta = \infty$ corresponds to a random sample).

problem is then to determine the weight of a particular subspectrum which is generated when $\underset{\sim}{H}_o$ has orientation (θ,ϕ) in the PMAS.

This can be accomplished by locating the membrane normal (z' intermediate axis) in the PMAS. The angle θ' (the distribution function has axial symmetry in the intermediate axis system) is simply the angle between $\underset{\sim}{H}_o$ and $\underset{\sim}{n}$; *i.e.*

$$\theta' = \cos^{-1}|(\underset{\sim}{n}\cdot\underset{\sim}{H}_o)| \qquad (4\text{-}22)$$

where $\underset{\sim}{n}\cdot\underset{\sim}{H}_o = X_n\cdot H_x + Y_n\cdot H_y + Z_n\cdot H_z$. This equation displays the explicit dependence of the oriented spectra on the location of the membrane normal in the PMAS.

As has already been mentioned, one quadrant contains all of the triplet subspectra. However, the integration has to be carried out over all quadrants, because the $\underset{\sim}{H}_o$ associated with a particular subspectrum will make different angles with $\underset{\sim}{n}$ depending upon which quadrant it is in. The optimal solution to this problem (to save computer time) is to define $D(\theta,\phi)$ as a sum over 4 possible quadrants (the other 4 are degenerate), *i.e.*

$$D(\theta,\phi) = \frac{1}{4}\sum_{i=1}^{4} D'(\cos^{-1}|\underset{\sim}{n}\cdot\underset{\sim}{H}_o^{(i)}|)\times\sin\theta/\sin\theta' \qquad (4\text{-}23)$$

where

$$H_o^{(1)} = (|H_x|\ |H_y|\ |H_z|)$$
$$H_o^{(2)} = (-|H_x|\ |H_y|\ |H_z|)$$
$$H_o^{(3)} = (|H_x|\ -|H_y|\ |H_z|)$$
$$H_o^{(4)} = (|H_x|\ |H_y|\ -|H_z|)$$

H_x, H_y, and H_z run from 0 to $|\underset{\sim}{H}_o|$. This technique allows the θ and ϕ integrations to be restricted to 0 to $\pi/2$, and $D'(\theta')$ need be calculated only for θ' ranging from 0 to $\pi/2$. Because $D'(\theta')$ can always be written as $\sin\theta' \times f'(\theta')$, we can rewrite eq. (4-23) as

$$D(\theta,\phi) = \frac{1}{4} \sum_{i=1}^{4} f'[|\cos^{-1}(\underset{\sim}{n}\cdot\underset{\sim}{H}_o^{(i)})|] \times \sin\theta \qquad (4\text{-}24)$$

It is the $f'(\theta')$ which are used in the actual computer simulations.

G. Computer Simulation of Parallel and Perpendicular Spectra

Figure 4-7 is a flow chart for the computer routine used to simulate the parallel and perpendicular peak ratios. First, $f_{\parallel}'(\theta')$ and $f_{\perp}'(\theta')$ were calculated in a separate program in intervals of $\pi/100$ for values of Δ between 0.1 and 1.6 in steps of 0.1. These values were read into the main program, and ratios were calculated for all values of Δ. X_n and Z_n were varied between 0 and 1; Z_n in steps of 0.05, and 10 equally spaced values of X_n for each Z_n.

H. Results

For each set of parameters X_n, Z_n and Δ, six ratios were calculated; Z/X, Z/Y_1, Z/Y_2 for both $\underset{\sim}{H}_o \parallel \underset{\sim}{H}_a$ and $\underset{\sim}{H}_o \perp \underset{\sim}{H}_a$. These ratios were compared with the experimental ones; an acceptable solution is one for which all six theoretical ratios lie within the limits of experimental error. Table

4-3 gives the experimental ratios with error limits for the *Rps. viridis* and *Rps palustris* signals. Experimental peak ratios were obtained by the same procedures used for the unoriented samples (see sec. 4.2).

For both organisms, only one region of solution exists. This region can be approximately described by a rectangular parallelpiped in (X_n, Z_n, Δ) space. The limits so obtained for X_n, Z_n and Δ are listed in table 4-5. Plots of 6 curves, $R_T - R_E$, for solution and non-solution regions, are shown in fig. 4-8.

The best fit to the experimental ratios is obtained with the values listed in table 4-4. Figure 4-9 portrays schematic representations of the orientation of the normal to the membrane in the PMAS of the special pair dimer.

Figure 4-10 compares the full theoretical and experimental spectra for random, parallel, and perpendicular orientations of *Rps. viridis* and *Rps. palustris*. Despite the distorting sweep artifacts, it is obvious that the qualitative features of the experimental spectra are reproduced; the conjunction of this fact with the quantitative fit of the peak ratios provides an adequate fitting criterion for the solutions.

I. Discussion

The solutions obtained for X_n, Z_n and Δ for both *Rps. viridis* and *Rps. palustris* fall within a reasonably narrow range of values. The region of solution was sharper for

TABLE 4-3 EXPERIMENTAL AMPLITUDE RATIOS OF MAGNETICALLY ALIGNED BACTERIA

$Z^{\pm}$, $X^{\pm}$, $Y_1^{\pm}$ and $Y_2^{\pm}$ refer to the amplitudes (in arbitrary units) of the triplet peaks as defined in section 4-2. The errors represent the range of possible values for the ratios as deduced from the repeatability of the amplitude measurements.

	$Z^{\pm}/X^{\pm}$	$Z^{\pm}/Y_1^{\pm}$	$Z^{\pm}/Y_2^{\pm}$
Rps. viridis			
Parallel	-1.2 ± .1	-4.1 ± .7	2.5 ± .3
Perpendicular	-1.7 ± .1	-9.6 ± 1.7	9.6 ± 1.7
Rps. palustris			
Parallel	-1.8 ± .2	-2.5 ± .2	2.5 ± .2
Perpendicular	-2.2 ± .1	-4.7 ± .5	6.1 ± .8

TABLE 4-4 ORIENTATION PARAMETERS FOR THE PRIMARY DONORS IN PHOTOSYNTHETIC BACTERIA

X_n, Y_n and Z_n are the calculated projections of the x", y" and z" principal magnetic axes onto the normal to the membrane. 1.7Δ is the distribution width (in radians) of the "wobble" angle, w. The values in parentheses are the angles between the normal to the membrane and the principal magnetic axes. They are related to the projections by $\theta_X = \cos^{-1} X_n$, etc. The values were determined by the best fit of the theoretical spectra to the experimental ratios given in Table 4-3.

	X_n	Y_n	Z_n	Δ
Rps. viridis	0.67(48°)	0.74(42°)	0.10(84°)	0.40
Rps. palustris	0.69(46°)	0.69(46°)	0.25(76°)	0.60

TABLE 4-5 BOUNDARY CONDITIONS FOR THE REGIONS OF SOLUTION

The regions of solution are given by a rectangular parallepiped, the dimensions of which are determined by X_n and Z_n which are the projections of the x" and z" magnetic axes onto the normal to the membrane, and Δ which is the disorder parameter as defined in the text. No solution outside these regions fell within experimental error.

Rps. viridis	$0.65<X_n<0.75$	$0.0<Z_n<0.15$	$0.3<\Delta<0.5$
Rps. palustris	$0.5<X_n<0.7$	$0.0<Z_n<0.3$	$0.4<\Delta<0.8$

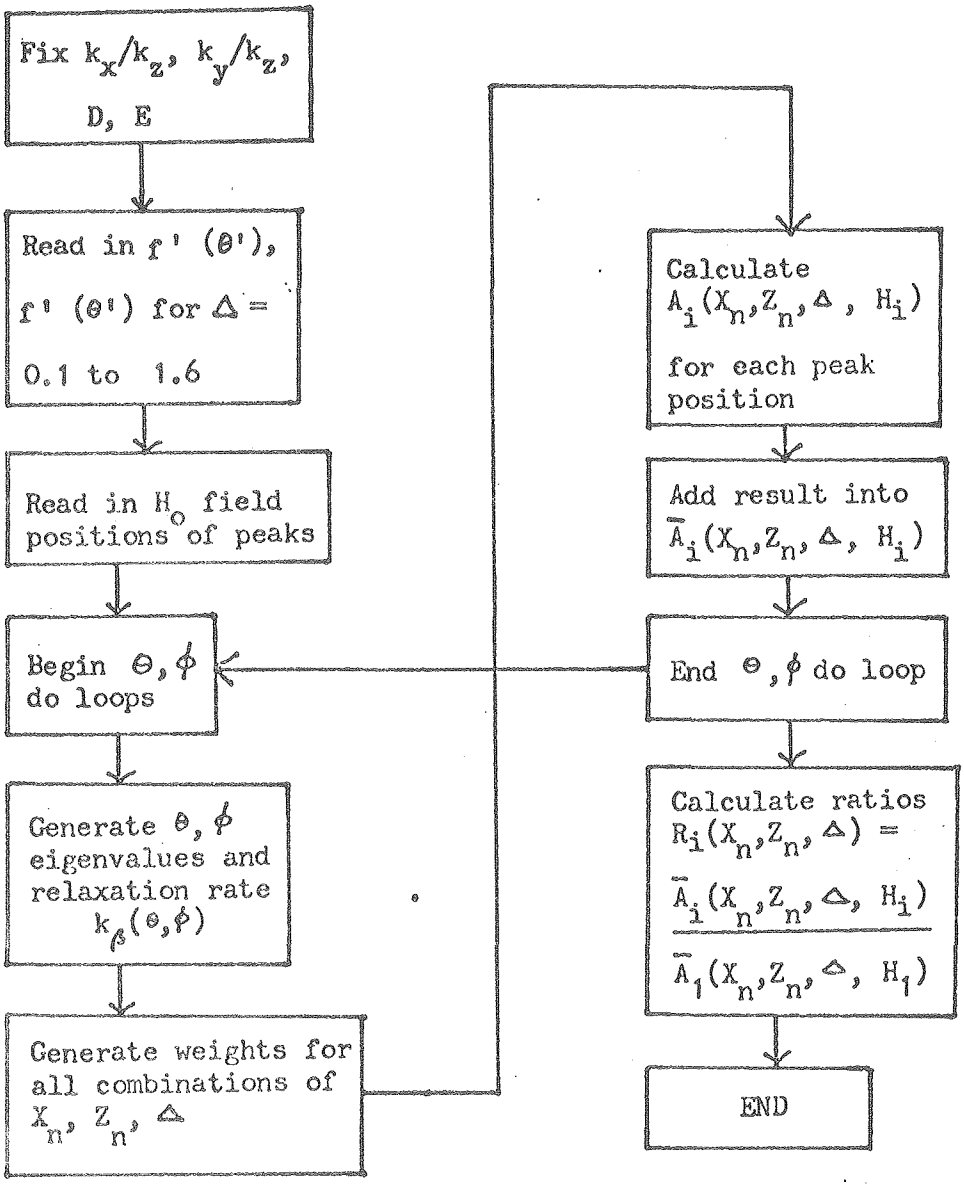

Figure 4-7. Flow chart for the computer program to calculate the ratio of peak amplitudes for the EPR spectra from the magnetically aligned whole cells of *Rps. viridis* and *Rps. palustris*.

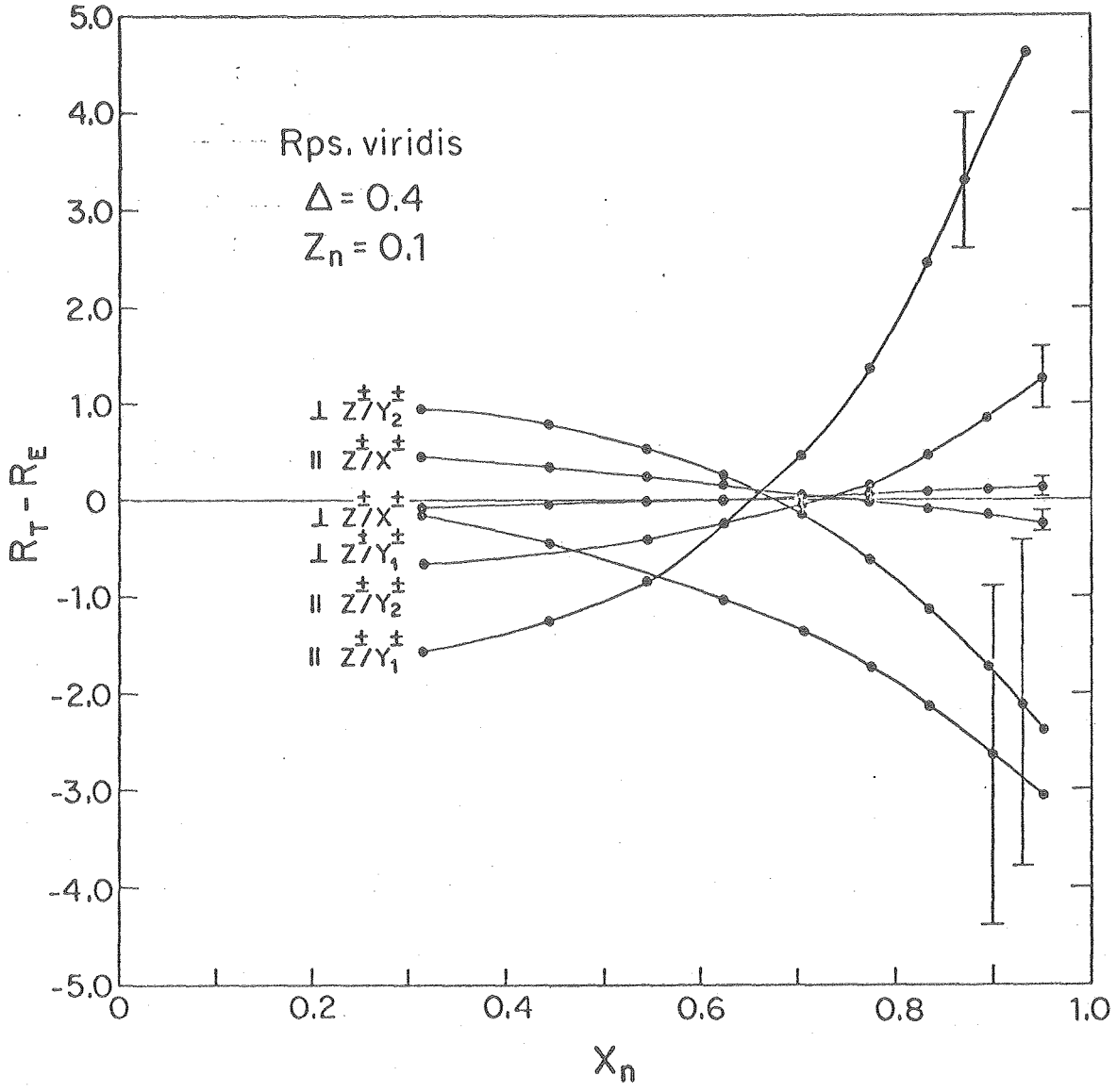

XBL7811-4376

Figure 4-8. (a) *Rhodopseudomonas viridis* plots of theoretical amplitude ratio minus experimental amplitude ratio, $R_T - R_E$, versus the projection, X_n, of the x" principal magnetic axes onto the normal to the membrane for $Z_n = 0.10$ and $\Delta = 0.40$.

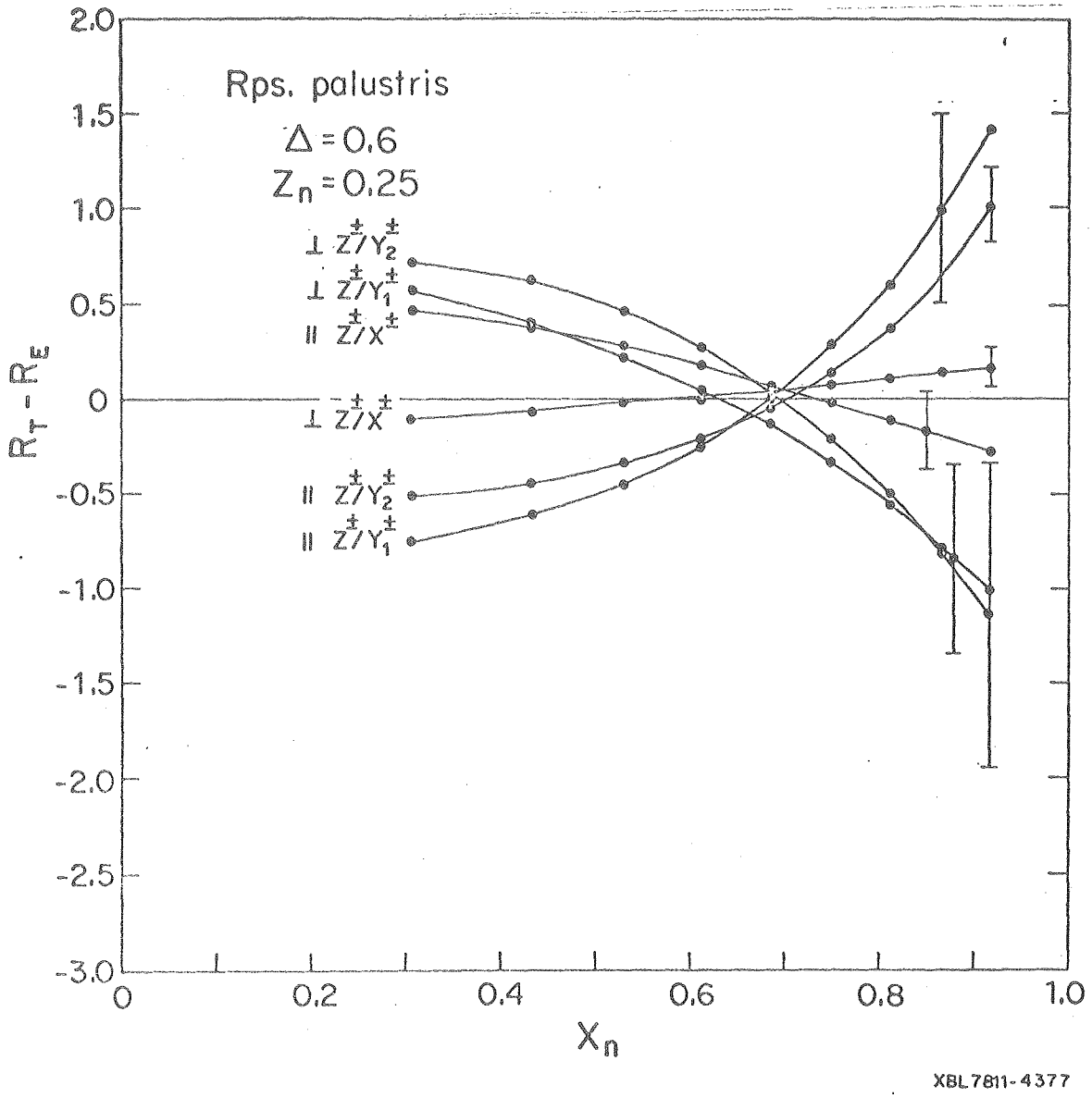

Figure 4-8. (b) *Rhodopseudomonas palustris* plots of theoretical ratio minus experimental amplitude ratio, $R_T - R_E$, versus the projection, X_n, of the x" principal magnetic axes onto the normal to the membrane for Z_n = 0.25 and Δ = 0.60.

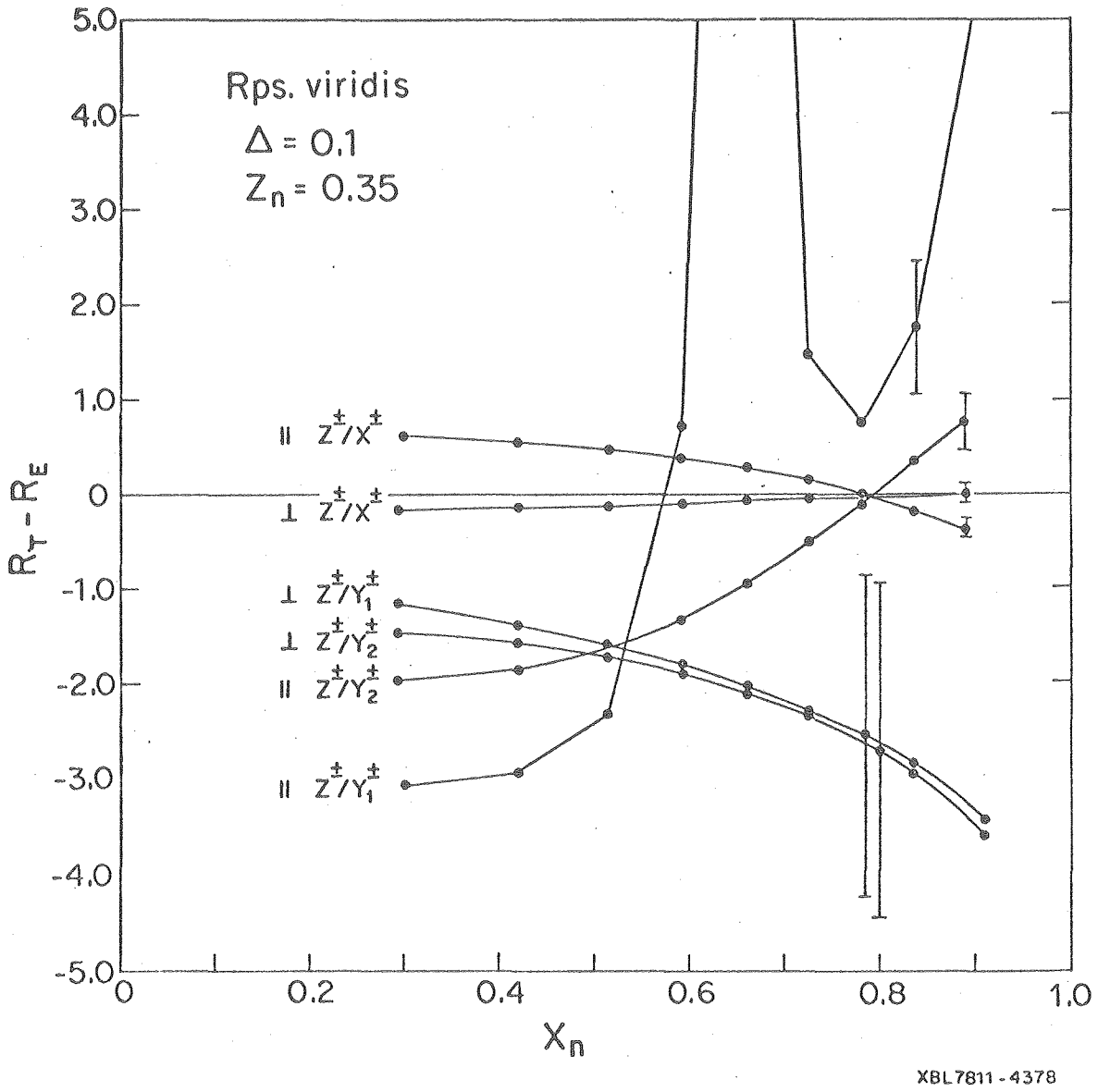

Figure 4-8 (c). *Rhodopseudomonas viridis* plots of theoretical minus experimental amplitude ratios versus the projection, X_n, of the x" principal magnetic axes onto the normal to the membrane for a typical non-solution region (*i.e.* one lying outside the experimental error).

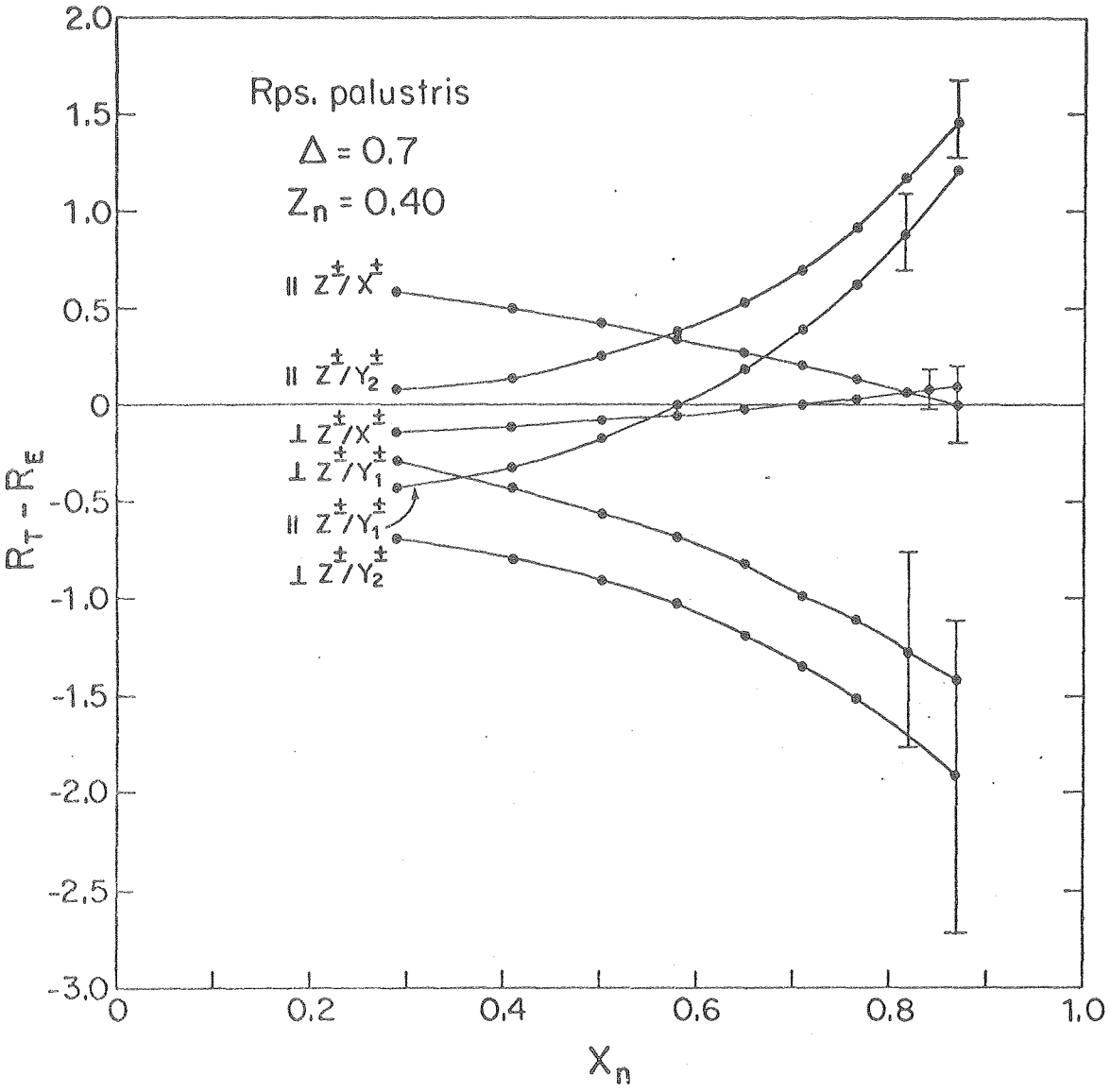

XBL7811-4379

Figure 4-8 (d). *Rhodopseudomonas palustris* plots of theoretical minus experimental amplitude ratios versus the projection, X_n, of the x" principal magnetic axes onto the normal to the membrane for a typical non-solution region (*i.e.* one lying outside the experimental error).

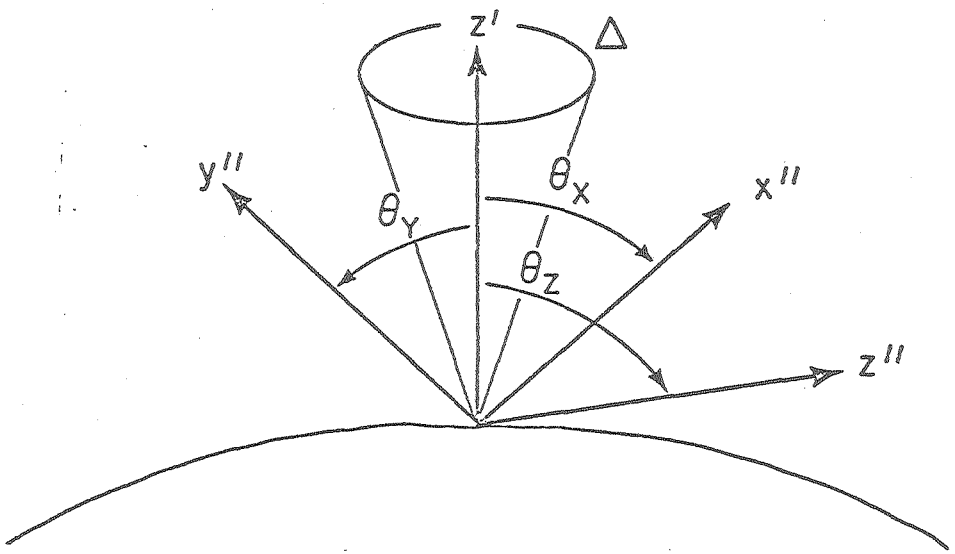

Figure 4-9. Orientation of the triplet magnetic axes of the primary donors in *Rhodopseudomonas viridis* and *Rhodopseudomonas palustris* sith respect to the cylindrical membrane surface. XBL 7810-4344

θ_X, θ_Y, θ_Z and Δ are given Table 4-5.

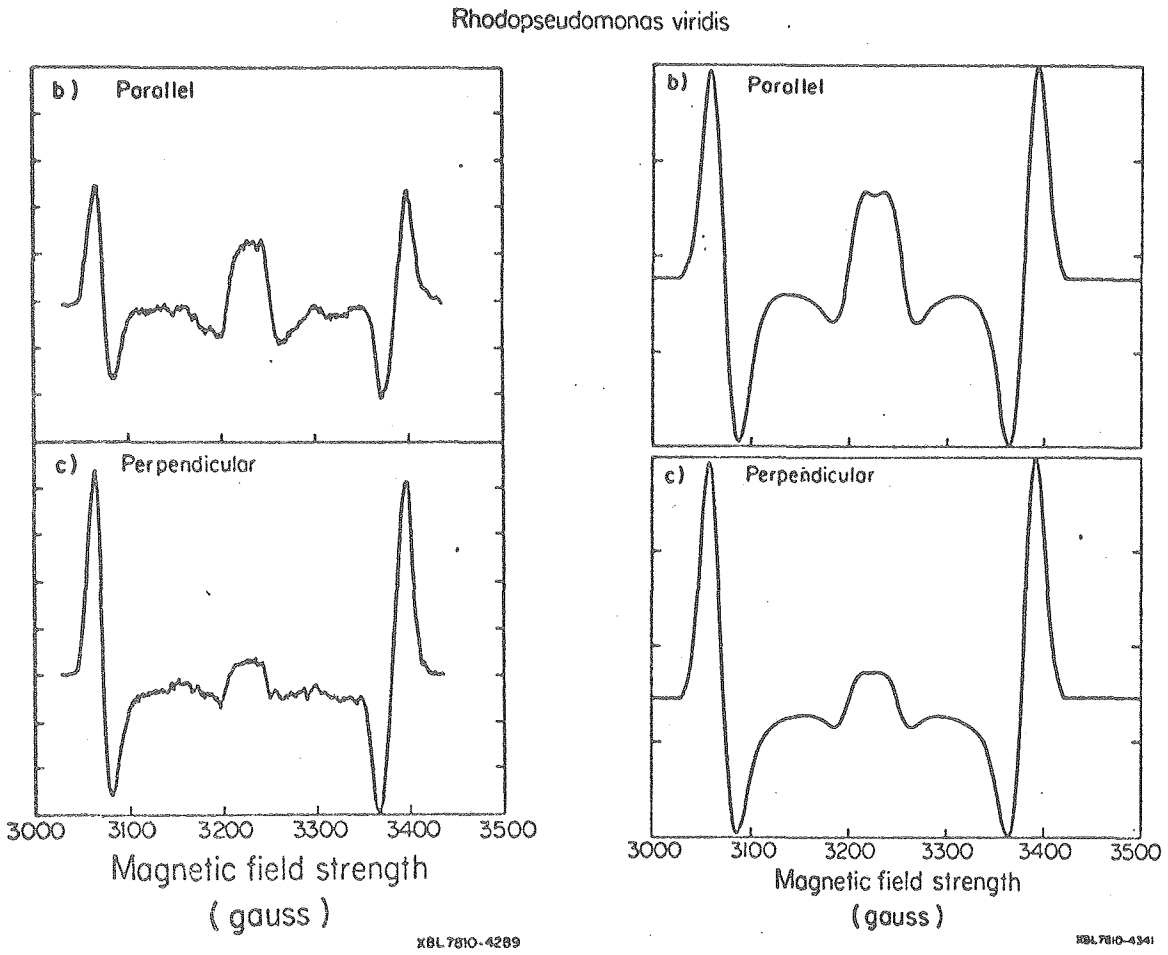

Figure 4-10. (a) Experimental (left) and theoretical (right) EPR spectra of the triplet from *Rps. viridis* for $\underset{\sim}{H}_o$ parallel and perpendicular to the alignment field $\underset{\sim}{H}_a$.

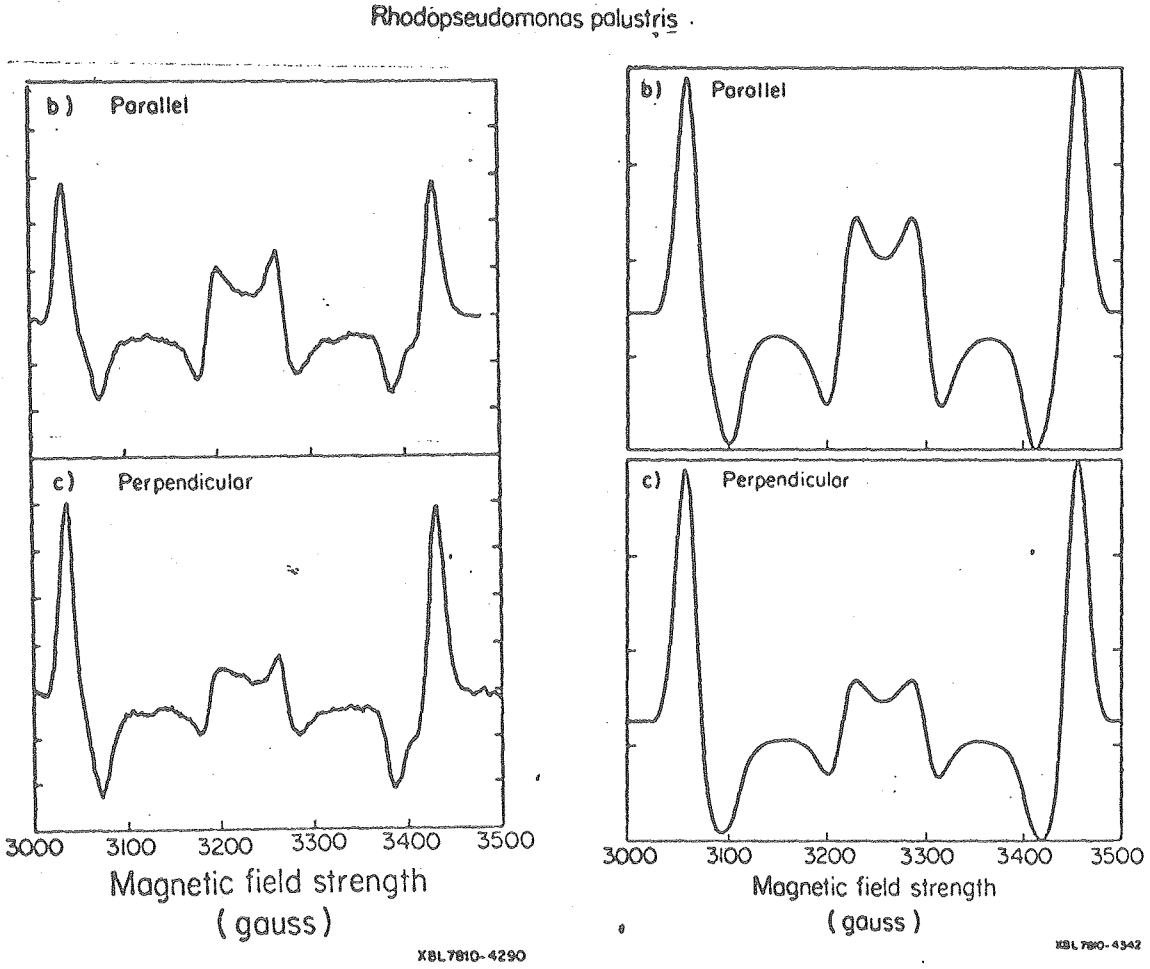

Figure 4-10. (b) Same as 4-10 (a) for *Rps. palustris*.

viridis reflecting the higher degree of orientation (*i.e.* smaller Δ) for this organism. We expect that as Δ becomes larger the uncertainty in the geometrical parameters would become greater, in the limit as $\Delta \rightarrow \infty$, no geometrical information would be present at all.

The above results demonstrate the utility of the theory of orientational averaging developed in Chapter 3. Without this theory, the averaging would have been extremely difficult and time consuming, and might well have entailed approximations which would have made the final results more questionable. The success of the theory in this application suggests others of a similar nature, for example, orienting benzpyrene intercalated into DNA.

4.4 Magnetophotoselection Studies on *Rps. spheroides* Reaction Centers

A. Introduction

The magnetophotoselection technique (MPS) has a purpose similar to that of the magnetic field alignment of whole cells; creation of a partially ordered ensemble of special pair triplet states. Here the ordering is accomplished by the use of plane-polarized, monochromatic light; the ordering is with respect to the optical transition excited by the wavelength of light used in the experiment. It is thus possible to locate this optical transition in the PMAS of the special pair bacteriochlorophyll dimer.

Previous workers have used MPS to obtain qualitative information from photosynthetic systems; these experiments were performed on chromatophores of *R. rubrum* (10). We employ a modification of the approach of sec. 4.3 to quantitatively determine the orientation of transition moments in the PMAS. Two transitions of *Rps. spheroides* are investigated; the special pair transition at 870 nm, and a bacteriopheophytin transition at 546 nm. Our results yield an approximate value for the angle between these transitions which is in agreement with the experiments of Vermeglio *et al.* using optical photoselection techniques (11).

Triplet EPR signals were measured, using the light modulation technique described in sec. 4.1, with the Zeeman field parallel and perpendicular to the direction of polarization of the light source. A broadband source was used to obtain a random spectrum (the plane polarization of such a source is irrelevant because of extensive energy transfer in the photosynthetic reaction center). Polarized, monochromatic light was obtained by the use of interference filters and polarizers [see reference (12) for experimental details].

We proceed in a manner analogous to sec. 4.3, *i.e.*

(1) Calculation of the distribution functions $D_{\parallel}(\theta,\phi)$ and $D_{\perp}(\theta,\phi)$ for the MPS experiment.

(2) Computer simulation of the relative peak heights (using the D, E, k_x/k_z, and k_y/k_z obtained in sec. 4.2) to determine P_x, P_y and P_z, the projections of the optical transition moments onto the principal magnetic axes of the triplet.

B. Calculation of the Distribution Function

The intermediate axis system z' axis can be taken to be the direction of the optical transition $\underset{\sim}{\mu}$, the laboratory z axis is the direction of the electric field polarization, $\underset{\sim}{E}$.

The probability A that a molecule will be excited by the polarized light is given by

$$A = \cos^2\theta' \tag{4-25}$$

where θ' is the angle between $\underset{\sim}{\mu}$ and $\underset{\sim}{E}$. For $\underset{\sim}{H}_o$ parallel to $\underset{\sim}{E}$, the angle between $\underset{\sim}{H}_o$ and $\underset{\sim}{\mu}$ (and thus z') is also θ', we therefore obtain the axially symmetric distribution function

$$D'_{\parallel}(\theta') = \cos^2\theta' \times \sin\theta' \tag{4-26}$$

where $\sin\theta'$ is the appropriate angular volume element. The perpendicular distribution function is easily worked out to be

$$D'_{\perp}(\theta') = (1-\cos^2\theta')\times\sin\theta' = \sin^2\theta' \times \sin\theta' \tag{4-27}$$

We now need to convert to the PMAS of the triplet. This is done exactly as in sec. 4-3, substituting $\hat{\mu}$ for $\underset{\sim}{n}$ ($\hat{\mu}$ is a unit vector in the direction of $\underset{\sim}{\mu}$)

$$\theta' = \cos^{-1}|\hat{\mu}\cdot\underset{\sim}{H}_o| \tag{4-28}$$

$$= \cos^{-1}|P_x H_x + P_y H_y + P_z H_z|$$

where P_x, P_y and P_z are the projections of $\hat{\mu}$ on the PMAS.

As in 4.3, we need to average over all quadrants; the net result is

$$D_{\parallel}(\theta,\phi) = \cos^2\{\sum_{i=1}^{4} \cos^{-1}|[\hat{\mu}\cdot\underset{\sim}{H}_o^{(i)}]|\} \times \sin\theta \quad (4\text{-}29)$$

$$D_{\perp}(\theta,\phi) = \sin^2\{\sum_{i=1}^{4} \cos^{-1}|[\hat{\mu}\cdot\underset{\sim}{H}_o^{(i)}]|\} \times \sin\theta \quad (4\text{-}30)$$

where the $\underset{\sim}{H}_o^{(i)}$ are as in eqs. (4-23).

C. Results

The computer simulation procedure is identical to that used in sec. 4-3, except that $D_{\parallel}(\theta,\phi)$ and $D_{\perp}(\theta,\phi)$ are given by eqs. (4-29) and (4-30) respectively. Also, no disorder parameter exists; the photoselection rule ($A \propto \cos^2\theta$) is taken to completely describe the ordering. We thus obtain values of P_x, P_y, and P_z (two of which are independent) for the 870 nm and 546 nm transition.

The results are summarized in Tables 4-6 to 4-8. Table 4-6 gives the experimental peak amplitude ratios for broadband and parallel and perpendicular spectra for the 870 nm and 546 nm transitions. Table 4-7 lists the best solutions, while Table 4-8 gives the acceptable range of solutions [described by a rectangle in (P_x,P_y) space].

Figure 4-11 displays the experimental and simulated parallel and perpendicular spectra for the two transitions. Figure 4-12 is a model of the orientations of the transition moments in the PMAS, calculated from the results in Table 4-2.

TABLE 4-6 EXPERIMENTAL TRIPLET STATE SIGNAL AMPLITUDE RATIOS

The amplitudes were measured at the key field positions indicated in figure 4-11. The pairs of measured intensities (*e.g.* X^+ and X^-) were found to be equal within experimental error. The amplitudes are therefore designated by a superscript ± (*e.g.* $X^{\pm}$). Numbers in parentheses indicate the range of acceptable ratios calculated from a fixed value for the uncertainty in the experimental amplitude determination.

	$Z^{\pm}/X^{\pm}$	$Z^{\pm}/Y_1^{\pm}$	$Z^{\pm}/Y_2^{\pm}$
882 nm			
1) parallel	-0.28(-.35,-.22)	3.7(13.0,1.8)	2.2(4.3,1.3)
2) perpendicular	-6.0 (-8.2,-4.0)	-3.6(-4.3,-3.1)	9.0(14.0,6.5)
550 nm			
1) parallel	-2.8(-3.6,-2.2)	-8.8(-23.5,-5.1)	-*
2) perpendicular	-1.6(-2.4,-1.1	-3.2(-7.3,-1.8)	1.6(2.4,1.1)

*$Y_2^{\pm}$ amplitude was approximately zero.

TABLE 4-7 PROJECTION OF THE OPTICAL TRANSITION MOMENTS ONTO THE PRINCIPAL MAGNETIC AXES OF THE TRIPLET STATE

The best fit of the calculated spectra to the experimental results are given by the projections P_x, P_y, and P_z.

	P_x	P_y	P_z
870 nm	.99	.014	.14
546 nm	.405	.405	.82

TABLE 4-8 BOUNDARY CONDITIONS FOR THE RECTANGULAR REGION OF SOLUTION

The regions of solution are given by rectangles, the dimensions of which are determined by P_x and P_z which are the projections of the transition moments onto the x and z principal magnetic axes, respectively.

870 nm	$.98 < P_x < 1.00$	$.10 < P_z < .16$
546 nm	$.33 < P_x < .63$	$.73 < P_z < .85$

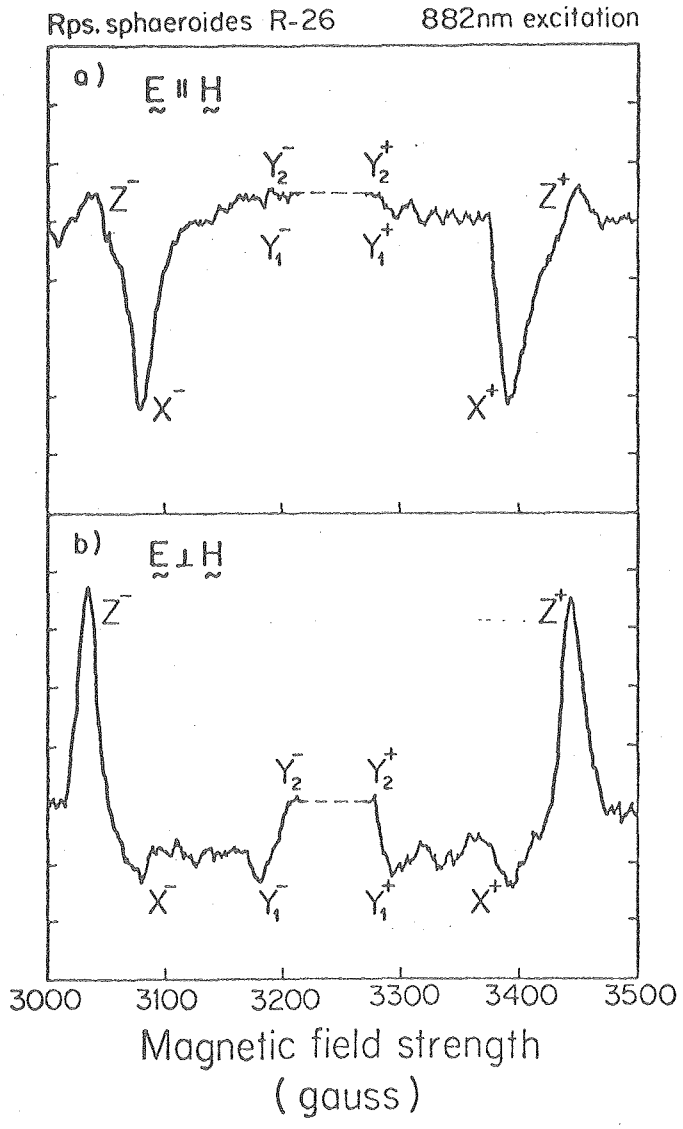

Figure 4-11. (a) Experimental triplet state spectra of *Rhodopseudomonas sphaeroides* R-26 generated by 882 nm polarized light, taken with $\underset{\sim}{E} \parallel \underset{\sim}{H}$ and $\underset{\sim}{E} \perp \underset{\sim}{H}$. The light-induced free radical signal at g = 2.0 has been omitted.

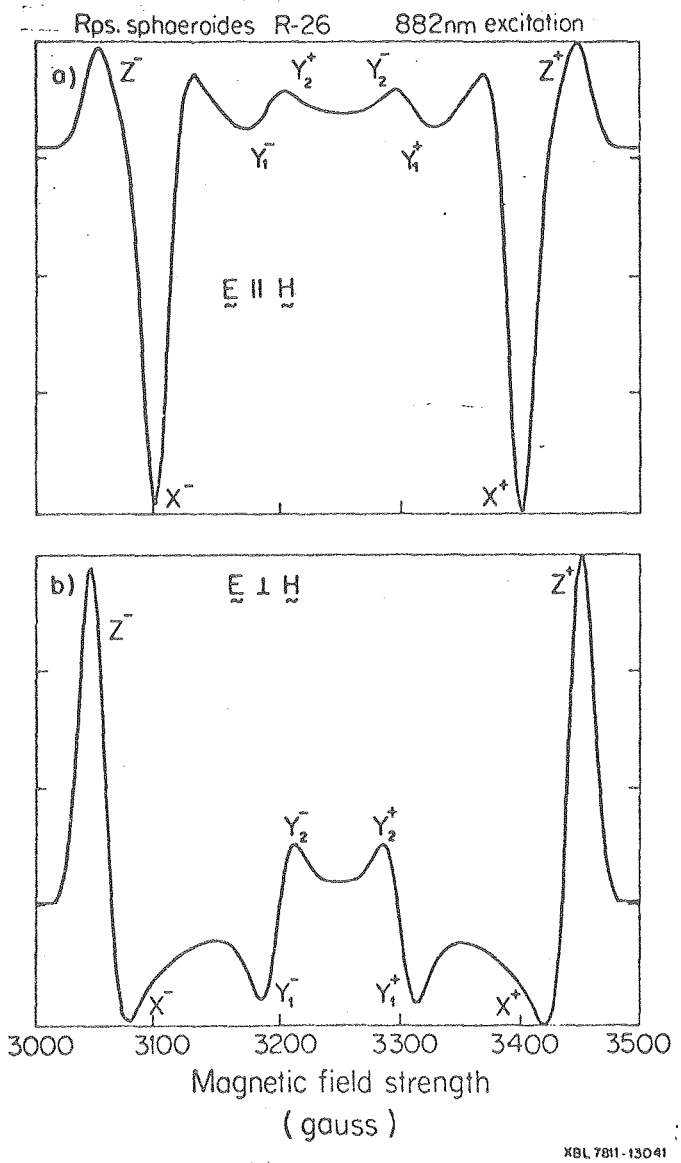

Figure 4-11. (b) Computer simulated 882 nm excited triplet state spectra of *Rhodopseudomonas sphaeroides* R-26. The spectra were calculated assuming a) $\underset{\sim}{E} \parallel \underset{\sim}{H}$, and b) $\underset{\sim}{E} \perp \underset{\sim}{H}$. The parameters used to calculate these spectra are given in Table 4-2 and 4-7. All computer simulations are normalized to the $|Z^{\pm}| + |X^{\pm}|$ peak amplitudes.

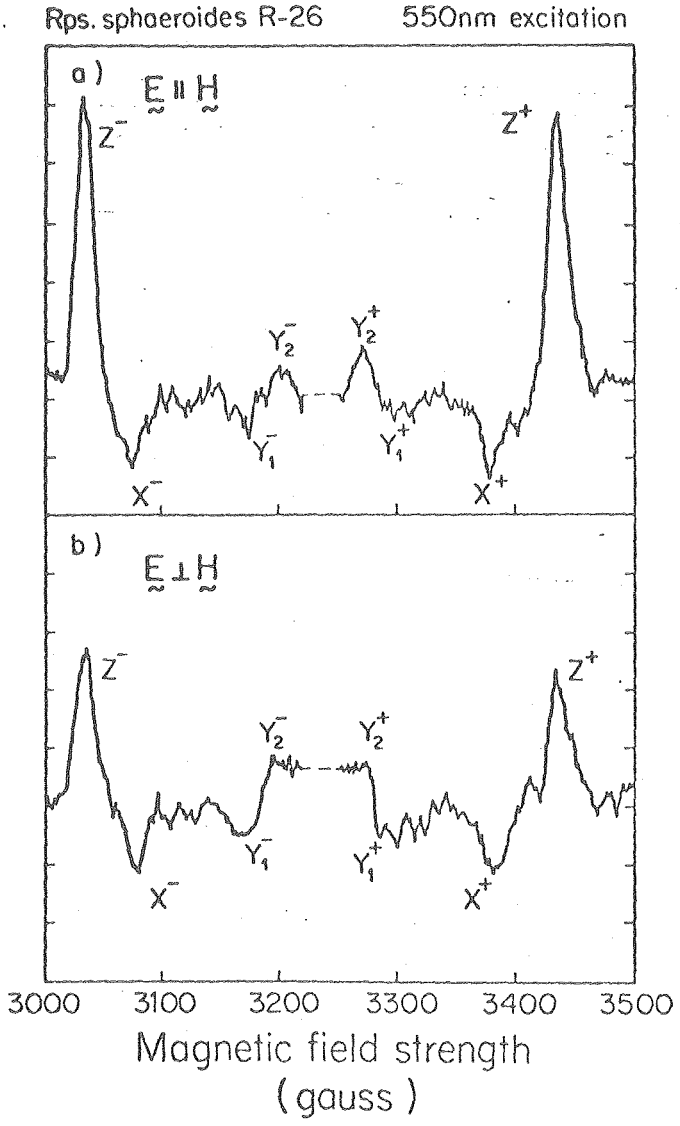

XBL 7812-13058

Figure 4-11. (c) Experimental triplet state spectrum of *Rhodopseudomonas sphaeroides* R-26 generated by 550 nm polarized light. Spectra taken with $\underset{\sim}{E} \parallel \underset{\sim}{H}$ (top) and $\underset{\sim}{E} \perp \underset{\sim}{H}$ (bottom). The light induced free radical signal at g = 2.0 has been omitted.

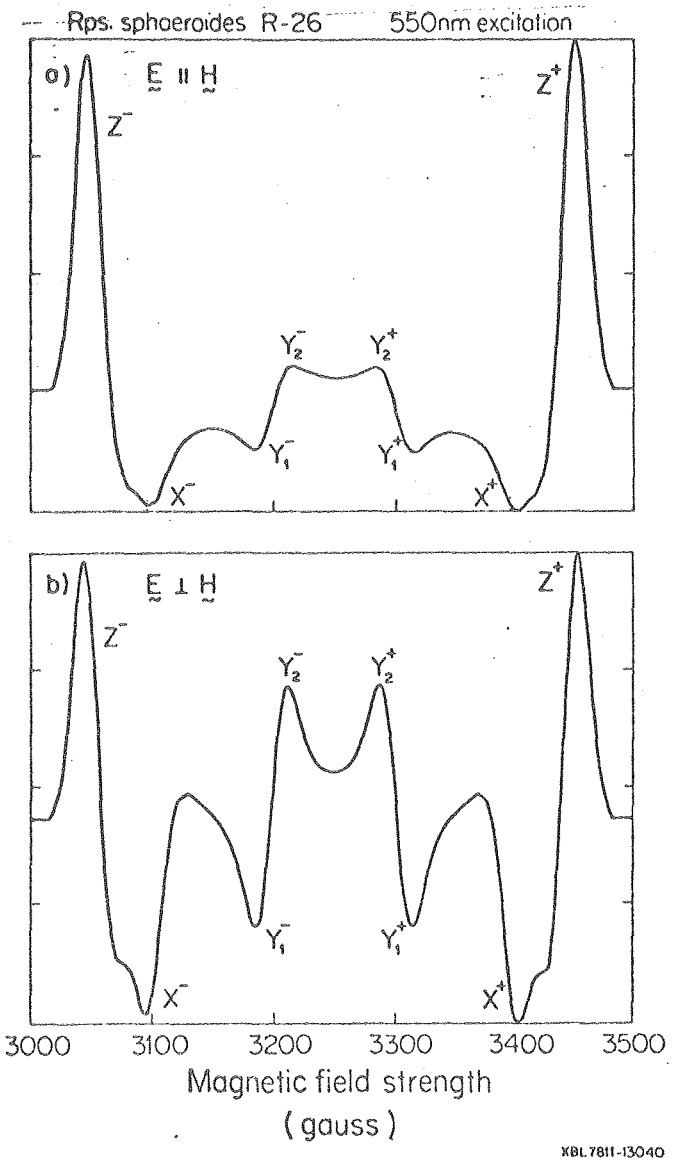

Figure 4-11. (d) Computer simulated 550 nm excited triplet state spectra of *Rhodopseudomonas sphaeroides*. The spectra were calculated assuming a) $\underset{\sim}{E} \parallel \underset{\sim}{H}$ and b) $\underset{\sim}{E} \perp \underset{\sim}{H}$. The parameters used to calculate these spectra are given in Table 4-2 and 4-7.

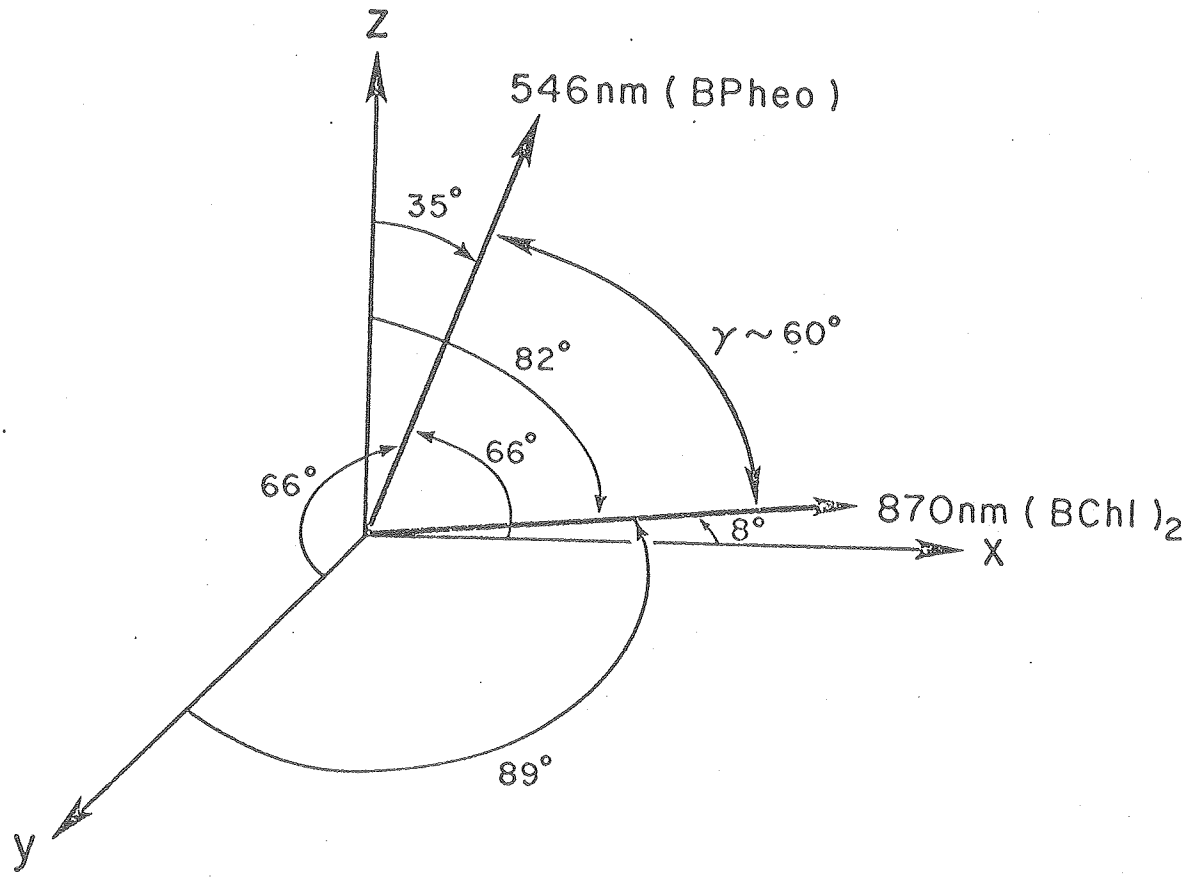

Figure 4-12. The orientation of the transition moments at 446 nm and 870 nm with respect to the principal magnetic axis system (x,y,z) of the triplet state. The angles were calculated from the projections given in Table 4-7 using the relations θ_x = arccos P_x, etc.

D. Discussion

1. 870 nm transition

This transition is believed to be a pure bacteriochlorophyll special pair Q_y transition (11). Our results indicate that it lies directly along the x magnetic axis of the triplet. Thus, any model constructed for the special pair dimer should have one of the exciton components of the Q_y transition along the X principal magnetic axis.

The projections for this simulation appear to have a very high degree of precision; this is due to the peculiar shape of the signal, in which the $X^{\pm}$ peaks are positive. Only a very large P_x value ($P_x > .98$) is able to generate such a spectrum.

2. 546 nm transition

At low temperatures the two bacteriopheophytin transitions (associated with two different molecules) are resolved at 530 nm and 546 nm (11). The exciting light is centered at 550 nm and so excites primarily the latter. The energy is then transferred to the special pair dimer where it produces the triplet P_R state in the usual manner. In the calculation, we assume that the geometry of the bacteriopheophytin is rigidly fixed with respect to the dimer.

The projections for this transition show a much wider range of solution, this is due to the poor signal-to-noise ratio achieved in the experiment. One might do better by using a laser excitation source.

The calculation of the angle between the two transitions is straightforward and agrees well with the value of Vermeglio *et al.* (59° *vs.* 60°). However, the uncertainty in the P_x value for the 546 nm transition makes this calculation of dubious value.

4.5 Conclusion

The studies in this Chapter have yielded a wealth of magnetic and geometrical information concerning the primary donor in bacterial photosynthesis. However, the geometrical information is fragmented; we cannot, from these results alone, locate the two bacteriochlorophyll molecules in the membrane, or determine their orientations with respect to other species.

The key to a unified picture of the reaction center will be the combining of various spectroscopic techniques. The present work thus needs to be supplemented by linear dichroism, absorption, circular dichroism and ODMR studies; the data from such studies needs to be analyzed carefully and quantitatively, as is done in this Chapter. Work in this direction is currently in progress, and I do not believe that it is too optimistic to expect to have a picture of this sort in a few years.

REFERENCES

1. H. Levanon and J.R. Norris. Chem. Rev. 78, 185 (1978).

2. H. Levanon and S. Vega. J. Chem. Phys 61, 2265 (1974).

3. C.J. Winscom. Z. Naturforsch. 30a, 571 (1975).

4. C.C. Felix and S.I. Weissman. Proc. Nat. Acad. Sci. USA 72, 4203 (1975).

5. R.H. Clarke, R.E. Connors, H.A. Frank and J.C. Hoch. Chem. Phys. Lett. 45, 523 (1977).

6. R.H. Clarke, R.E. Connors and H.A. Frank. Biochem. Biophys. Res. Comm. 71, 671 (1976).

7. A.J. Hoff. Biochim. Biophys. Acta 440, 765 (1976).

8. J. Breton. Biochem. Biophys. Res. Comm. 59, 1011 (1974).

9. G. Paillotin, A. Vermeglio and J. Breton. Biochim. Biophys. Acta 545, 249 (1979).

10. M.C. Thurnauer and J.R. Norris. Biochem. Biophys. Res. Comm. 73, 501 (1976).

11. A. Vermeglio, J. Breton, G. Paillotin and R. Cogdell. Biochim. Biophys. Acta. 501, 514 (1978).

12. H.A. Frank, J. Bolt, R. Friesner and K. Sauer. Biochim. Biophys. Acta. in press (1979).

CHAPTER 5

DEVELOPMENT OF ELECTRON SPIN POLARIZATION IN PHOTOSYNTHETIC ELECTRON TRANSFER BY THE RADICAL PAIR MECHANISM

5.1 Introduction

For a number of years, P430 was thought to be the primary acceptor in PSI (1). The first evidence that an earlier acceptor might exist was obtained by MacIntosh and Bolton (2), who observed a reversible light-induced EPR signal at low temperature when centers A and B were chemically reduced. This signal has g values of 2.08, 1.92, and 1.76; the species giving rise to it has been labelled "X". Redox titrations indicate that the midpoint potential of X is more negative than that of P430, as would be expected if its place in the electron transport chain is intermediate between P430 and P700.

Somewhat later, spin polarization was first detected in signals from broken spinach chloroplasts by Blankenship *et al.* (4). The polarized signal appears as a fast kinetic component in measurements of the time dependence of EPR Signal I using a 1 mHz phase sensitive detection system. Typical kinetic traces of the EPR intensity *versus* time are shown in fig. 5-1.

Additional information was obtained by the discovery of a "flow effect". In the original experiments, a suspension of chloroplasts was circulated through the EPR cell by a pump to avoid decomposing the samples. It was observed that the

kinetic traces at certain field positions altered dramatically when flow was stopped (5); a typical pair of flow and no-flow traces is shown in fig. 5-1. Profiles of the flow and no-flow spectra as a function of field position are shown in fig. 5-2.

The flow effect can be accounted for by the orientation of the disk-shaped chloroplasts in a velocity gradient. PSI particles or *Chlorella pyrenoidosa*, which do not orient in the flow gradient (their morphology is roughly isotropic), yield polarized spectra similar to fig. 5-2NF (*i.e.*, no-flow) under both flow and no-flow conditions. This result suggests that the altered lineshape is due to some anisotropic paramagnetic species which is rigidly bound in the thylakoid membrane and which influences the spin polarization.

A series of experiments were done (5) from which it was inferred that the polarized signal arises from a non-Boltzmann population of $P700^+$ radicals. However, $P700^+$ is isotropic. It was therefore hypothesized that the flow effect is a consequence of magnetic interaction of $P700^+$ with an anisotropic acceptor species. The radical pair mechanism provides a theoretical model in which such an interaction could occur.

It is the purpose of this Chapter to develop a quantitative model for the generation of the spin polarized signal due to PSI which reproduces the flow and no-flow results described above. We proceed in the following

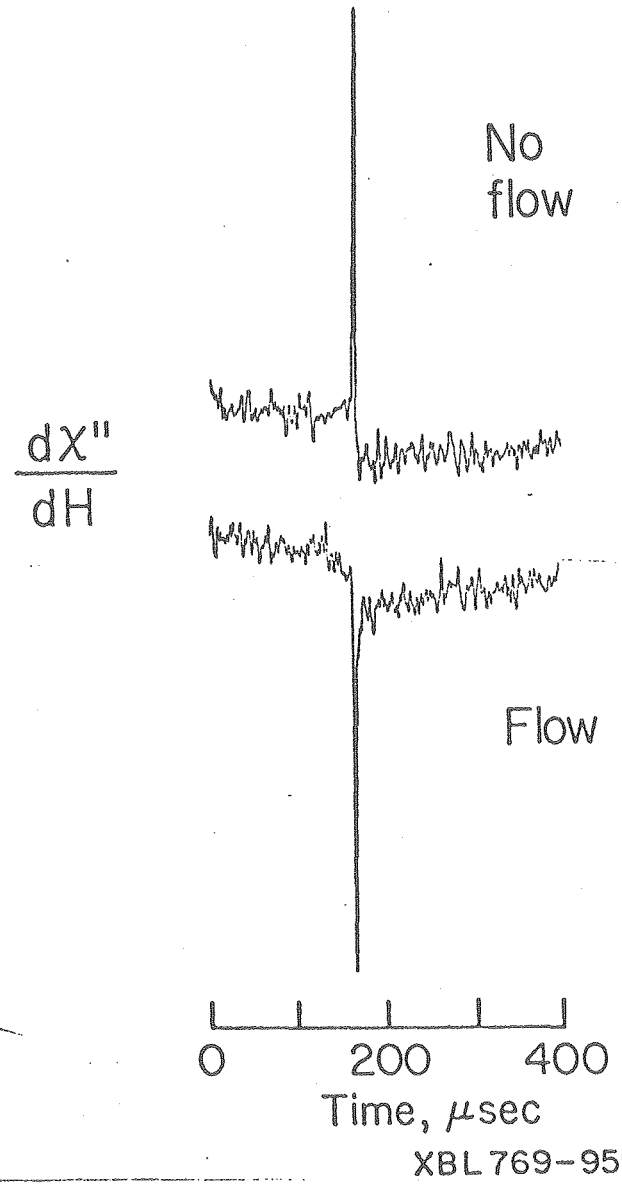

Figure 5-1. Kinetic traces of the EPR signal from spinach chloroplasts. The signal under flowing (bottom) and non-flowing (top) conditions for a single field position are contrasted (from reference 5).

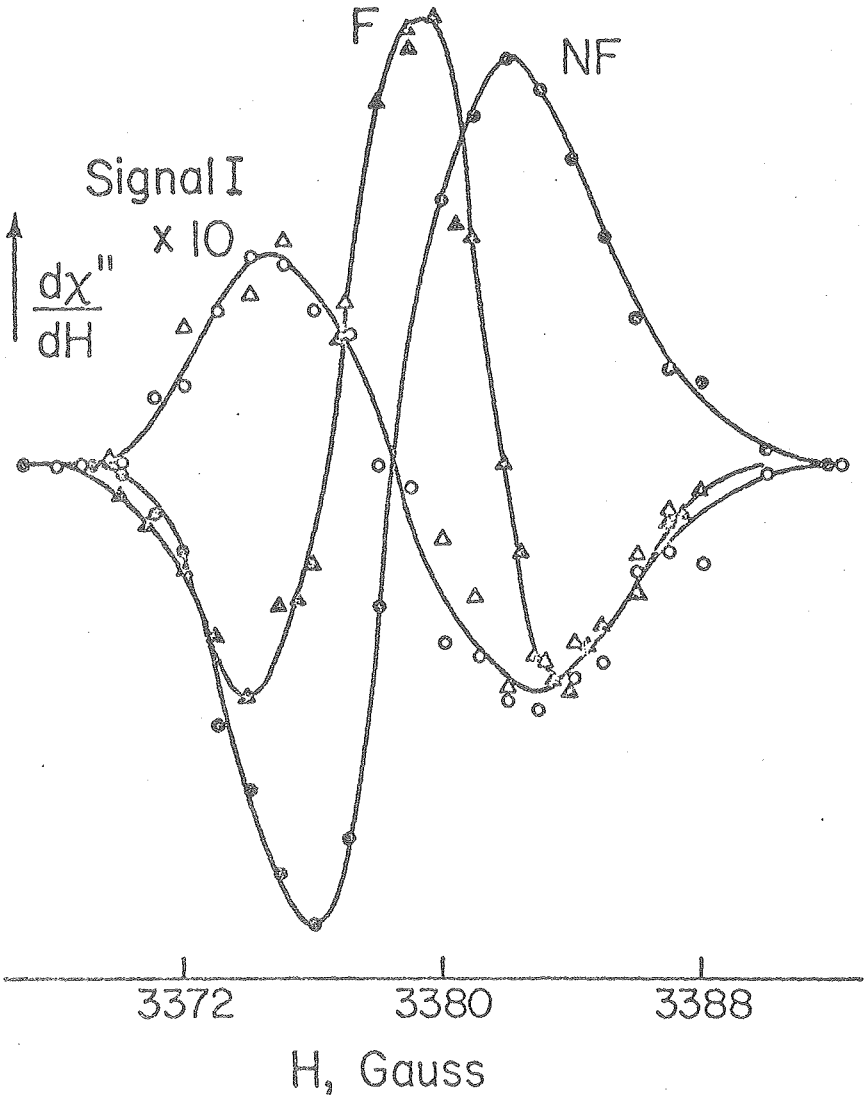

Figure 5-2. EPR spectra of the emission signal and signal I in spinach chloroplasts under flow and no flow conditions. Signal I: △, flowing sample and ○, non-flowing sample. Polarized signal: ▲, flowing sample and ●, non-flowing sample. Flow rate, 0.6 ml/min; microwave power, 25 mW; 4G modulation amplitude; chlorophyll content, 2.5 mg/ml. Each point in the emission signal spectrum is the average of 200 events obtained with a 10 μsec time constant. The amplitude of Signal I is multiplied by 5 for the purpose of display (from reference 5).

stepwise fashion:

(1) Formulation of a theoretical model for the evaluation of spin polarization in membrane-bound radicals, including the effects of g tensor anisotropy.

(2) Construction of the possible sequences of electron transfer events in PSI.

(3) Calculation of the predicted spin polarized signals from the hypotheses listed in (2) using the theory developed in (1).

(4) Comparison of the predictions of (3) with the experimental results. This results in the confirmation of a particular hypothesis, *i.e.* that the sequence of acceptors is

$$P700 \rightarrow A_1 \rightarrow A_2 \rightarrow P430$$

where A_2 is X, and A_1^- is an isotropic molecular species with a g value close to that of $P700^+$, possibly a Chl^- anion.

The existence of A_1 was suggested by the optical experiments of Sauer *et al.* (6) These authors monitored the kinetics of reduction of $P700^+$ following flash excitation in reduced PSI membrane fragments, and found evidence for the existence of two acceptors preceding ferredoxins A and B. Further confirmation of this work has been obtained by Ke and Shuvalov (7), who measured a light-induced difference spectrum attributable to A_1. The resultant spectrum is consistent with the hypothesis that A_1 is a chlorophyll species.

5.2 The Radical Pair Mechanism

A. Introduction to Spin Polarization

Consider an ensemble E of identical spin $\frac{1}{2}$ systems in a high magnetic field $\underset{\sim}{H}_o$. The members of E are aligned either parallel or antiparallel to $\underset{\sim}{H}_o$, *i.e.* the spin wavefunction is either $|\alpha\rangle$ or $|\beta\rangle$.

If the spin system is at thermodynamic equilibrium, the fraction of ensemble members in the α state as compared to the β state is given by the Boltzmann factor

$$\frac{n_\alpha}{n_\beta} = \frac{e^{-E_\alpha/kT}}{e^{-E_\beta/kT}} \qquad (5\text{-}1)$$

where E_α and E_β are the energies of the α and β states, respectively. The EPR intensity is proportional to the population difference, $n_\alpha - n_\beta$.

However, if it is possible (*e.g.* in fast kinetic experiments) to observe the ensemble prior to the establishment of equilibrium, one may detect a non-Boltzmann population of spin states. Such an ensemble is said to be spin polarized; the polarization, ρ, is proportional to the value of $n_\alpha - n_\beta$. ρ is defined to be +1 when all spins are in the α state, and -1 when all spins are in the β state.

The above definition applies strictly only to non-interacting ensembles of spin $\frac{1}{2}$ particles. It is possible to extend the definition to more complex systems. In the

general case, one needs to look at the equilibrium populations of the set of spin sublevels, and define a polarized ensemble in terms of deviations from these equilibrium populations. We now consider a specialized example; an interacting two-spin system which at some future time will undergo a non-adiabatic separation to two separate spin $\frac{1}{2}$ systems.

Let the wavefunction of the coupled system be ψ; this will be a linear combination of the direct product states, $\alpha(1)\beta(1)$, $\alpha(1)\beta(2)$, $\alpha(2)\beta(1)$, and $\alpha(2)\beta(2)$. The non-adiabatic decoupling will separate ψ into two non-correlated states ϕ_1 and ϕ_2, where $\phi_1 = \alpha(1)$ or $\beta(1)$, and $\phi_2 = \alpha(2)$ or $\beta(2)$. The net result is two non-interacting ensembles E_1 and E_2, with populations $n_{1\alpha}$, $n_{1\beta}$, $n_{2\alpha}$, and $n_{2\beta}$.

We can then calculate the polarizations ρ_1 and ρ_2 of E_1 and E_2 from the above formula, *e.g.* $\rho_1 = n_{1\alpha} - n_{2\alpha}$. The probability of producing an $\alpha(1)$ or $\beta(1)$ state from the coupled system is proportional to the expectation value of the z component of spin of electron 1, S_{1z}, on ψ; we can thus write (assuming that $\rho_1 + \rho_2 = 0$)

$$\begin{aligned} \rho_1 &= 2\langle\psi|S_{1z}|\psi\rangle = \langle\psi|S_{1z}-S_{2z}|\psi\rangle \\ \rho_2 &= 2\langle\psi|S_{2z}|\psi\rangle = -\rho_1 \end{aligned} \qquad (5\text{-}2)$$

where ρ_1 and ρ_2 have been normalized so as to fall between +1 and -1.

The time dependence of ρ is found by solving the time dependent Schroedinger equation for $\psi(t)$ and substituting into eq. (5-2). The experimental value of the polarization

is determined by integrating over time in accordance with the experimental conditions.

B. The Genesis of Radical Pair Theory

The radical pair mechanism was originally proposed to explain the anamolous spin polarization that develops in radicals observed in solution after creation of a radical pair or after a spin selective reaction. Eventually the radical pair constituents diffuse away from one another to produce the two non-interacting spin $\frac{1}{2}$ ensembles described in A; these ensembles were sometimes found to be spin polarized, with the polarization dependent upon the hyperfine interactions and g values of the two radical species.

The first adequate quantitative explanation of this phenomenon was given by Adrian (8), who calculated $\psi(t)$ for the radical pair by including the effects of radical-radical diffusion on the magnetic interactions in a simple manner (the exchange interaction was taken to be a step function). He concluded that it is the difference in magnetic environments (*e.g.* g tensor and hyperfine values), which leads to spin polarization, and that it is necessary for the radicals to diffuse apart and then return for substantial polarization (relative to the equilibrium population difference) to develop.

The above problem is difficult because three-dimensional diffusive motion is quite complex. More sophisticated models were therefore developed by Freed (stochastic-Liouville approach) (9) and Adrian (vector model) (10) which are qualitatively similar to Adrian's original formulation both conceptually and in predicted results, but treat the diffusive motion more rigorously.

We shall be concerned with a simpler problem than the one posed above; a system of membrane-bound radicals where the non-adiabatic separation occurs via electron transfer. For this case, Adrian's original theory is an accurate representation, and it remains only to incorporate physical characteristics relevant to the membrane bound systems (*e.g.* anisotropy, radical lifetimes). In the sections that follow we review Adrian's theory from the context of the above physical system, and develop a set of appropriate spin polarization equations.

C. Development of the Spin Polarization Equations

As a paradigmatic example we treat in detail a simplified two spin system. The system contains two molecules, a donor (D) and an acceptor (A), initially in their ground states, and rigidly fixed with respect to one another. As a first step D is excited to its first excited state, D*, by absorption of a photon. The electron transfer reaction $D^*A \rightarrow D^+A^-$ then occurs; this produces a radical pair state. At some

time τ the electron leaves A^- for a further acceptor; the final result is an ensemble of D^+ molecules in either an α or β state. We proceed to calculate the time-dependent polarization for this ensemble by determining the time-dependent coupled spin wave function $\psi(t)$ and substituting into eq. 5-2

The spin Hamiltonian for D* is given by

$$\mathcal{H}_{D^*} = g_D \beta H_o S_z + J_D S_{1z} S_{2z} + \Sigma A_i^{(D)} M_{iz}^{(D)} S_z \qquad (5\text{-}3)$$

where we have neglected the dipolar interaction and assumed that $\hat{g}_D$, $\hat{J}_D$, and $\hat{A}_i^{(D)}$ are isotropic. The pure singlet

$$|S\rangle = \frac{1}{\sqrt{2}} [\alpha(1)\beta(2) - \alpha(2)\beta(1)]$$

is an eigenstate of this Hamiltonian; because of the selection rule $\Delta S = 0$ for an electronic transition, the excitation of D to D* prepares the system in a singlet state.

After electron transfer we have a new magnetic Hamiltonian, the radical pair Hamiltonian;

$$\mathcal{H}_{RP} = g_D \beta H_o S_{1z} + g_A \beta H_o S_{2z} + [\Sigma A_i^{(D)} M_{iz}^{(D)}] S_{iz} + [\Sigma A_j^{(D)} M_{jz}^{(D)}] S_{2z} - J_{RP}(2 S_{1z} S_{2z} + \tfrac{1}{2}) \qquad (5\text{-}4)$$

where g_A, $A^{(A)}$ and J_{RP} are isotropic but may have different values from g_D, $A_{Di}^{(D)}$, and J_D. In particular, the exchange interaction will be greatly reduced in the radical pair owing to decreased orbital overlap.

If $g_D \neq g_A$, or $(\Sigma\ A_j^{(A)} M_{jz}^{(A)}) \neq (\Sigma\ A_i^{(D)} M_{iz}^{(D)})$, the singlet $|S\rangle$ is not an eigenfunction of $\mathcal{H}_{RP}$. The correct eigenfunctions can be determined by splitting $\mathcal{H}_{RP}$ into two parts;

$$\mathcal{H}_D = \tfrac{1}{2}(g_D + g_A)\beta H_o S_z - J_{RP}(2S_{Az}S_{Dz} + \tfrac{1}{2})$$

$$+ \tfrac{1}{2}[\Sigma_i\ A_i^{(D)} M_{iz}^{(D)} + \Sigma_j\ A_j^{(D)} M_{jz}^{(D)}] \cdot S_z$$

$$\mathcal{H}_{OD} = \tfrac{1}{2}(g_D - g_A)\beta H_o + \tfrac{1}{2}[\Sigma_i\ A_i^{(D)} M_{iz}^{(D)} - \Sigma_j\ A_D^{(A)} M_{jz}^{(A)}]$$

$$\times (S_{Dz} - S_{Az}) \qquad (5\text{-}5)$$

where we have now labelled the spin operators by S_{Dz} and S_{Az} (corresponding to the electron on D and A, respectively) and

$$S_z = S_{Dz} + S_{Az}$$

$\mathcal{H}_D$ is diagonal in the basis $\{S, T_o, T_{+1}, T_{-1}\}$. $\mathcal{H}_{OD}$ generates one off-diagonal matrix element,

$$\langle S|\mathcal{H}_{OD}|T_o\rangle = \tfrac{1}{2}(g_D - g_A)\beta H_o + \tfrac{1}{2}[\Sigma_i\ A_i^{(D)} M_{iz}^{(D)} - \Sigma_j\ A_j^{(A)} M_{jz}^{(A)}]$$

$$= H_{AD} \qquad (5\text{-}6)$$

The Hamiltonian matrix is thus

$$\mathcal{H}_{RP} = \begin{array}{c|cccc} & S & T_o & T_{+1} & T_{-1} \\ \hline S & -J & H_{AD} & 0 & 0 \\ T_o & H_{AD} & J & 0 & 0 \\ T_{+1} & 0 & 0 & J+\bar{g}\beta H & 0 \\ T_{-1} & 0 & 0 & 0 & J-\bar{g}\beta H \end{array} \qquad (5\text{-}7)$$

where $\bar{g} = (g_A + g_D)/2$, and we have omitted the diagonal hyperfine energies (these will be added later in accordance with sec. 1-3).

The four eigenstates are obtained by diagonalizing $\mathcal{H}_{RP}$:

$$\begin{aligned}
\phi_1 &= |T_{+1}\rangle & E_1 &= J + \bar{g}\beta H \\
\phi_2 &= |T_{-1}\rangle & E_2 &= J - \bar{g}\beta H \\
\phi_+ &= [(\omega+J)/2\omega]^{1/2}|S\rangle + [(\omega-J)/2\omega]^{1/2}|T_o\rangle & E_+ &= \omega \\
\phi_- &= [(\omega-J)/2\omega]^{1/2}|S\rangle - [(J+\omega)/2\omega]^{1/2}|T_o\rangle & E_- &= -\omega
\end{aligned} \tag{5-8}$$

where $\omega = (H_{AD}^2 + J_{RP}^2)^{1/2}$.

Calculation of $\psi(t)$ is now straightforward. We first determine $\psi(0)$;

$$\psi(0) = |S\rangle = \langle\phi_+|S\rangle|\phi_+\rangle + \langle\phi_-|S\rangle|\phi_-\rangle \tag{5-9}$$

because $\langle\phi_1|S\rangle = \langle\phi_2|S\rangle = 0$. We can write

$$\psi(t) = \sum_i c_i(t)\phi_i \tag{5-10}$$

Now, $\mathcal{H}_{RP}$ is not explicitly time dependent; the wave-function evolves with time because it was prepared in a non-stationary state in the radical pair basis. For such a system the solution of the time dependent Schroedinger equation for the coefficients $c_i(t)$ is trivial;

$$i\hbar\frac{\partial\psi}{\partial t} = \mathcal{H}\psi \tag{5-11}$$

$$\Rightarrow \quad \sum_i i\hbar \frac{\partial c_i(t)}{\partial t} |\psi_i> = \sum E_i \psi_i c_i(t)$$

Multiplying by ψ_j and integrating;

$$i\hbar \frac{\partial c_j}{\partial t} = E_j \tag{5-12}$$

$$\ell n \frac{c_j(t)}{c_j(0)} = \int_0^t -\frac{E_j}{i\hbar}\, dt$$

$$\Rightarrow \quad c_j(t) = c_j(0) e^{-iE_j t/\hbar}$$

Substituting into eq. (5-10), and using eq. (5-9) to determine the $c_j(0)$,

$$\psi(t) = c_+(0) e^{-iE_+ t/\hbar} |\phi_+> + c_-(0) e^{-iE_- t/\hbar} |\phi_-> \tag{5-13}$$

where $E_+ = \omega$, $E_- = -\omega$, $c_+(0) = <\phi_+|S>$, and $c_-(0) = <\phi_-|S>$.

The spin polarization, $\rho(t)$, can now be found by substituting eq. (5-13) into eq. (5-2) and evaluating this. The resultant expression is

$$\rho(t) = \frac{2H_{AD}{}^{\circ}J}{\omega^2} \sin^2 \omega t \tag{5-14}$$

We will wish to consider a more general case in which $\psi(0)$ is given, not by $|S>$, but by some linear combination $c_S(0)|S> + c_T(0)|T_o>$. The development proceeds as above except that $c_+(0)$ and $c_-(0)$ are now given by

$$c_+(0) = c_S(0)\cdot\langle\phi_+|S\rangle + c_T(0)\cdot\langle\phi_+|T_o\rangle$$
$$c_-(0) = c_S(0)\cdot\langle\phi_-|S\rangle + c_T(0)\cdot\langle\phi_-|T_o\rangle \qquad (5\text{-}15)$$

The spin polarization is then

$$\begin{aligned}\rho(t) = {} & [c_T(0)c_S^*(0) + c_T^*(0)c_S(0)] \\ & \times \{\cos^2\omega t + [(H_{AD}^2 - J^2)/\omega^2]\sin^2\omega t\} \\ & + (iJ/\omega)[c_T(0)c_S^*(0) - c_T^*(0)c_S(0)](\sin 2\omega t) \\ & + 2(JH_{AD}/\omega^2)\sin^2\omega t[|c_S(0)|^2 - |c_T(0)|^2] \end{aligned} \qquad (5\text{-}16)$$

D. Modification of the Radical Pair Mechanism to Include Tensor Anisotropy

Inclusion of g tensor anisotropy in eq. (5- 4) is straightforward, we rewrite the radical pair Hamiltonian as

$$\begin{aligned}\mathcal{H}_{RP} = {} & \beta \underset{\sim}{H}_o[\hat{g}_D\cdot\underset{\sim}{S}_D + \hat{g}_A\cdot\underset{\sim}{S}_A] - J(2\underset{\sim}{S}_D\cdot\underset{\sim}{S}_A + \tfrac{1}{2}) \\ & + \sum_i A_i^{(D)}\underset{\sim}{I}_i^{(D)}\cdot\underset{\sim}{S}_D + \sum_j A_j^{(A)}\underset{\sim}{I}_j^{(A)}\cdot\underset{\sim}{S}_A \end{aligned} \qquad (5\text{-}17)$$

where all the terms retain identical meanings as in eq. (5-4), but $\hat{g}_A$ and $\hat{g}_D$ are now tensor quantities.

Solutions to this Hamiltonian are obtained by diagonalizing the $\mathcal{H}_{RP}$ matrix in the basis set $\{S, T_o, T_{+1}, T_{-1}\}$. In Appendix D, we evaluate the matrix elements of $\mathcal{H}_{RP}$ and show that

(1) The spins are quantized in the direction of the effective field, $\underset{\sim}{h}' = \underset{\sim}{H}_o\cdot(\hat{g}_A + \hat{g}_D)$

(2) For small values of g anisotropy [*i.e.* max $(|g_{ii} - \bar{g}|) \ll \bar{g}$] the $\langle S|\mathcal{H}_{RP}|T_\pm\rangle$ matrix elements are negligible.

$$(3)\quad H_{AD} = \langle S|\mathcal{H}_{RP}|T_o\rangle = \frac{1}{2}\beta \underset{\sim}{H}_o \cdot (\underset{\sim}{\hat{g}}_A - \underset{\sim}{\hat{g}}_D)\cdot\hat{z} + \frac{1}{2}\sum_i [A_i^{(D)} M_{iz}^{(D)}] \qquad (5\text{-}18)$$

where $\hat{z}$ is a unit vector in the direction of $\underset{\sim}{h}'$, and $m_{iz}^{(A)}$ is the z component of the nuclear spin of the ith nucleus on molecule D. Note that the off-diagonal matrix element is now orientation dependent.

From points (1) and (2) we can adopt an S-T_o basis set, with the α and β spin functions quantized in the direction of $\hat{z}$.

The Hamiltonian matrix is then

	S	T_o
S	+J	H_{AD}
T_o	H_{AD}	-J

This is identical to the matrix obtained from eq. (5-4), except that H_{AD} is given by eq. (5-18). The expressions derived previously for the eigenvectors (eq. 5-8), eigenvalues (5-8), and spin polarization (eq. 5-16) can therefore be utilized as they are. In the following section we apply these results to calculate the spin polarization for membrane-bound radicals.

5.3 CIDEP of Membrane-Bound Radicals

A. General Theory

The radical pair mechanism described in Chapter 1 has been applied primarily to diffusive systems. In these systems, it is necessary for the two radicals to diffuse apart and then re-encounter one another in order for appreciable polarization to develop.

To simplify the ensuing calculations, we set $|c_S(0)|^2 = 1$, $|c_T(0)|^2 = 0$, corresponding to the assumption of creation of the radical pair from an initial singlet state (see the Discussion for the justification of this assumption in Photosystem I). The results which follow could easily be generalized by retaining the terms dependent upon $c_S(0)$ and $c_T(0)$.

The simplified expression for the polarization during a time interval t of constant J is, from eq. (5-14)

$$\rho(t) = (2H_{AD}J/\omega^2) \sin^2\omega t \qquad (5\text{-}20)$$

This expression will be larger than the thermal population difference ($\sim 10^{-3}$ at room temperature) only if H_{AD} and J are of comparable magnitude for a time interval $\sim \omega^{-1}$. Because ω^{-1} is typically of the order of 10^{-9} sec, and the diffusion correlation time is $\sim 10^{-12}$ sec, this condition is ordinarily not satisfied for freely diffusing radicals in solution, and the net polarization upon initial separation of the radicals is negligible. After a re-encounter,

other terms in eq. (5-16) become significant, and the polarization develops as described by Adrian's model.

We consider here a system in which the radical species are bound to a membrane at fixed sites. A radical pair is produced by transfer of an electron from a donor molecule (D) to an initial acceptor (A_1). The electron is then transferred to successive acceptors in a fixed sequence.

We shall assume that all of the electron transfers are irreversible. This assumption is not necessary, but it simplifies the calculations considerably. (It is a good assumption in Photosystem I, since the electron transfer has a quantum efficiency greater than 90%) (17). Then, transfer away of an electron is analogous to diffusion. However, there can be no "return" of the radical pair, and the development of polarization has an origin distinct from that of diffusive systems.

The development of spin polarization on D^+ is a consequence of the time evolution of the coupled spin wavefunctions of the unpaired electrons on D^+ and A_n^-. This process will change the polarization with time as long as there is a large enough exchange coupling, J_n, between D^+ and A_n^-. We therefore must consider the interaction of all radical pairs formed by successive electron transfer in which J_n is appreciable.

We will assume that J_n is zero for $n \geq 3$, because $A_3 \ldots A_n$ are presumably too distant from D^+ to have a

significant exchange coupling. Then, there are two reasonable models for the development of polarization. The one-site model assumes that J_2 is also negligible, and that only the interaction $D^+ - A_1^-$ need be considered. The two-site model assumes that both J_1 and J_2 are significant, and that the interaction $D^+ - A_2^-$ must be included in a calculation of the spin polarization.

B. One Site Model

An acceptor radical A_n^- is characterized by a lifetime, τ_n, which determines the duration of the existence of the radical pair $D^+ - A_n^-$. (This is in fact the case in Photosystem I, where $P700^+$ has a lifetime of 30 msec which is much longer than the lifetimes of either A_1^- or A_2^-). The prabability that the radical pair will exist for time t is given by e^{-t/τ_n}. The time-averaged polarization for the one site model is then

$$\rho(\tau_1) = \frac{2}{\tau_1} \int_0^\infty e^{-t/\tau_1} (H_1 J_1/\omega_1^2) \sin^2 \omega_1 t \, dt \qquad (5\text{-}21)$$

$$= 4H_1 J_1 \tau_1^2/(1 + 4\omega_1^2 \tau_1^2)$$

where H_1 is the off-diagonal matrix element H_{AD} for the radical pair $D^+ - A_1^-$, and $\omega_1 = (H_1^2 + J_1^2)^{1/2}$.

Equation (5-21) predicts a large value for ρ for suitable values of J_1 and τ_1. This is possible because, in contrast to the diffusive system, τ_1 may well be of the order of ω^{-1}. Thus, if J_1 is of the order of H_1, eq. (5-21) may attain values greatly in excess of the thermal population difference.

C. Two Site Model

For this model we need to calculate the net polarization on D^+ after the electron leaves A_2. The spin wave function at the time of transfer to A_2 (*i.e.* immediately after the electron has left A_1) is given by

$$\psi_1(t_1) = |S\rangle\cdot[\cos(\omega_1 t_1) - (J_1/\omega_1)\sin(\omega_1 t_1)] - |T_o\rangle\,[(H_1/\omega_1)\sin(\omega_1 t_1)] \qquad (5\text{-}22)$$

where t_1 is the duration of existence of $D^+ - A_1^-$.

The polarization after the radical pair $D^+ - A_2^-$ has existed for time t_2 can be found by obtaining the coefficients $c_S(t_1)$, $c_T(t_1)$ from eq. (5-22) and substituting into eq. (5-16).

$$\rho(t_1,t_2) = \frac{2H_1J_1}{\omega_1^2}\sin^2\omega_1 t_1\left(1 - \frac{2J_2^2}{\omega_2^2}\sin^2\omega_2 t_2\right) + \frac{J_2H_1}{\omega_1\omega_2}\sin(2\omega_1 t_1)\sin(2\omega_2 t_2) + \frac{2H_2J_2}{\omega_2^2}\sin^2\omega_2 t_2\left(1 - \frac{2H_1^2}{\omega_1^2}\sin^2\omega_1 t_1\right)$$

Time averaging over t_1 and t_2, we obtain

$$\rho(\tau_1,\tau_2) = \frac{4H_1J_1\tau_1^2}{1+4\omega_1^2\tau_1^2}\cdot\left(1-\frac{4J_2\omega_2^2}{1+4\omega_2^2\tau_2^2}\right)$$

$$+\frac{4J_2H_1\tau_1\tau_2}{1+4\omega_1^2\tau_1^2}\cdot\left(\frac{1}{1+4\omega_2^2\tau_2^2}\right)$$

$$+\frac{4H_2J_2\tau_2^2}{1+4\omega_2^2\tau_2^2}\cdot\left(1-\frac{4H_1^2\tau_1^2}{1+4\omega_1^2\tau_1^2}\right) \qquad (5\text{-}24)$$

5.4 Orientation Effects

We now investigate the effect of g tensor anisotropy on the expressions for the polarization derived in the previous section. The effect arises from the dependence of the matrix elements H_n on the orientation of the radicals in the applied magnetic field $\underset{\sim}{H}_o$. We shall restrict our interest to a situation where only one radical involved in the development of spin polarization on D^+ is anisotropic; the coordinate system defining the orientation is then chosen to be the principal axis system of the anisotropic species. The location of $\underset{\sim}{H}_o$ is specified by a magnitude, $|H|$, and the spherical polar angles θ and ϕ.

$$\rho_i = \frac{2}{\pi}\int_0^{\pi/2}\int_0^{\pi/2}\rho_i(\theta,\phi)P(\theta,\phi)\,d\theta d\phi \qquad (5\text{-}25)$$

where $P(\theta,\phi)$ is the probability that the radicals possess orientation (θ,ϕ) relative to $\underset{\sim}{H}_o$, and $\rho_i(\theta,\phi)$ is the spin

density developed on D^+ in hyperfine state i from either eq. (5-21) or eq. (5-24), with $H_n(\theta,\phi)$ given by eq. (D-10) of Appendix D.

We anticipate the next section and assume that the g tensor of D^+ is predominantly isotropic. For the one site model, we assume that A_1 is anisotropic; then, substitution of eqs. (5-21) and (5-18) into (5-25) yields, with suitable rearrangement,

$$\rho_i(\text{one site}) = \frac{8}{\pi}\tau_1^2 J_1 \cdot \left[\int_0^{\pi/2}\int_0^{\pi/2} \frac{\Delta g_1(\theta,\phi)P(\theta,\phi)\, d\theta d\phi}{I_1(\theta,\phi)} + \frac{\alpha_i}{2}\int_0^{\pi/2}\int_0^{\pi/2} \frac{P(\theta,\phi)\, d\theta d\phi}{I_1(\theta,\phi)}\right] \tag{5-26}$$

where

$$\Delta g_n = -\frac{1}{2}[g_n^x \sin^2\theta\cos^2\phi + g_n^y \sin^2\theta\sin^2\phi + g_n^z \cos^2\theta - g_D] \tag{5-27}$$

g_n^x, g_n^y, and g_n^z are the principal g tensor components of A_n^-, g_D is the isotropic g value of D^+, α_i is the total hyperfine field, $\sum_j A_j^{(D)} M_{ji}^{(D)}$, of D^+ in hyperfine state i, and $I_n(\theta,\phi) = 1 + 4\omega_n^2(\theta,\phi)\tau_n^2$.

Defining

$$U_n = \frac{2}{\pi}\int_0^{\pi/2}\int_0^{\pi/2} \frac{\Delta g_n(\theta,\phi)P(\theta,\phi)\, d\theta d\phi}{I_n(\theta,\phi)} \tag{5-28}$$

$$V_n = \frac{2}{\pi}\int_0^{\pi/2}\int_0^{\pi/2} \frac{d\theta d\phi\ \ P(\theta,\phi)}{I_n(\theta,\phi)} \tag{5-29}$$

we have

$$\bar{\rho}_i(\text{one site}) = 4\tau_1^2 J_1 (U_1 + \frac{\alpha_i}{2} V_1) \tag{5-30}$$

For the two site model, we again anticipate the next section and assume that the g tensor of only A_2^- is anisotropic, and that $g_1 = g_D$ are both scalars. Then, noting that $H_1 = \alpha_i/2$ (since $\Delta g_1 = 0$) and that both H_1 and ω are orientation-independent, we obtain

$$\bar{\rho}_i(\text{two site}) = \frac{\alpha_i}{2}\left[\frac{4J_1\tau_1^2}{1+4\omega_1^2\tau_1^2}\cdot(1-4J_2^2\tau_2^2V_2)\right.$$

$$+\frac{4J_2\tau_1\tau_2}{1+4\omega_1^2\tau_1^2}\cdot V_2 + 4\tau_2^2J_2V_2\cdot\left(1-\frac{4H_1^2\tau_1^2}{1+4\omega_1^2\tau_1^2}\right)\Big]$$

$$+4U_2\tau_2^2J_2\cdot\left(1-\frac{4H_1^2\tau_1^2}{1+4\omega_1^2\tau_1^2}\right) \qquad (5\text{-}31)$$

The experimental EPR intensity I_D of D^+ as a function of field position H is given by

$$I_D(H) = \sum_{\substack{\text{all hyperfine}\\ \text{configurations}\\ \text{of } D^+}} (-\bar{\rho}_i)\, e^{(H-H_i^\circ)^2/\delta^2} \qquad (5\text{-}32)$$

where H_i° is the center of hyperfine line i, and δ is the half-width of the individual hyperfine lines. Note that a positive value of $\bar{\rho}_i$ results in a negative EPR intensity, *i.e.* $\bar{\rho}_i > 0$ means that hyperfine line i will be found in emission. This is the case because ρ is defined as $N_\alpha - N_\beta$, and an excess population of the state higher in energy (α) leads to a net emission of radiation.

In the next section, we examine the ability of eqs. (5-30) and (5-31) to predict the intensity patterns of the signals observed in Photosystem I, and thereby deduce a mechanism for the development of this polarization.

5.5 CIDEP in Photosystem I

A. General Discussion

Figure 5-2 displays the CIDEP signals from flow oriented and from randomly oriented broken spinach chloroplasts. The effect of the velocity gradient in the configuration of the EPR spectrometer is to orient the short axis of the thylakoid membranes in the chloroplasts normal to the applied magnetic field (5,11).

Reference (5) presents arguments to support the view that the CIDEP signals from both the oriented and the unoriented systems are due to the $P700^+$ cation radical. We shall adopt this as a working hypothesis which is supported by the calculations which follow.

The possible assignments of electron acceptors in photosystem I and the results of the previous section suggest two alternate schemes for the development of spin polarization: (1) acceptor A_1 is the species X, polarization develops as in the one-site model; (2) acceptor A_1 is a small organic molecule, possibly Chl, and A_2 is X, polarization develops as in the two-site model.

We have rejected two other conceivable schemes. A one-site model with Chl as A_1 would be inappropriate because it would not account for the orientation dependence of the polarized signal. A two-site model with X as A_1, bound Fd (center A or B) as A_2, would fail to correctly predict the mixed-emissive-enhanced absorptive pattern of the oriented signal for much the same reason as the one-site model (see the analysis of the one-site model for details), *i.e.* the term proportional to the hyperfine field of $P700^+$ would be too small.

It has been shown (11) that the x component of the g tensor of X^- (1.78) is oriented parallel to the short axis of the thylakoid membranes. Thus, the result of flow orientation is to align the g_x component normal to $\underset{\sim}{H}_o$.

The effect of orientation upon the development of polarization can now be determined for both the one and two-site models. The only orientation-dependent terms in eqs. (5-30) and (5-31) are the integrals U_i and V_i. We first note that U_1(one site) = U_2(two site), and V_1(one site) = V_2(two site), since all of these integrals involve the g tensor components, lifetime, and J value of the same anisotropic radical, X^-. We therefore drop the subscripts, and refer to these integrals as U and V, respectively.

For a random orientation (no flow), $P(\theta,\phi) = \sin\theta$ for all θ,ϕ, and

$$U^{NF} = \frac{2}{\pi} \int_0^{\pi/2} \int_0^{\pi/2} \frac{\Delta g_x^{NF} \sin\theta \, d\theta d\phi}{1 + 4\tau_x^2[J_x^2 + H_x^2(\theta,\phi)]} \qquad (5\text{-}33)$$

where τ_x is the lifetime of X^-, J_x is the exchange interaction between $P700^+$ and X^-, $H_x = (\alpha_i/2) + \Delta g_x^{NF}$, and $\Delta g_x^{NF}(\theta,\phi) = -(1.78 \sin^2\theta\cos^2\phi + 1.90 \sin^2\theta\sin^2\phi + 2.09 \cos^2\theta) + 2.0026$.

$$V^{NF} = \frac{2}{\pi} \int_0^{\pi/2} \int_0^{\pi/2} \frac{\sin\theta \, d\theta d\phi}{1 + 4\tau_x^2(J_x^2 + H_x^2)} \qquad (5-34)$$

For the oriented system, we set $\phi = \pi/2$ [*i.e.* $P(\theta,\phi) = \delta(\phi - \frac{\pi}{2})$]. Then, U and V are given by

$$U^F = \frac{2}{\pi} \int_0^{\pi/2} \frac{g_x^F(\theta) \, d\theta}{1 + 4\tau_x^2[J_x^2 + H_x^2(\theta)]} \qquad (5-35)$$

$$V^F = \frac{2}{\pi} \int_0^{\pi/2} \frac{d\theta}{1 + 4\tau_x^2[J_x^2 + H_x^2(\theta)]} \qquad (5-36)$$

where $\Delta g_x(\theta) = 1.90 \sin^2\theta + 2.09 \cos^2\theta - 2.0026$, and $H_x(\theta) = \Delta g_x(\theta) + \alpha_i/2$.

We have set g_D (the isotropic g value of the donor radical) equal to 2.0026, the experimental value for $P700^+$.

We can now evaluate the predictions for the polarized $P700^+$ lineshape in the context of the two models described above. There are three important experimental observations which a successful model must explain:

(1) The EPR spectrum from the unoriented sample is in total emission, *i.e.* the polarization is positive across the entire hyperfine field of $P700^+$. The signal

from the oriented system displays a mixed emissive-enhanced absorptive pattern; the polarization changes sign near $\alpha_i = 0$.

(2) The integrated area ratio for either polarized signal to the relaxed $P700^+$ signal is approximately 13:1 (*i.e.*, the population difference, $|N_\alpha - N_\beta|$, is more than 10 times the thermal value at 300°K, 10^{-3}). Because relaxation has already begun when the EPR measurements are made, the calculated area ratios should be in excess of 13:1.

(3) The area ratio of the unoriented signal to the oriented signal is between 1:1 and 2:1 (this number is at present experimentally uncertain).

B. One Site Model

We make the simplifying approximation that $|\Delta g_1| + |J_1| \gg |\alpha_i/2|$, since α_i for $P700^+$ is typically a few gauss (the peak to peak linewidth of the steady-state $P700^+$ signal is 7.5 G). Then, $\omega_1^2 \sim (\Delta g_1)^2 + J_1^2$, and we can write eq. (5-30) as

$$\bar{\rho}_i(\text{one site}) = k_1[\alpha_i + \Delta\underline{g}_1] \qquad (5\text{-}37)$$

where $k_1 = 2V\tau_1^2 J_1$, and $\Delta\underline{g}_1 = 2U/V$.

The $\Delta\underline{g}_1$ term is mathematically isomorphic to the Δg_1 value difference term in Adrian's original formulation. Both k_1 and $\Delta\underline{g}_1$ are independent of α_i.

The orientation dependence of eq. (5-37) is easily described. The integral U decreases by a factor of 10 to 100 upon orientation, *i.e.* $10 < U^{NF}/U^{F} < 100$. The integral V is relatively insensitive to orientation, $V^{NF}/V^{F} \sim 1$ for a wide range of τ_1 and J_1. Thus, $k_1^{NF}/k_1^{F} \sim 1$, and $10 < \Delta g_1^{NF}/\Delta g_1^{F} < 100$. The absolute amplitudes of Δg_1^{NF} and k_1 are dependent upon the specific values of τ_1 and J_1.

The one-site model correctly predicts the unoriented signal to be in total emission. Δg_1^{NF} is large and positive, the net polarization of the signal is sufficiently greater than the thermal population difference to account for the 13:1 area ratio of the polarized to unpolarized signal.

However, the one-site model fails completely for the oriented signal. The integral V is always small; therefore, k_1 is always small, less than .0025. Since Δg_1 is inversely proportional to k_1, the hyperfine term α_i is dominated by Δg_1 even for the oriented system. Furthermore, the total polarization for the oriented system is insufficient to account for the observed area ratios. Even for the most favorable values of τ_1 and J_1, the one-site model predicts that the oriented signal be much smaller than the unoriented signal (a factor of 10 or more) and in total emission. We therefore conclude that the one-site model is incapable of explaining our results.

C. Two Site Model

The polarization equation for the two-site model can be written as

$$\bar{\rho}_i(\text{two site}) = k_2(\alpha_i + \Delta g_2) \qquad (5\text{-}38)$$

where

$$k_2 = \frac{2J_1\tau_1^2}{1 + 4\omega_1\tau_1^2} + V\cdot[2\tau_1^2 J_2 + \frac{2\tau_1 J_2 \tau_2}{1 + 4\omega_1^2\tau_1^2}(1 - J_1 J_2 \tau_1\tau_2)]$$

$$\Delta g_2 = 2U\tau_2^2 J_2/k_2$$

We have again assumed that $|\alpha_i| \ll |J_1|$ and $|\alpha_i| \ll \Delta g_2$, so that ω_1, ω_2 are independent of α_i, and the term $[4H_1^2\tau_1^2/(1 + 4\omega_1^2\tau_1^2)] \ll 1$ in eq. (5-31), and thus has been neglected. Both k_2 and Δg_2 are then independent of α_i.

The major difference between the one and two site models is the amplitude of k. k_1 is directly proportional to the integral V, which is small for all values of τ_x and J_x. k_2 is a sum of two terms, one proportional to V and one independent of V. It is this second term, $2J_1\tau_1^2/(1 + 4\omega_1^2\tau_1^2)$, which can have a relatively large amplitude for appropriate values of τ_1 and J_1. This term arises from the interaction between $P700^+$ and A_1^-, and is large because Δg_1 is zero, so that $H_1 \ll J_1$. Effectively, the interaction of $P700^+$ with A_1^- produces a substantial polarization term proportional to the hyperfine field of $P700^+$. The corresponding term in the one site model is small because the only radical pair

interaction available here is $P700^+ - X^-$. For this radical pair, the g value difference is quite large relative to α_i for almost all orientations of X^-.

The experimental signals can be generated from eq. (5-38) when k_2 is sufficiently large (so that the polarized signals have enough amplitude relative to the relaxed signal) and when the average value of α_i (2-3 gauss) falls between g_2^F and g_2^{NF}. Then, for the oriented system the term linear in α_i dominates, the sign of $\bar{\rho}_i$ is governed by the sign of α_i, and a mixed emissive-enhanced absorptive signal results. For the unoriented system, the sum $(\alpha_1 + \Delta g_2)$ is positive for all values of α_i, and the polarized signal is seen in total emission.

In the next section, we simulate the polarized signals quantitatively by substituting eq. (5-38) into eq. (5-32) and summing over all configurations of the $P700^+$ hyperfine system.

5.6 Results of Calculations with the Two-Site Model

We first calculated an EPR spectrum for an isolated, relaxed $P700^+$ radical, assuming that it is an oxidized chlorophyll dimer (12). The relative amplitudes of the hyperfine coupling constants were obtained from NMR studies, (13) the magnitudes were scaled to the ENDOR result for the largest coupling constant (14).

The narrowing of the polarized signal (see Discussion) was introduced phenomenologically by decreasing the hyperfine

coupling constants. An identical adjustment was used to simulate the signals for both the oriented and unoriented systems.

Figure 5-3 displays the dependence of the EPR lineshape on the value of Δg_2 in eq. (5-38). For $\Delta g_2 < 0.7$ G, a nearly symmetrical mixed emissive-enhanced absorptive pattern results. For $\Delta g_2 > 4$ G, the signal is essentially in total emission. For 0.7 G $< \Delta g_2 <$ 4 G, a lineshape intermediate between the two previous cases is found.

The integrated area of a polarized signal depends linearly on k_2, and in a complicated fashion upon Δg_2. Table 5-1 lists the integrated area of $|dI/dH|$ as a function of Δg_2; the area of the unpolarized signal is set equal to 1.0, and the polarized signals normalized to this. The net integral area relative to the thermal equilibrium value for signal I at 300°K is found by multiplying the value in table 5-1 by $k_2/.001$ (.001 is the thermal population difference at 300°K).

From these results we can set limits on k_2 and Δg_2 such that the three fitting criteria for the experimental signals described above are satisfied. The general lineshape analysis requires that $0 < \Delta g_2^F < 0.7$ G, while $\Delta g_2^{NF} > 4$ G. Since the polarized signals have an area 3.5 - 6 times greater than that of the unpolarized signal when k_2 is set equal to .001, we require that $k_2/.001 > 3.7$, so that the net area

TABLE 5-1 RELATIVE AREA OF THE POLARIZED SIGNAL AS A FUNCTION OF Δg_2

(Signal I = 1.0)

Δg_2	Area
0.0	3.6
0.1	3.6
0.2	3.6
0.5	3.6
1.0	3.7
2.0	4.0
5.0	6.0
10.0	10.5

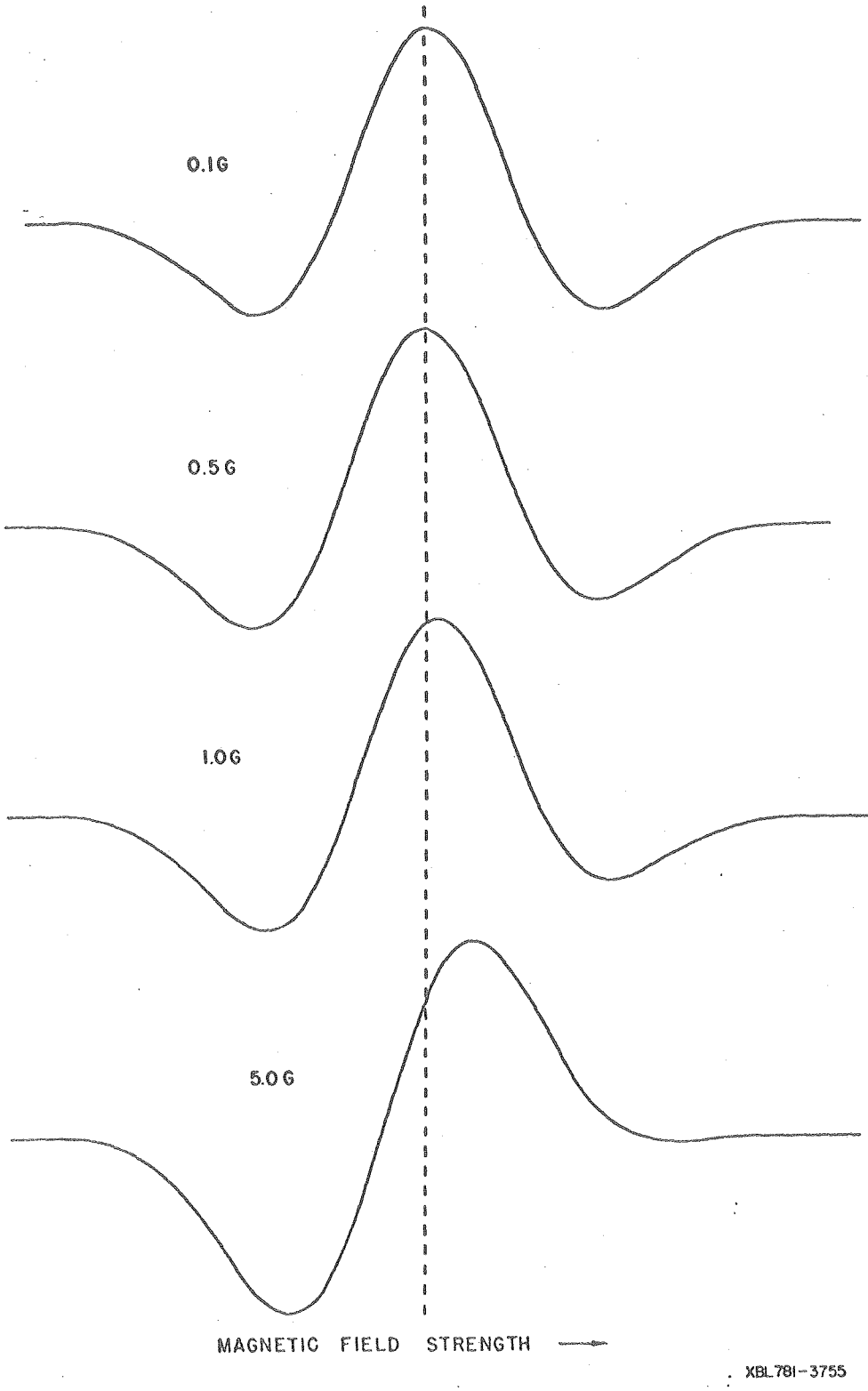

Figure 5-3. Simulated EPR spectra for the polarized signal for Δg_2 = 0.1 G, 0.5 G, 1.0 G and 5.0 G.

ratio is greater than 13:1. An upper limit of 2:1 on the area ratio of the oriented and unoriented signals can be insured by setting the limit $\Delta g_2^{NF} < 6.5$ G.

The values of k_2, Δg_2^F, and Δg_2^{NF} are determined by the parameters τ_1, τ_2, J_1 and J_2. Table 5-2 presents several sets of parameters for which k_2, Δg_2^F, and Δg_2^{NF} fall within the limits prescribed above. The exact values of the individual exchange energies or lifetimes are not critical; a small change in τ_n or J_n will produce a correspondingly small change in the simulated EPR spectrum.

It is clearly not possible to deduce the absolute magnitudes of any of the parameters from the data available at present. We can, however, set some limits on τ_1 and J_1. It is necessary that $\tau_1 \geq 250$ psec, and $J_1 < 200$ G, in order for k_2 to be greater than .0037. Once τ_1 and J_1 are fixed, a limited set of pairs (τ_2, J_2) will generate acceptable values of Δg_2^F and Δg_2^{NF}.

For a comparison of theory and experiment, we chose a value of τ_1 which is comparable to the lifetime of I^- observed in photosynthetic bacteria. We also chose $J_1 > J_2$, because A_1 is presumably in closer proximity to $P700^+$. The resulting values of J_1 and J_2 are reasonable ones for exchange interactions between organic molecules separated by 5 - 25 Å (15). They are also within the neighborhood of exchange interactions observed between electron acceptors in photosynthetic bacteria (16).

TABLE 5-2

Calculated Values of k_2, Δg_2^F and Δg_2^{NF} for selected values of τ_1, τ_2, J_1 and J_2. Area ratios are also calculated using Table 5-1.

J_1(G)	J_2(G)	τ_1(nsec)	τ_2(nsec)	k_2	Δg_2^{NF}(G)	Δg_2^F(G)	$\frac{A^F_{pol}}{A_{sig.I}}$	$\frac{A^{NF}}{A^F}$
10	75	1.0	2.1	.029	.45	5.7	106	1.84
50	10	0.35	0.35	.0046	.29	5.3	16.6	1.74
50	20	1.0	1.0	.0111	.17	5.1	40.0	1.69
100	10	0.35	0.35	.0045	.28	5.0	16.6	1.67
100	10	1.0	2.1	.067	.07	4.5	241	1.58
150	10	0.35	0.35	.0039	.33	6.0	13.1	1.92
150	20	1.0	0.35	.0047	.27	4.9	16.6	1.65
150	10	3.5	35	.0047	.076	6.4	16.9	2.02
100	150	0.35	0.035	.0051	.54	5.4	18.4	1.76
50	50	3.5	35	.0128	.08	4.5	46.1	1.58
75	3.5	0.35	35	.0047	.13	5.0	16.7	1.67

Figure (5-4) displays the theoretical and experimental EPR signals for the oriented and unoriented samples. The amplitudes of the theoretical signals, which are larger than the experimental signals, are reduced to account for the effects of relaxation. It is seen that excellent agreement is obtained within the limits of experimental error.

5.7 Discussion

The two-site model successfully predicts most of the important features of the polarized signals arising from oriented and unoriented chloroplasts. Many of the values of τ_1, τ_2, J_1 and J_2 which generate the correct lineshapes are consistent with what is known about early photosynthetic events. The model is relatively insensitive to the details of the calculations, *i.e.* small errors in the polarization function (as are introduced by neglect of $S\text{-}T_{\pm 1}$ mixing) would have a minimal effect on the predicted lineshapes and area ratios.

We believe that our results provide compelling (although indirect) evidence for the existence of an acceptor in Photosystem I preceding X. A radical pair mechanism with X as the initial acceptor is inconsistent with the mixed emissive-absorptive lineshape and relative area of the oriented signal. The presence of an earlier acceptor with an isotropic g value close to that of $P700^+$ provides a simple and satisfying explanation for these

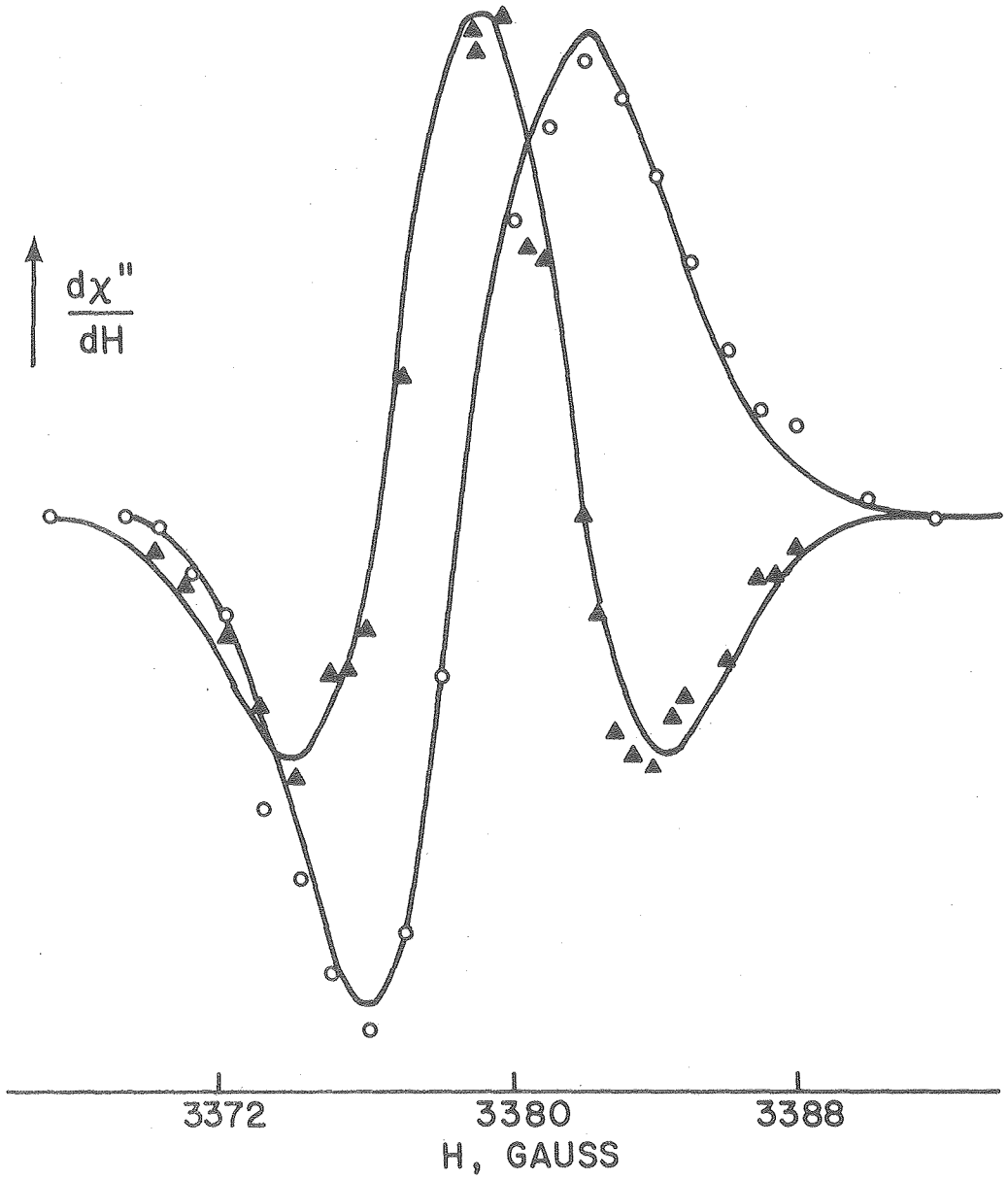

XBL775-4394

Figure 5-4. Calculated and experimental EPR spectra for the oriented and unoriented polarized signal from spinach chloroplasts. Values of the parameters used in the simulation are τ_1 = 0.35ns, τ_2 = 35ns, J_1 = 75G and J_2 = 3.5G. Solid triangles are experimental intensities for flow oriented chloroplasts. Open circles are experimental intensities for unoriented chloroplasts. Solid lines are theoretical curves.

features. The most likely candidate for A_1 at present is chlorophyll, because it is known to be present in sufficient quantity in reaction center preparations, and Chl^- has the requisite g tensor properties. Also, the midpoint reduction potential of chlorophyll a is 0.78 V (*vs.* NHE, in dimethylsulfoxide), (17) which is consistent with its role as an earlier acceptor than X. In analogy with photosynthetic bacteria, pheophytin might also be considered as a suitable candidate for A_1. However, Thornber *et al.* have found no pheophytin in enriched Photosystem I preparations (18). However, we have no direct information concerning the chemical identity of A_1.

The assignment of X as A_2 is also supported by our results. The alignment of the high field component of the g tensor of A_2 normal to the plane of the thylakoid membrane is required to produce the transformation from a totally emissive spectrum to a mixed emissive-enhanced absorptive spectrum upon orientation. Neither ferredoxin signal (centers A or B) displays the proper orientation in the membrane to generate the observed lineshape changes (11). The observation that the simulation of the oriented and unoriented signals, assuming that A_2 is X, gives excellent quantitative agreement is convincing evidence that this interpretation is valid.

Reference (4) proposed a triplet mechanism for the development of spin polarization. This can now be eliminated, because it never predicts a mixed emissive-enhanced absorptive lineshape. The triplet and radical pair mechanisms are

the only theories proposed to date to explain chemically induced spin polarization. The model presented here thus appears to be the only reasonable explanation which fits the experimental results.

The radical pair theory as developed by Adrian appears to be applicable to membrane-bound systems of radicals; the fundamental driving mechanism of spin polarization is, as in diffusive systems, $S\text{-}T_o$ mixing. The simple approach taken here provides an adequate explanation for the experimental results to date; however, more sophisticated treatments are possible and may be needed in the future. One could, for example, allow back transfer of an electron, or postulate more than one site for the electron in X, or investigate the possibility that at room temperature reduced or unreduced X may have appreciable unpaired spin density due to mixing in of low lying excited spin states. Development along these lines may become profitable when more data are available.

We have assumed throughout our calculations that the initial radical pair state is a singlet. This can be justified qualitatively without invoking any EPR results. The initial state of $P700^*$ is surely a singlet. If the rate of electron transfer from $P700^*$ to A_1 is comparable to that observed in bacterial systems (< 20 psec), (19,20) there would be insufficient time for intersystem crossing

to a triplet state to occur. Also, the unusual spin polarization of the reaction center triplet state in bacteria can be explained if electron transfer occurs from the excited singlet state (21). A spin flip as a consequence of electron transfer is quantum mechanically forbidden. We thus expect the radical pair to initially have the same singlet character as $P700^*$.

The narrowing of the polarized signal relative to the relaxed $P700^+$ signal is an interesting phenomenon for which we currently do not have a completley satisfying explanation. The polarized signal from the unoriented sample has a peak-to-peak linewidth of 5.6 G, as compared to the value of 7.5 G measured for the relaxed $P700^+$ signal. The polarized signal from the oriented sample is the derivative of a mixed emissive-enhanced absorptive lineshape, and therefore its linewidth cannot be compared directly with those of the other signals. However, good simulation of the oriented signal requires that the starting linewidth be narrowed to the value of 5.6 G found for the unoriented signal.

The above observations are not predicted by the radical pair mechanism. The polarization is either a constant across the hyperfine field (Δg_2 large) or linear in α_i(Δg_2 small). Neither of these polarization functions leads to a

symmetrical narrowing of the hyperfine envelope of the $P700^+$ signal. Furthermore, one would not expect the effect to be identical for the oriented and unoriented systems.

One explanation of the narrowing is that, immediately following photo-oxidation, the unpaired electron on $P700^+$ is delocalized over 3 or 4 chlorophyll molecules. The steady-state $P700^+$ complex is believed to be a strongly coupled chlorophyll dimer; (16) delocalization of the unpaired electron over two molecules leads to a narrowing of $\sqrt{2}$ compared to the Chl^+ monomer EPR signal. Full delocalization over 3 or 4 molecules would result in a further narrowing of $\sqrt{3/2}$ or $\sqrt{4/2}$, respectively; the experimental narrowing is between these two values. Following electron transfer, the oxidized reaction center complex reaches a new equilibrium structure which favors delocalization over only two chlorophylls.

Reference (5) discusses other hypotheses concerning the narrowing phenomenon. Verification of these proposals will require further theoretical and experimental work.

There are many interesting areas of future research which are suggested by this Chapter. Further EPR and optical experiments on photosystem I are needed to evaluate details of the two-site model, determine values for lifetimes and exchange interactions, and determine the identity of A_1. An approach similar to the one described here can also be applied to the CIDEP signals reported from photosynthetic bacteria (22).

REFERENCES

1. B. Ke. Biochim. Biophys. Acta 301, 1 (1973).

2. A.R. McIntosh and J.R. Bolton. Biochim. Biophys. Acta 430, 555 (1976).

3. B. Ke, E. Dolan, K. Sugahara, R.M. Hawkridge, S. Demeter and E.R. Shaw, in Photosynthetic Organelles, a special edition of Plant Cell Physiol. No. 3., Jap. Soc. Plant. Physiol, p. 187 (1977).

4. R.A. Blankenship, A. McGuire and K. Sauer. Proc. Nat. Acad. Sci. USA 72, 4943 (1975).

5. G.C. Dismukes, A. McGuire, R.A. Blankenship and K. Sauer. Biophys. J. 21, 239 (1978).

6. K. Sauer, P. Mathis, S. Acker and J.A. Van Best. Biochim. Biophys. Acta 503, 120 (1978).

7. B. Ke. and V. Shuvalov, in Frontiers of Biol. Energetics, Eds. P.L. Dutton, J.S. Leigh and A. Scarpa, Academic Press, NY, in press (1979).

8. F.J. Adrian. J. Chem. Phys. 54, 3918 (1971).

9. J.H. Freed and J.B. Petersen. Adv. Mag. Res. 8, 1 (1976).

10. L. Monchick and F.J. Adrian. J. Chem. Phys. 68, 4376 (1978).

11. G.C. Dismukes and K. Sauer. Biochim. Biophys. Acta 504, 431 (1978).

12. J.J. Katz and J.R. Norris, in Current Topics in Bioenergetics Vol. 5 (D.R. Sandai and L. Packer, eds.) p. 41 (1973).

13. J.K.M. Sander and J.C. Waterton. J. Chem. Soc. D. Chem. Commun., 247 (1976).

14. H. Scheer, J.J. Katz and J.R. Norris. J. Amer. Chem. Soc. 99, 1372 (1977).

15. E.K. Metzner, Ph.D. Thesis. University of California, Berkeley, CA. Lawrence Radiation Laboratory Report - UCRL 3356 (September, 1974).

16. R.C. Prince, D.M. Tiede, J.P. Thornber and P.L. Dutton. Biochem. Biophys. Acta 462, 467 (1977).

17. G. Dryhurst in Electrochemistry of Biological Molecules, p. 412 (1977).

18. J.P. Thornber, R.S. Alberte, I.A. Hunter, J.A. Shiozawa and K.S. Kan. Brookhaven Symp. Biol. 28, 148 (1976).

19. K.J. Kaufmann, P.L. Dutton, T.L. Netzel, J.S. Leigh and P.M. Rentzepis. Science 188, 1301 (1975).

20. D. Holton, M.W. Windsor, W.W. Parson and J.P. Thornber. Biochim. Biophys. Acta 501, 112 (1978).

21. M.C. Thurnauer, J.J. Katz and J.R. Norris. Proc. Nat. Acad. Sci. 72, 3270 (1975).

22. A.J. Hoff, P. Gast and J.C. Romijn. FEBS Letters 73, 185 (1977).

CONCLUSION

The results presented in Chapters 3, 4, and 5 suggest further experimental and theoretical projects. Some of these are currently in progress, while others are at present tentative speculations. Below is summarized a program for logical continuations and new directions.

A. Theory of Orientation Averaging

We are extending the density of states approach developed in Chapter 3 to other types of spectroscopic experiments. A detailed paper on linear dichroism and a more general one outlining a linear response theory of partially ordered ensembles are in preparation. A calculation of time-dependent fluorescence depolarization due to rotational diffusion of an anisotropic protein molecule is also in progress.

B. Orientation of Electron Transport Cofactors in Photosynthetic Systems

We are investigating the orientation of the I and X (QFe) acceptor in *Rps. viridis* by EPR spectroscopy of magnetically aligned intact bacteria. We include in our calculations the Q^--Fe magnetic interactions and the I^--(X^-) interactions. Computer simulations of the random and oriented signals from Q-Fe^-, $Q^-FeQ^=$, and $I^-Q^-FeQ^=$ are planned.

We are also using absorption circular dichroism and linear dichroism measurements to determine the relative mutual orientations of Chl molecules in Chl proteins and

reaction centers. The initial calculations are being carried out on antenna BChl protein of the R-26 mutant of *Rps. spheroides*, which has only two Chl molecules per protein. We hope to extend our methods to the *Rps. viridis* reaction center, which has already been studied via EPR (Chapter 4).

C. Spin Polarization in Photosystem I

During the past year several new results have been obtained. Warden has observed the CIDEP signal by direct detection and claims that the flow effect disappears; he has reproduced our results when detection is carried out by 100 kHz field modulation. This report is very puzzling and may require a reformulation of the theory of Chapter 5. Thurnauer and Norris have used the spin echo method to monitor the polarized signal; their results, although at present only tentative, are also peculiar. A polarized signal has also been observed by MacIntosh and Bolton and by our laboratory at low temperatures; interpretation of this signal in a sensible manner has yet to be accomplished.

My objective at this point is construction of a coherent theory which satisfactorily explains all of the above results. At present I am inclined to believe that the core of the theory in Chapter 5 will be retained and that clarification will come when an accurate representation of what it is that each experiment is measuring can be made. The theory will then have to be extended to incorporate experimental effects which have up to now been ignored.

D. Final Remarks

The emphasis in this thesis has been an application of theory to photosynthesis. However, I believe that the approach taken here can be profitably applied to other biological systems. Speculations in this regard would be too vague to be worthwhile, and I shall not be more specific at this point. It is my hope that physical chemists investigating any biological system have found the ideas in the preceding pages, both general and particular, to have been stimulating, suggestive, or perhaps even concretely useful.

APPENDIX A

The matrices that describe the rotation are defined as follows. $R_{\hat{u}}(\phi)$ is the rotation matrix for rotation counterclockwise through an angle ϕ about an axis in the $\hat{u}$ direction. The matrix elements of $R_{\hat{u}}(\phi)$ are given by

$$[R_{\hat{u}}(\phi)]_{ij} = \cos(\angle x_i x'_j) \qquad \text{(A-1)}$$

where $(\angle x_i x'_j)$ is the angle between the ith axis of the original coordinate system and the jth axis of the coordinate system obtained after the rotation.

APPENDIX B

Equation (38) is obtained from equation (32) by the following substitution:

$$\cos u = \frac{-1}{\sin^2\theta'}\,(1 + \cos^2\theta' - 2\cos^2 v_1) \quad . \qquad (B\text{-}1)$$

The upper limit at $\cos v_1 = \cos\theta'$ is transformed to $\cos u = -1$, or $u = \pi$. The lower limit at $\cos v_1 = 1$ is transformed to $\cos u = +1$ or $u = 0$. From equation (B -1), one can readily obtain

$$dv_1 = \frac{\sin u \sin^2\theta'\, du}{4 \sin v_1 \cos v_1} \qquad (B\text{-}2)$$

$$\cos^2 v_1 = \tfrac{1}{2}(1 + \cos^2\theta' + \cos u \sin^2\theta') \qquad (B\text{-}3)$$

and

$$\sin v_1 = [\tfrac{1}{2} \sin^2\theta'(1-\cos u)]^{1/2} \qquad (B\text{-}4)$$

Substitution into equation (37) yields

$$\mathcal{D}_{\parallel}'(\theta') = \frac{\sin\theta'}{N_{\parallel}'} \int_0^{\pi} h(v_1)[\sin u \sin^2\theta'\, du]/\{4[\tfrac{1}{2}\sin^2\theta'(1-\cos u)]^{1/2}$$

$$\times [\tfrac{1}{2} + \frac{\cos^2\theta'}{2} + \frac{\sin^2\theta'}{2}\cos u - \cos^2\theta']^{1/2}\} \qquad (B\text{-}5)$$

which simplifies to

$$\mathcal{D}_{\parallel}(\theta) = \frac{\sin\theta'}{2N_{\parallel}'} \int_0^{\pi} h(v_1)\, du \qquad (B\text{-}6)$$

where

$$v_1 = \cos^{-1}\{[\tfrac{1}{2}(1+\cos^2\theta'+\cos u \sin^2\theta')]^{1/2}\}.$$

APPENDIX C

Using equations (31) and (40e), the perpendicular density of states can be written down

$$\mathcal{D}_1'(\theta') = \frac{\sin\theta'}{N_1'} \int_{v_1} \int_{v_2} \frac{h(v_1)}{\cos v_1 \sin\mu \cos v_2} dv_1 dv_2 \qquad (C-1)$$

Solving equation (40e) for $\sin\mu$ and substituting into equation (C-1) yields

$$\mathcal{D}_1'(\theta') = \frac{\sin\theta'}{N_1'} \int_{v_1} \frac{h(v_1)}{\cos v_1} dv_1 \int_{v_2} \frac{dv_2}{\cos v_2}$$

$$\times \{1-[(\cos\theta'+\sin v_1 \sin v_2)/(\cos v_1 \cos v_2)]^2\}^{-1/2} \qquad (C-2)$$

The denominator of the v_2 integral is quadratic in $\sin v_2$. When expanded and factored, $\mathcal{D}'(\theta')$ simplifies to

$$\mathcal{D}_1'(\theta') = \frac{\sin\theta'}{N_1'} \int_{v_1} dv_1 \; h(v_1) \int_{v_2} dv_2 \{[\sin(\theta'-v_1)$$

$$-\sin v_2][\sin(\theta'+v_1)+\sin v_2]\}^{-1/2} \qquad (C-3)$$

The v_2 integration is performed over the region where the integrand is real; *i.e.* the $\sin v_2$ quadratic is greater than zero. This requirement means the v_2 integration is from $-(\theta'+v_1)$ to $(\theta'-v_1)$. Now, make the substitution $x = \sin v_2$ and equation (C-3) becomes

$$\mathcal{D}_1'(\theta') = \frac{\sin\theta'}{N_1'} \int_{v_1} dv_1 \; h(v_1) \int_{-\sin(\theta'+v_1)}^{\sin(\theta'-v_1)} dx\{(x-1)(x+1)$$

$$\times [x-\sin(\theta'-v_1)][x+\sin(\theta'+v_1)]\}^{-1/2} \qquad (C-4)$$

The x integral is an elliptic integral of the first kind where the limits of integration are two roots of the quartic in x. Using equation 254.00 in Byrd & Freidman[1], the x integration can be performed. The end result for $\mathcal{D}_1'(\theta')$ is

$$\mathcal{D}_1'(\theta') = \frac{\sin\theta'}{N_1'} \int_0^{\pi/2} h(v_1)\, G(\theta', v_1)\, dv_1 \qquad (C-5)$$

where $G(\theta', v_1)$ is given by equation (42) and the limits of the v_2 integration are by inspection 0 and $\pi/2$.

[1] P.F. Byrd and M.M. Friedman. Elliptic Integrals for Scientists and Engineers. (Springer-Verlag, Berlin, 1971).

APPENDIX D

The radical pair Hamiltonian given in eq. (1) can be split into two parts

$$\mathcal{H}_{RP} = \mathcal{H}_D + \mathcal{H}_{OD} \tag{D-1}$$

where

$$\mathcal{H}_D = \tfrac{1}{2}\beta\vec{H}_o\cdot(\hat{g}_A + \hat{g}_D)\cdot(\vec{S}_A + \vec{S}_D) + J\vec{S}_A\cdot\vec{S}_D$$
$$+ \tfrac{1}{2}[\sum_i \underline{A}_i^{(D)}\vec{I}_i^{(D)} + \sum_j \underline{A}_j^{(A)}I_j^{(A)}]\cdot(\vec{S}_A + \vec{S}_D)$$

$$\mathcal{H}_{OD} = \tfrac{1}{2}\beta\vec{H}_o\cdot(\hat{g}_D - \hat{g}_A)\cdot(\vec{S}_D - \vec{S}_A)$$
$$+ \tfrac{1}{2}(\sum_i \underline{A}_i^{(D)}\vec{I}_i^{(D)} - \sum_j \underline{A}_j^{(A)}\vec{I}_j^{(A)})\cdot(\vec{S}_D - \vec{S}_A)$$

$\mathcal{H}_D$ is diagonal in the basis $\{|S\rangle, |T_o\rangle, |T_{+1}\rangle, |T_{-1}\rangle\}$, provided that the spin functions $|\alpha\rangle$ and $|\beta\rangle$ are quantized in the direction of the effective field

$$\hat{z} = (\hat{g}_A + \hat{g}_D)\cdot\vec{H}_o/||(\hat{g}_A + \hat{g}_D)\cdot\vec{H}_o|| \tag{D-2}$$

The radical pair eigenfunctions and energies depend upon the off-diagonal elements of the above basis set of the operator $\mathcal{H}_{OD}$. We now show that, for small g tensor anisotropy, the mixing of $|S\rangle$ with $|T_{+1}\rangle$ and $|T_{-1}\rangle$ is of negligible importance, and an $|S\rangle - |T_o\rangle$ basis set is sufficient for calculation of the polarization. We also derive an approximate expression for the matrix element $\langle S|H_{OD}|T_o\rangle \equiv H_{AD}$ as a function of orientation of radicals A^- and D^+.

We shall assume that the donor radical is isotropic, with scalar g value g_D. We choose as a coordinate system the principal axis system of the acceptor radical. Then

$$\vec{H}_o = |\vec{H}|(\sin\theta\cos\phi \ , \ \sin\theta\sin\phi \ , \ \cos\theta) \qquad \text{(D-3)}$$

$$\hat{g}_A = \begin{bmatrix} g_A^x & 0 & 0 \\ 0 & g_A^y & 0 \\ 0 & 0 & g_A^z \end{bmatrix}$$

$$g_D = \begin{bmatrix} g_D & 0 & 0 \\ 0 & g_D & 0 \\ 0 & 0 & g_D \end{bmatrix}$$

We define

$$\bar{g}_A = \frac{1}{3}(g_A^x + g_A^y + g_A^z) \qquad \text{(D-4)}$$

$$\Delta x = \bar{g}_A - g_A^x$$

$$\Delta y = \bar{g}_A - g_A^y$$

$$\Delta z = \bar{g}_A - g_A^z$$

$$g_+ = \bar{g}_A + g_D$$

$$g_- = g_D - \bar{g}_A$$

We wish to calculate the matrix elements $\langle S|H_{OD}|T_o\rangle$, $\langle S|H_{OD}|T_{+1}\rangle$, and $\langle S|H_{OD}|T_{-1}\rangle$. We first define

$$H_{OD} = H_{HF} + H_{\Delta g} \tag{D-5}$$

where

$$H_{HF} = \frac{1}{2}\left(\sum_i \underline{A}_i^{(D)} \vec{I}_i^{(D)} - \sum_j \underline{A}_j^{(A)} \vec{I}_j^{(A)}\right)\cdot(\vec{S}_D - \vec{S}_A)$$

$$H_{\Delta g} = \frac{1}{2}\beta \vec{H}_o \cdot (\hat{g}_D - \hat{g}_A)\cdot(\vec{S}_D - \vec{S}_A)$$

Because we are interested in the spin polarization of the donor radical, we set the sum over the acceptor hyperfine field equal to its ensemble average, i.e.

$$\sum_j \underline{A}_j^{(A)} m_j^{(A)} \rightarrow \langle \Sigma \underline{A}_j^{(A)} m_j^{(A)} \rangle = 0 \tag{D-6}$$

The nuclear spin operators $I_i^{(D)}$ are quantized in the direction of the effective field, $\hat{z}$. Then

$$\langle S|H_{HF}|T_{\pm 1}\rangle = 0 \tag{D-7}$$

$$\langle S|H_{HF}|T_o\rangle = \frac{1}{2}\sum_j \underline{A}_j^{(D)} m_j^{(D)}$$

where $m_j^{(D)}$ is the projection of $I_j^{(D)}$ on $\hat{z}$.

The matrix elements of $H_{\Delta g}$ must now be evaluated. Substitution of (3A) and (4A) into (5A) yields

$$\langle S|H_{\Delta g}|T_o\rangle = \frac{1}{2}\beta|\vec{H}|\{\cos^2\phi\sin^2\theta(g_+ - \Delta x)(g_- + \Delta x) \tag{D-8}$$

$$+ \sin^2\theta\sin^2\phi(g_+ - \Delta y)(g_- + \Delta y) + \cos^2\theta(g_+ - \Delta z)(g_- + \Delta z)\}$$

$$\{\cos^2\phi\sin^2\theta(g_+ - \Delta x)^2 + \sin^2\theta\sin^2\phi(g_+ - \Delta y)^2$$

$$+ \cos^2\theta(g_+ - \Delta z)^2\}^{-1/2}$$

In general, the matrix elements $\langle S|H_{\Delta g}|T_{\pm 1}\rangle$ will be complex. Since we intend to show only that these matrix elements are a small perturbation, we compute the absolute magnitudes.

$$|\langle S|H_{\Delta g}|T_{\pm 1}\rangle| = \left[\frac{\beta}{2}||(\hat{g}_D-\hat{g}_A)\cdot\vec{H}_o||^2-(\langle S|H_{\Delta g}|T_o\rangle)^2\right]^{1/2}$$

We now make the approximation

$$g_- \sim \Delta x,\Delta y,\Delta z \ll g_+$$

Then, algebraic manipulation of (8A) leads to

$$\langle S|H_{\Delta g}|T_o\rangle \approx \frac{1}{2}\beta|\vec{H}|\left[g_- -(\cos^2\phi\sin^2\theta\Delta x + \sin^2\phi\sin^2\theta\Delta y + \cos^2\theta\Delta z)\right] \quad \text{(D-9)}$$

$$|\langle S|H_{\Delta g}|T_{\pm 1}\rangle| \approx \left[(g_--\Delta x)^2\cos^2\phi\sin^2\theta + (g_--\Delta y)^2\sin^2\theta\sin^2\phi + (g_--\Delta z)\cos^2\theta - (\langle S|H_{\Delta g}|T_o\rangle)^2\right]^{1/2}$$

This gives as a final expression for $\langle S|H_{OD}|T_o\rangle$

$$\langle S|H_{OD}|T_o\rangle \equiv H_{AD} = \frac{1}{2}\Sigma\, \underline{A}_j^{(D)}M_j^{(D)} + \frac{1}{2}\beta|\vec{H}|\left[g_D - (g_A^x\cos^2\phi\sin^2\theta + g_A^y\sin^2\phi\sin^2\theta + g_A^z\cos^2\theta)\right] \quad \text{(D-10)}$$

We estimate the effects of $T_{\pm 1}$ mixing by calculating the ensemble average value

$$\langle\langle S|H_{\Delta g}|T_{\pm 1}\rangle\rangle = \frac{2}{\pi}\int_0^{\pi/2}\int_0^{\pi/2}\langle S|H_{\Delta g}|T_{\pm 1}\rangle \sin\theta\, d\theta d\phi$$

$$\approx \left[\frac{1}{3}(\Delta x^2 + \Delta y^2 + \Delta z^2)\right]^{1/2}\cdot\frac{1}{2}\beta|\vec{H}| \quad \text{(D-11)}$$

Substitution of values of Δx, Δy, and Δz for the species X^- yields

$$\langle|\langle S|H_{\Delta g}|T_{\pm 1}\rangle|\rangle \approx \beta|\vec{H}|\cdot(0.13) \quad \text{(D-12)}$$

The mixing coefficients, $C_{ST_{\pm 1}}$, are given to first order by

$$C_{ST_{\pm 1}} \propto |\langle S|H_{OD}|T_{\pm 1}\rangle|/(E_S - E_{T_{\pm 1}}) \qquad \text{(D-13)}$$

$$= \beta|\vec{H}|(0.13)/g\beta|\vec{H}| \approx \quad (.0325).$$

This 3.25% mixing in of the $T_{\pm 1}$ states leads to an error of less than 3% in the calculated polarization.

TECHNICAL INFORMATION DEPARTMENT
LAWRENCE BERKELEY LABORATORY
UNIVERSITY OF CALIFORNIA
BERKELEY, CALIFORNIA 94720